Modulation of endoplasmatic reticulum Ca^{2+} storage by Amyloid Precursor Protein and its cleavage products

Thesis
Submitted for a Doctoral Degree in Natural Sciences
at the Department of Biology
Ludwig Maximilians University, Munich, Germany

Submitted by
Runa Hamid
From Bareilly, India

Munich 2005

Modulation of endoplasmatic reticulum Ca^{2+} storage by Amyloid Precursor Protein and its cleavage products

Dissertation
zur Erlangung des Doktorgrades
- Dr. rer. nat.-
des Fachbereichs Biologie
der Ludwig Maximilian Universität, München

Vorgelegt von
Runa Hamid
aus Bareilly, Indien

München 2005

Declaration

I solemnly declare that this Dissertation is solely my own work and I have not taken any impermissible aid in completing it.

Ich versichere hiermit ehrenwörtlich, daß die Dissertation von mir selbständig, ohne unerlaubte beihilfe angefertigt ist.

(Runa Hamid)

Thesis work completed at:
Centre of Neuropathology and Prion research
Feodor-Lynen Str.23,
81377- Munich, Germany

First reviewer: Prof. Dr. Elisabeth Weiss
Second reviewer: PD Dr. Angelika Böttger
Supervisor: Prof. Dr. Jochen Herms

Thesis submitted on: 21st October, 2005
Date of oral examination: 29th May, 2006

Angefertigt am:
Zentrum für Neuropathologie und Prion forschung
Feodor-Lynen str.23
81377- München, Deutschland

Erstgutachter: Prof. Dr. Elisabeth Weiss
Zweitgutachter: PD Dr. Angelika Böttger
Sondergutachter: Prof. Dr. Jochen Herms

Dissertation eingereicht am: 21st Oktober, 2005
Tag der mündlichen prüfung: 29th Mai, 2006

With love

to

My parents

Table of Contents

Abbreviations and units .... -1-

1 Summary .... - 5 -

2 Introduction .... - 7 -

2.1 Alzheimer's disease .... - 7 -

2.2 Pathology of Alzheimer's disease .... - 8 -

2.2.1 Amyloid Plaques .... - 8 -

2.2.2 Neurofibrillary tangles .... - 9 -

2.3 Genetics of Alzheimer's disease .... - 9 -

2.3.1 The Presenilin .... - 10 -

2.3.2 The Amyloid Precursor Protein .... - 12 -

2.3.2.1 Amyloid Precursor Protein gene .... - 12 -

2.3.2.2 Amyloid Precursor Protein expression .... - 12 -

2.3.2.3 Amyloid Precursor Protein processing .... - 13 -

2.4 Cellular Ca^{2+} homeostasis .... - 19 -

2.4.1 "Ca^{2+} ON" mechanisms .... - 20 -

2.4.2 "Ca^{2+}OFF" mechanisms .... - 21 -

2.5 Alzheimer's disease and Ca^{2+} dyshomeostasis .... - 22 -

2.5.1 Presenilins and Ca^{2+} dyshomeostasis .... - 23 -

2.5.2 Amyloid Precursor Protein and Ca^{2+} dyshomeostasis .... - 24 -

2.5.3 Mitochondrial dysfunction and Ca^{2+} homeostasis .... - 26 -

3 Aim of the study .... - 30 -

4 Materials .... - 31 -

4.1 Cell lines .... - 31 -

4.1.1 Human embryonic kidney cells (HEK293 cells) .... - 31 -

4.1.2 Human neuroglioma cells (H4 cells) .... - 31 -

4.1.3 Primary culture of mouse astrocytes .... - 31 -

4.2 Bacterial strain .... - 31 -

4.3 Plasmids .... - 32 -

4.4 Microscopes .... - 32 -

4.5 Filter sets - 32 -
4.6 Antibodies - 33 -
4.7 Commercial kits - 33 -
4.8 Buffers - 33 -
  4.8.1 Buffers for Ca^{2+} imaging - 33 -
  4.8.2 Buffers for crude mitochondrial extraction - 34 -
  4.8.3 Buffers for western blotting - 35 -
  4.8.4 Buffer for agarose gel electrophoresis - 36 -
  4.8.5 Growth medium for bacterial cultures - 36 -
4.9 Equipments - 37 -
4.10 Chemicals - 38 -
4.11 Other materials - 39 -
4.12 Softwares - 40 -
5 Methods - 41 -
5.1 Cell culture - 41 -
5.2 Preparation of primary culture of mouse astrocytes - 41 -
5.3 Freezing of mammalian cells - 42 -
5.4 Thawing of mammalian cells - 42 -
5.5 DNA isolation from rodent tails - 42 -
5.6 Genotyping - 43 -
5.7 Agarose gel electrophoresis - 44 -
5.8 Ca^{2+} Imaging - 44 -
5.9 *In vitro* Ca^{2+} calibration - 48 -
5.10 Analysis of mitochondrial membrane potential - 48 -
5.11 Bioluminescent ATP assay - 49 -
5.12 Isolation of mitochondria from cultured cells - 49 -
5.13 Bradford method of protein estimation - 50 -
5.14 Western Blotting - 51 -
5.15 Preparation of electrocompetent cells - 51 -
5.16 Electrotransformation - 52 -
5.17 Plasmid isolation (Midi prep) - 53 -

5.18 Transient transfection .... - 53 -
5.19 Statistical analysis .... - 54 -
6 Results .... - 55 -
6.1 An enhanced cytosolic concentration of Ca^{2+} was observed in cells lacking APP or its C-terminal cleavage products. .... - 55 -
6.2 ER Ca^{2+} storage is modulated in cells lacking *APP* or its C-terminal cleavage products. .... - 60 -
6.3 Cells lacking AICD have decreased ATP production and enhanced mitochondrial membrane potential. .... - 67 -
6.4 The basal cytosolic free Ca^{2+} level was enhanced and ER Ca^{2+} was reduced on inhibition of oxidative phosphorylation .... - 71 -
6.5 Responses of cells lacking AICD were reversed on the application of Complex I and II substrates. .... - 75 -
6.6 AICD was not detected in isolated mitochondria. .... - 78 -
6.7 Responses of cells lacking AICD was reversed on application of Li^{2+} .... - 80 -
7 Discussion .... - 84 -
7.1 AICD regulates cellular Ca^{2+} homeostasis .... - 84 -
7.2 AICD regulates Ca^{2+} buffering by ER through mitochondrial ATP generation .... - 85 -
7.3 AICD might regulate Ca^{2+} homeostasis and mitochondrial function through gene transcription. .... - 87 -
7.4 AICD might regulate mitochondrial function directly .... - 89 -
7.5 AICD and Alzheimer's Disease .... - 89 -
7.6 Consequences of gamma secretase inhibitors as therapeutic drug targets for Alzheimer's disease .... - 93 -
8 Literature .... - 94 -
Acknowledgements .... -114-
Curriculum vitae .... -116-

Abbreviations and units

AA	Amino acid
AD	Alzheimer's disease
ADAM	a disintegrin and metalloprotease
AICD	APP intracellular domain
Aph-1	Anterior pharynx defective protein-1
APLP	Amyloid precursor like protein
APP	Amyloid precursor protein
$App^{0/0}$	Amyloid precursor protein knockout
APPs	soluble APP
Aβ	Amyloid beta peptide
BACE	Beta site APP cleaving enzyme
BCIP	5-bromo-4-chlor-indolyl-phosphate
BP1	APP binding protein 1
BSA	Bovine serum albumin
Ca^{2+}ATPase	Calcium ATPase
CCE	Capacitative calcium entry
CPA	Cyclopiazonic acid
CSF	Cerebrospinal fluid
C-terminus	Carboxyl terminus
CTFs	Carboxy terminal fragments
DMEM	Dulbecco's modified eagle's medium
Dox	Doxycycline
DTT	Dithiothreitol
EDTA	Ethylenediamine tetra aceticacid
EOFAD	Early onset of familial Alzheimer's disease
ER	Endoplasmatic reticulum
FAD	Familial Alzheimer's disease
FCCP	Carbonyl cyanide 4-trifluoro-methoxyphenylhydrazone
FCS	Foetal calf serum

GSK	Glycogen synthase kinase
H4 cells	Human neuroglioma cells
HBSS	Hank’s basal salt solution
Hek cells	Human embryonic kidney cells
ICD	Intracellular domain
IDE	Insulin degrading enzyme
IP_3	Inositol-1,4,5-triphosphate
IP_3R	Inositol-1,4,5-triphosphate receptor(s)
KPI	Kunitz protease inhibitor
LDL	Low density lipids
MAP	Microtubule associated protein
NaCN	Sodium cyanide
NBT	Nitroblue tetrazolium chloride
NFT	Neurofibrillary tangles
NICD	Notch intracellular domain
PAT	Protein interacting with APP tail
PDL	poly-D-lysine
PEN-2	Presenilin enhancer protein-2
PHF	Paired helical fragment
PiP2	Phosphatidyl inositol-4,5-biphosphate
PLC	Phospholipase C
PMCA	Plasmamembrane calcium ATPase
PS1	Presenilin 1
PS2	Presenilin 2
ROCC	Receptor operated calcium channels
ROS	Reactive oxygen species
RYR	Ryanodine receptor
$sAPP_\alpha$	soluble alpha APP ectodomain
$sAPP_\beta$	soluble beta APP ectodomain
SDS	Sodium dodecyl sulphate
SERCA	Sarcoendoplasmic reticulum calcium ATPase

SOCC	Store operated calcium channel
SR	Sarcoendoplasmic reticulum
TACE	Tumor necrosis factor alpha converting enzyme
TBS	Tris buffered saline
TGN	*trans*-Golgi network
TMPD	2,3,5,6-tetramethyl-p-phenylenediamine
TNF	Tumor necrosis factor
VOCC	Voltage operated calcium channels
VSV tag	Vesicular somatitis virus tag
α-secretase	alpha secretase
β-secretase	beta secretase
γ-secretase	gamma secretase
ε-secretase	epsilon secretase

Units

µF	microfarad
µg	microgram
µl	microlitre
µm	micrometer
µM	micromolar
bp	base pair
cm	centimeter
hrs	hours
kb	kilobase
kDa	kilodalton
kV	kilovolt
M	molar (= moles per liter)
mA	milliampere
mg	milligram
MHz	megahertz
min	minute

ml	milliliter
mm	millimeter
mM	millimolar
ng	nanogram
nm	nanometer
^{o}C	degree Celsius
pmol	picomole
rpm	revolutions per minute
v/v	volume per volume
w/v	weight per volume
x g	relative centrifugal force
%	percent

1 Summary

The work presented in this thesis is aimed to contribute to the understanding of the physiological role of APP and its underlying mechanism controlling the Ca^{2+} homeostasis. In addition, it aims to understand the pathophysiological role of Amyloid precursor protein (APP) and its cleavage products in Alzheimer's disease (AD) particularly focussing on the disturbances in normal Ca^{2+} homeostasis resulting from altered APP processing. A central hypothesis to the pathogenesis of AD is that the accumulation of amyloid-β peptide (Aβ) and/or Aβ-containing plaques play an important role in the development of the disease. Mutations in *APP*, *Presenilin 1* (PS1), or *Presenilin 2* (PS2) are linked to the inherited forms of the disease and result in an increased production of Aβ, particularly of the Aβ42 isoform. Most mutations in *APP*, *PS1*, or *PS2* that are associated with Familial Alzheimer's Disease (FAD) alter the γ-secretase cleavage, resulting in increased levels of Aβ42 species and affecting the generation of corresponding C-terminal fragments (CTFs), for instance, the APP intracellular domain (AICD). Recently, several studies have indicated that not only altered production of Aβ42 affect neuronal survival, but also the CTFs, predominantly AICD, have a critical pathophysiological role by modulating neuronal Ca^{2+} homeostasis.

In the present study, the mechanism by which APP or its cleavage products maintains Ca^{2+} homeostasis, is investigated in more detail by analyzing free cytosolic Ca^{2+} concentration in different cell types under various experimental conditions. In all the cell types analyzed, it was consistently observed that the loss of γ-secretase derived APP C-terminal fragment, AICD, enhances the basal resting cytosolic Ca^{2+} levels and reduce intracellular endoplasmatic reticulum (ER) Ca^{2+} storage. The correlation of enhanced resting Ca^{2+} and reduced ER Ca^{2+} storage strongly indicate an alteration of the mechanisms involved in Ca^{2+} buffering by the ER.

One of the most important mechanisms involved in the removal of Ca^{2+} from cytosol, to maintain the resting Ca^{2+} concentration, is mediated by Calcium ATPases (Ca^{2+}ATPases) that pumps Ca^{2+} from the cytosol into the ER lumen. This process is strongly ATP dependent. The mitochondrial membrane potential (or proton motive force) is the central bioenergetic parameter that controls ATP synthesis, therefore both mitochondrial membrane potential using rhodamine-123 fluorescent probe and ATP production using a bioluminescent assay were determined. Cells lacking AICD fragments were found to exhibit a lower ATP generation and a higher mitochondrial membrane potential. These results indicate a dysfunction of ATP synthase as a consequence of loss of AICD. Indeed blockade of mitochondrial ATP synthase by oligomycin in AICD expressing cells led to the similar alterations in Ca^{2+} storage as in the cells lacking AICD. On the other hand, administration of mitochondrial substrates on AICD non-expressing cells exhibited responses analogous to AICD expressing cells. Collectively, our data suggest that AICD is critically involved in mitochondrial ATP synthesis through a γ-secretase dependent signalling pathway controlling ATP dependent cellular mechanisms such as the cellular Ca^{2+} storage.

2 Introduction

2.1 Alzheimer’s disease

Age related impairment of memory and of cognitive functions, defined as ‘dementia’, is a brain disorder that seriously affects a person’s capability to carry out day to day activities. The most common form of dementia is ‘Alzheimer’s disease’, accounting for 60-80% of all dementia cases. This involves the part of brain that control thought, memory and language. AD affects 7-10% of individuals older than 65 years and up to 40% of persons older than 80 years (Evans et al., 1989). The word “Alzheimer’s” is named after a German doctor, Dr. Alois Alzheimer. In 1907, he described this condition in a 51 year old woman who died of an unusual mental illness showing impaired memory, orientation problems and disturbed behaviour (Alzheimer, 1907; Alzheimer et al., 1995). In the woman’s brain tissue he found abnormal clumps (now called neuritic or amyloid plaques) and tangled bundles of fibres (now called neurofibrillary tangles) (Fig 2.1).

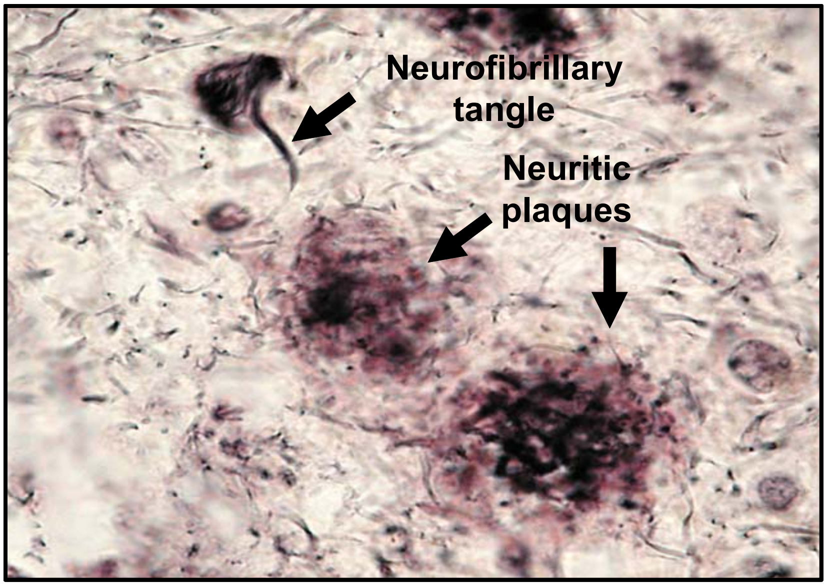

Fig 2.1: Photograph of an original section of the first case described by Alois Alzheimer in 1907 (from the archives of Dept. of Neuropathology, Munich). Photograph shows a neurofibrillary tangle and the neuritic plaques.

Today, these plaques and tangles in the brain are considered signs of Alzheimer's disease. Early and objective diagnosis is however still impossible and only definitive by pathological diagnosis of the brain postmortem.

2.2 Pathology of Alzheimer's disease

Clinically, the disease is initially characterized by subtle short-term memory problems and orientation disturbances. As the disease progresses, all higher cognitive functions become affected and the patients become completely dependent. The pathology of AD is restricted to the central nervous system and is pathologically characterized by the presence of extracellular senile amyloid plaques and intracellular neurofibrillary tangles. In addition, amyloid deposits in the walls of cerebral blood vessels (cerebral amyloid angiopathy), loss of neuronal cell bodies and synapses, as well as severe reactive astrogliosis can be observed.

2.2.1 Amyloid Plaques

Amyloid plaques are complex lesions composed of diverse amyloid peptides and associated molecules, degenerating neuronal processes and reactive glia (Dickson, 1997). Two types of extracellular amyloid deposits have been identified: neuritic and non-neuritic (diffuse plaques). The neuritic plaques, which measure 20-200 µm across, consist principally of an amyloid core surrounded by swollen abnormal processes, called dystrophic neurites. Biochemically, the most important component of the amyloid core is Aβ, a 4 kDa peptide proteolytically derived from the 110-130 kDa APP (Glenner and Wong, 1984; Robakis et al., 1987). Although Aβ is the major component of the amyloid deposits, other molecules are also known to be associated with these deposits i.e. α1-antichymotrypsin, α2-macroglobulin, LDL-receptors related protein, acetylcholine esterase, laminin, glycosaminoglycans, and the apolipoproteins.(Strittmatter and Roses, 1995; Bronfman et al., 1996; Van Uden et al., 2000). On the other hand, non-neuritic plaques differ from neuritic plaques, in that, they do not contain an amyloid core and, at most, only few or no neuritic processes. While both plaque types are found in the brains of non-demented old people, large number of neuritic plaques are only found in the brains of AD patients. Amyloid plaques are particularly abundant in the neocortex, the hippocampus, and the amygdale regions of the brain.

2.2.2 Neurofibrillary tangles

The second pathological hallmark in brain of AD patients is intracellular neurofibrillary tangles (NFT). The tangles consist mainly of paired helical filaments (PHF) of about 10 nm which are wound into helices. Some are straight filaments of about 15 nm interspersed with PHF. Extensive biochemical and immunological studies of these poorly soluble filaments demonstrated that the principal and probably the sole protein subunit is hyperphosphorylated protein Tau, a major neuronal microtubule-associated protein (MAP) (Kosik et al., 1986; Nukina and Ihara, 1986; Wood et al., 1986; Grundke-Iqbal et al., 1986a; Grundke-Iqbal et al., 1986b; Wischik et al., 1988; Lee et al., 1991).

In AD, about 95% of Tau filaments are in the form of PHF, while the remainder are straight filaments (Spillantini and Goedert, 1998). In normal brain, Tau protein binds to and stabilize microtubules, in contrast to PHF where Tau is unable to bind to microtubules.

2.3 Genetics of Alzheimer’s disease

Most cases of AD are sporadic, which means that the emergence of clinical symptoms occur in the seventh decade of life. However, less than 1% of AD cases show clinical symptoms at an early age and are inherited in an autosomal-dominant mendelian fashion (Van Gassen and Van Broeckhoven, 2000). These are referred to as FAD. Despite the disparity in the age of onset, both forms share common histopathological features: the extracellular deposition of neuritic and non-neuritic plaques that are composed of Aβ and intracellular NFT.

Three genes have been identified associated with early onset of familial Alzheimer's disease (EOFAD): *the PS1, PS2 and APP genes* located at chromosomes 14, 1, and 21 respectively (Hardy and Higgins, 1992; Hardy, 1997).

2.3.1 The Presenilin

Mammalian PS1 and PS2 are evolutionary conserved integral membrane proteins with a molecular weight of 50 kDa, each is predicted to traverse the membrane 6-10 times. The amino and carboxyl termini are both oriented towards the cytoplasm (Hutton and Hardy, 1997). Endoproteolytic cleavage generates two fragments that remain associated. The presenilin holoproteins and their endoproteolytically cleaved fragments are components of high molecular weight protein complexes that reside in the ER and the Golgi apparatus (Annaert et al., 1999). The amino acid sequence identity between PS1 and PS2 is approximately 60% as a whole and about 90% within the transmembrane domain. Human *PS1* and *PS2* express distinctly in human tissue. *PS1* is transcribed uniformly throughout the brain and peripheral tissue. On the other hand, *PS2* is transcribed at relatively low levels in the brain, except for the high levels in corpus callosum. It is highly expressed in some peripheral tissue, such as pancreas, heart, and skeletal muscle (Rogaev et al., 1997). It has been well established that presenilins are required for the γ-secretase cleavage of APP to generate Aβ and AICD and also for the S3 cleavage of Notch family receptors generating notch intracellular domain (NICD) (Kopan and Goate, 2000). Presenilins are important components of γ-secretase assembly along with other components: Nicastrin, aph-1 and Pen-2 (*see below*).

In contrast to mutations in the *PS1* gene, mutations in the *PS2* gene are rare causes of FAD. Approximately 50% of EOFAD cases are associated with mutation in the *PS1* gene (Tandon et al., 2000). To date, at least 73 different pathological mutations have been reported in the *PS1* gene, some of which are shown in fig 2.2 (Tandon and Fraser, 2002). The majority are missense mutations. Mutations in presenilins cause increased generation of Aβ42. Two of the important mutations identified are of two highly conserved aspartate residues in the transmembrane domains 6 and 7 of PS1 (Asp257 and Asp385). These mutations inhibit the biological function of presenilin required for γ-secretase activity (Wolfe et al., 1999). It has been shown that PS1 D385N mutation acts like a dominant negative mutation (Steiner et al., 1999b). Both aspartate residues at 257 and 385 are supposed to form the catalytic centre of the γ-secretase complex (Edbauer et al., 2003; Iwatsubo, 2004). PS1 with A257 and A385 mutations integrate poorly into the heteromeric complex of γ-secretase, raising the possibility that these transmembrane domain mutations disable PS1 structurally (Yu et al., 2000a).

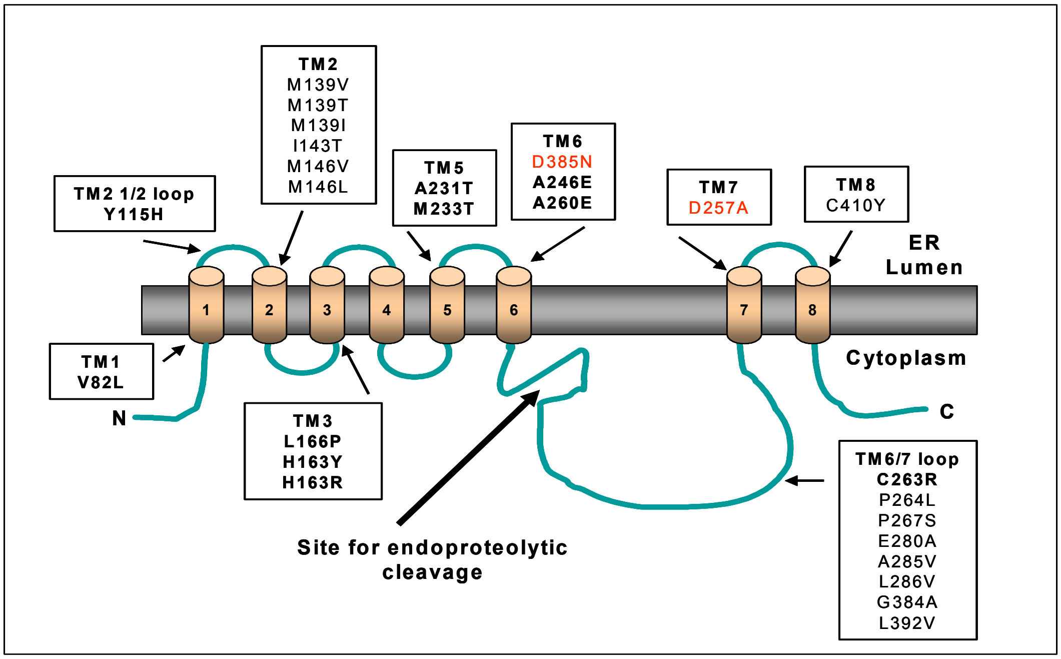

TM2
M139V
M139T
M139I
I143T
M146V
M146L
TM5
A231T
M233T
TM6
D385N
A246E
A260E
TM2 1/2 loop
Y115H
TM7
D257A
TM8
C410Y
ER
Lumen
1
2
3
4
5
6
7
8
Cytoplasm
TM1
V82L
N
C
TM3
L166P
H163Y
H163R
TM6/7 loop
C263R
P264L
P267S
E280A
A285V
L286V
G384A
L392V
Site for endoproteolytic cleavage

Fig 2.2: Schematic representation of PS1 showing eight transmembrane domains (TM). The boxes indicate some of the mutations identified in various regions of PS1. Mutations of two highly conserved aspartate residues (shown in red) in the transmembrane domain 6 and 7 inactivate γ-secretase activity and reduce Aβ and AICD generation (Diagram is compiled from the information in Steiner and Haass, 2000 and Tandon and Fraser, 2002)

2.3.2 The Amyloid Precursor Protein

2.3.2.1 Amyloid Precursor Protein gene

The human *APP* gene is 400 kb located in the mid portion of the long arm of chromosome 21 (Tanzi et al., 1987; Goldgaber et al., 1987). The amino acid (AA) sequence deduced from the *APP* cDNA predicted a large precursor of 695 AA, with a single hydrophobic stretch near its carboxyl terminal, containing properties of a membrane spanning domain, a 17 residue signal peptide for transport into ER and two consensus sequences for N-glycosylation in the large ectodomain (Kang et al., 1987). The *APP* gene consist of 18 exons and is alternatively spliced to generate at least 10 different APP variants (Octave, 1995). The three major spliced variants are *APP770* when all exons are present, while *APP751* lacks exon 8 and *APP695* lacks exon 7 and 8.

2.3.2.2 Amyloid Precursor Protein expression

From the early stages of embryonic development, APP mRNA is detectable in most tissues (Fisher et al., 1991; Lorent et al., 1995). *APP* is widely expressed throughout the body with particularly high expression in brain and kidney. Expression of *APP* in a variety of cell types, ranging from neurons to glial cells, platelets, endothelial cells, epithelial cells and fibroblasts, suggest an important role for APP in fundamental cellular processes (Arai et al., 1991; Forloni et al., 1992; Mattson, 1997),

APP is evolutionarly conserved and detected in a variety of mammals. Homologous proteins have also been identified in lower organisms, including *Saccharomyces cerevisae*, *Caenorhabditis elegans* and *Drosophila melanogaster* (Rosen et al., 1989; Daigle and Li, 1993; Zhang et al., 1994) . Two mammalian proteins that are highly homologous to APP are Amyloid precursor like protein 1 and 2 (APLP1 and APLP2). The discovery of APLPs classifies APP as a member of a multigene family (Wasco et al., 1992; Slunt et al., 1994). APP, APLP1 and APLP2 have the structure of type I integral membrane glycoproteins with a major extracellular component and a short cytoplasmic tail. All the three proteins are processed in a similar way leading to the secretion of large ectodomains. The expression of *APLP2* overlaps largely with that of *APP*, whereas *APLP1* is primarily expressed in the nervous system. The APLPs do not contain Aβ-like sequence (Wasco et al., 1993; Zhong et al., 1996), therefore do not seem to play a role in AD.

2.3.2.3 Amyloid Precursor Protein processing

APP is cotranslationally translocated into the ER by its signal peptide and matures through the central secretory pathway, with only a small percentage of holoproteins reaching the cell surface where it is acted upon by different secretases and is cleaved. About 23 AA hydrophobic stretch near its C-terminal region serves as an anchor in internal membranes (ER, Golgi, *trans*-Golgi network, endosome and in plasmalemma.)

There are two major pathways through which APP can be processed and are known as either non-amyloidogenic pathway or amyloidogenic pathway (Fig 2.3) (Selkoe, 1994; Octave, 1995; De Strooper and Annaert, 2000)). In the non-amyloidogenic pathway, the principal cleavage is performed by a protease named α-secretase that cleaves within the Aβ sequence and precludes the formation of Aβ. In amyloidogenic pathway, cleavage involves β-secretase and eventually results in production of Aβ-peptide.

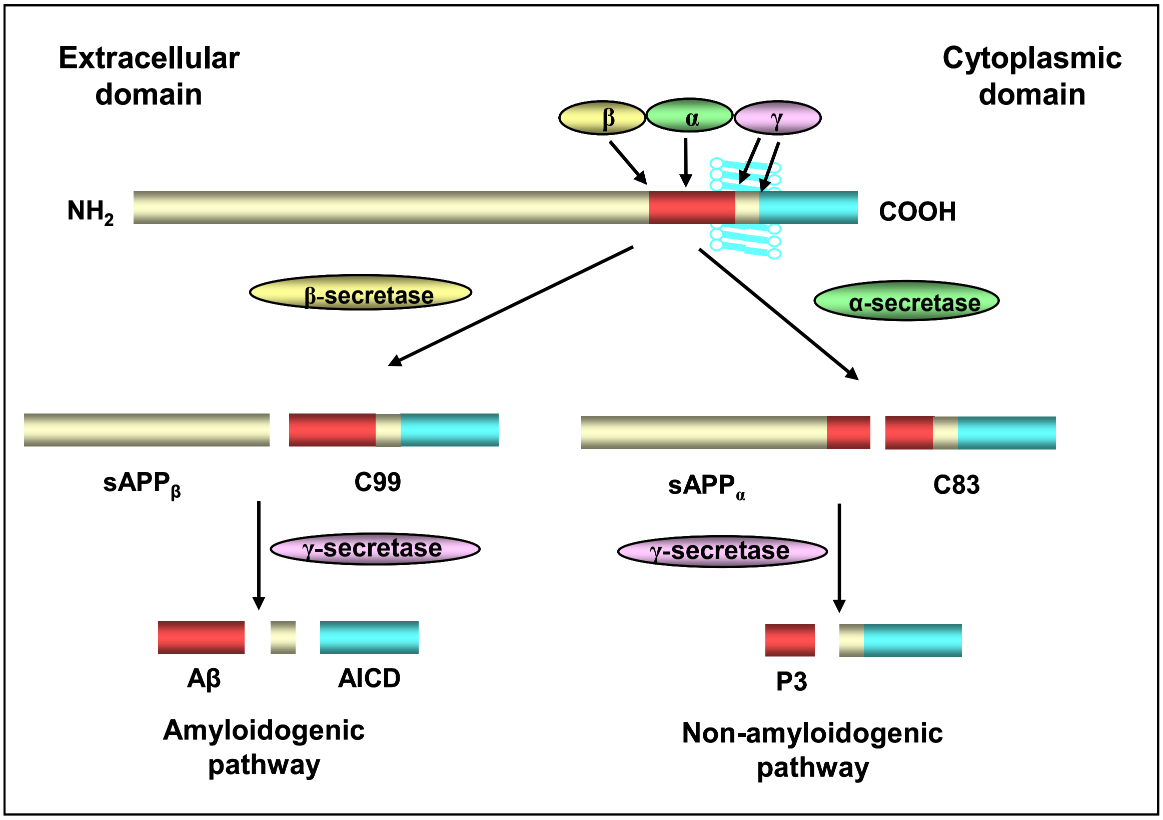
Extracellular domain
Cytoplasmic domain
β
α
γ
NH2
COOH
β-secretase
α-secretase
sAPPβ
C99
sAPPα
C83
γ-secretase
γ-secretase
Aβ
AICD
P3
Amyloidogenic pathway
Non-amyloidogenic pathway

Fig 2.3: Schematic representation of the proteolytic processing of APP. APP undergoes two endoproteolytic pathways that either preclude the formation of Aβ (Non-amyloidogenic pathway) or cause the formation of Aβ (Amyloidogenic pathway). In non-amyloidogenic pathway cleavage by α-secretase occurs within the Aβ domain (between residues 16 and 17 of Aβ sequence, shown in red). This results in the release of soluble N-terminus sAPPα and a membrane anchored C-terminus named as C83 fragment. α-secretase cleavage is followed by γ-secretase cleavage to liberate the P3 peptide. In amyloidogenic pathway, APP is first cleaved by β-secretase at the N-terminus region of the Aβ sequence. This cleavage generates a slightly shorter soluble N-terminus sAPPβ fragment and a membrane anchored C-terminus fragment named as C99. Cleavage by β-secretase is followed by γ-secretase that occurs first at the recently elucidated ε-site within the transmembrane domain liberating 50 AA fragment known as APP intracellular domain (AICD) and then at the γ-secretase site after residue 40 or 42 of Aβ domain to liberate Aβ40 or Aβ42.

Non-amyloidogenic pathway

APP is synthesized as an integral membrane protein, and becomes N- and O-glycosylated, sulphated, phosphorylated and endoproteolytically processed during its transit from ER to the cell surface. In the non amyloidogenic pathway, APP is predominantly cleaved by α-secretase, between amino acid 16 and 17 of the amyloid region, precluding the formation of Aβ-peptide (Fig 2.3) (Anderson et al., 1991; Wang et al., 1991; Zhong et al., 1994). This cleavage results in the release of the large soluble fragment of APP (100-120 kDa), named as sAPPα, and the generation of a truncated membrane anchored C-terminal fragment of about 10 kDa named as α-stub or C83 fragment (Weidemann et al., 1989; Schubert et al., 1989; Esch et al., 1990; Sisodia et al., 1990). α-secretase cleavage occurs intracellularly, predominantly after N- and O-glycosylation and sulphation, in a late compartment of the secretory pathway as well as at the plasma membrane. The 10 kDa C-terminal fragment is further processed to generate a secreted P3 peptide, by γ-secretase cleavage, which has been hypothesized to occur in early endosomes (Haass and Selkoe, 1993; Checler, 1995; Selkoe, 1998). The biological significance of P3 and its role, in amyloidogenesis, if any, remains obscure. As cleavage of APP by α-secretase destroys the Aβ sequence, it is generally thought that the α-secretase pathway extenuate amyloid formation, although this has not been demonstrated clearly. In addition, the C-terminally truncated form of APP released by α-secretase may have trophic actions (Small, 1998) which could antagonize the neurotoxic effects of aggregated Aβ (Mok et al., 2000). Most recently two members of ADAM (a disintegrin and metalloprotease) family, tumor necrosis factor-α (TNF-α) converting enzyme (TACE or ADAM-17) and ADAM-10, are reported as most interesting candidate for α-secretases (Buxbaum et al., 1998; Lammich et al., 1999).

Amyloidogenic pathway

Since the first proteolytic processing event defined for APP was “normal” α-secretory cleavage within the Aβ region, it was assumed that “abnormal” or pathological processing must occur to generate the Aβ-peptide, necessitating an unusual cleavage in the transmembrane domain of APP. This concept was revivified when Aβ peptides were detected in the conditioned medium of many cultured cells and in the cerebrospinal fluid of cognitively normal individuals

(Seubert et al., 1992; Shoji et al., 1992; Haass et al., 1992b; Busciglio et al., 1993). Subsequent extensive biochemical analysis demonstrated that Aβ is generated by endoproteolytic cleavage of APP by β-secretase followed by γ-secretase (Fig 2.3) (Haass and Selkoe, 1993). β-secretase cleavage of APP releases a truncated soluble ectodomain of APP, named sAPPβ (Seubert et al., 1993) and generates a membrane retained amyloidogenic C-terminal fragment of about 12 kDa, named as β-stubs or C99 fragments. C99 fragments are further processed by γ-secretase to generate Aβ peptides of varying lengths i.e. between 40 and 42 AA and a residual C-terminal fragment of nearly 7 kDa, named as AICD (APP intracellular domain) (Fig 2.3).

The subcellular compartment of Aβ generation is still not clearly identified. However, an approximate localization can be established by defining where one can detect their respective cleavage products i.e. sAPPβ, C99 and the amyloid peptides Aβ40 and Aβ42. Generation of Aβ-peptides was observed to be dependent on re-internalization of cell surface APP that escapes α-secretase cleavage. This was evidenced most clearly by the detection of radio-iodinated Aβ, following reinternalization of radio-iodinated cell surface APP (Koo and Squazzo, 1994). The internalization of APP is believed to employ the cytoplasmic domain of APP which contains a YENPTY signal mediating endocytosis of APP. The cells lacking this domain of APP show decreased Aβ formation (Golde et al., 1992; Haass et al., 1993; Lai et al., 1995). Moreover, agents interfering with the acidification of subcellular compartments, i.e. ammonium chloride and chloroquine, inhibit the production of Aβ (Shoji et al., 1992; Haass et al., 1993). This implies that Aβ is generated in an acidic compartment following endocytosis, which could be congruent with early endosomes. Since, Aβ formation was not completely abolished by inhibition of reinternalization of APP, an additional pathway independent of APP reinternalization might exist.

Using a variety of control experiments including brefeldin A and temperature blocks, pulse chases, immunocytochemistry and addition of an ER retrieval signal to APP, it was surprisingly found that Aβ42 is produced in high amounts in neuronal ER while the *trans*-Golgi network (TGN) was found to be the site for Aβ40 generation (Hartmann et al., 1997; Cook et al., 1997).

In contrast to α- and γ-secretases, β-secretase appears to be a sequence specific endoprotease (Citron et al., 1995). Radio sequencing demonstrates that Aβ isolated from amyloid plaques and cell lines, predominantly begins at the Asp +1 residue of Aβ (Gouras et al., 1998; Cai et al., 2001). Interestingly, a mutation in APP called Swedish mutation (so called because it was discovered in a Swedish family) is located near the β-secretase cleavage site causes FAD. This mutation is double mutation which involves amino acid substitution of Lys-Met→AsnLeu and is located immediately N-terminal to the β-secretase cleavage start site (Asp) of APP (Fig 2.4). The expression of this mutant causes APP to be a much better substrate for β-secretase and dramatically increases secretion of Aβ starting at Asp+1 (Citron et al., 1992; Cai et al., 1993) .

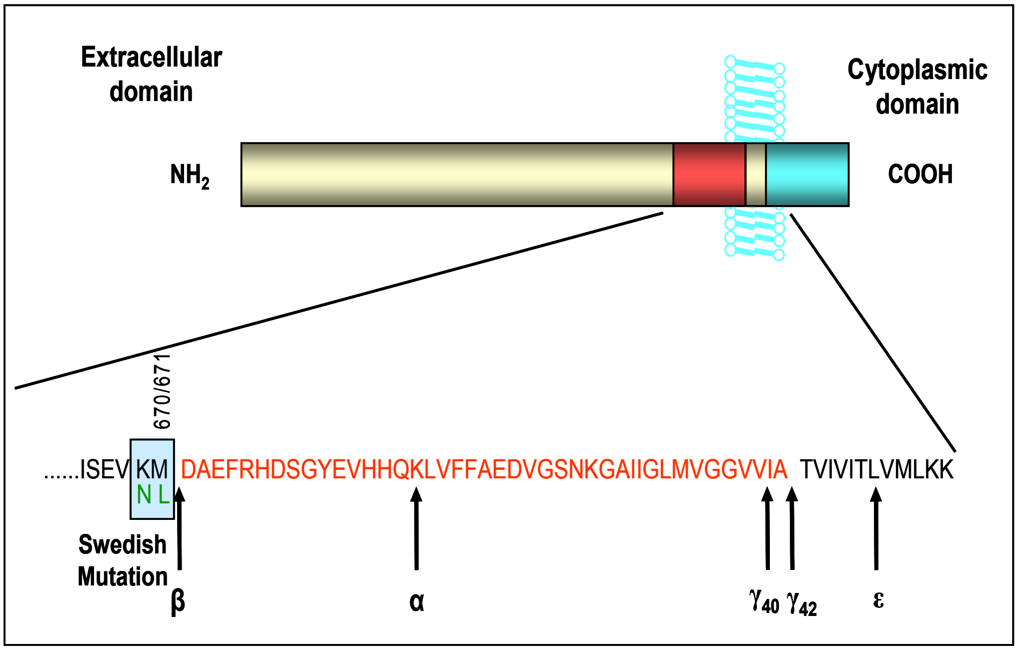
Extracellular domain
Cytoplasmic domain
NH2
COOH
670/671
......ISEV KM DAEFRHDSGYEVHHQKLVFFAEDVGSNKGAIIGLMVGGVVIA TVIVITLVMLKK
N L
Swedish Mutation
β
α
γ40 γ42
ε

Fig 2.4: The sequence of APP containing the Aβ domain (shown in red) and transmembrane region is expanded and shown as single letter amino acid code. The shaded vertical box indicates the Swedish double mutation which is located immediately N-terminus to the β-secretase cleavage start site. The normal cleavage site of β, α, γ, ε-secretases are indicated by arrows.

β-secretase activity in cells efficiently cleaves only membrane bound APP. On the other hand, transfection of APP constructs lacking the transmembrane domain are not cleaved by β-secretase (Citron et al., 1992). This implies that β-secretase is likely to be a membrane bound protease or, alternatively, it could be tightly associated with a membrane protein. β-secretase shows maximal activity at acidic pH, since agents that disrupt intracellular pH also inhibit β-secretase activity (Haass et al., 1993; Knops et al., 1995; Haass et al., 1995a). Moreover, β-secretase activity is highest in the acidic subcellular compartments of the secretory pathway, including the golgi apparatus and endosomes (Koo and Squazzo, 1994; Haass et al., 1995b). These data suggest that the active site of β-secretase is located within the lumen of acidic intracellular compartments. Recently, a most interesting candidate for β-secretase called β-site APP cleaving enzyme 1 (BACE1, also called Asp2 and memapsin2), a novel transmembrane aspartic protease has been identified by four independent groups. BACE 1 exhibits all the properties of β-secretase and as a key enzyme that initiates the formation of Aβ (Hussain et al., 1999; Sinha et al., 1999; Vassar et al., 1999; Yan et al., 1999).

Cleavage by γ-secretase takes place at multiple sites in C99 fragments, generating Aβ molecule that ends at amino acids 38, 39, 40, 42 or 43 of the Aβ domain. However the most abundant species found *in vivo* are Aβ40 and Aβ42. Among these Aβ42 is the most amyloidogenic form. Cell based systems that have been used to characterize γ-secretase generate 80-90% Aβ40 and 10-20% Aβ42, consistent with the ratio found in plasma and cerebrospinal fluid of humans (Mehta et al., 2001; Ertekin-Taner et al., 2001). Mutations in *APP*, *PS1* and *PS2* genes that cause EOFAD result in a selective increase in Aβ42 production (Esler and Wolfe, 2001). Since γ-secretase mediated cleavage of APP defines the C-terminus of Aβ, it is likely that activity of this enzyme contributes substantially to the rate of developing sporadic as well as familial AD. γ-secretase shows unusual properties of cleavage within the lipid bilayer where it hydrolyses the β-secretase generated membrane tethered C-terminal fragment of APP (named C99) in a water excluded environment. Several lines of evidence suggest that presenilins are closely related to γ-secretase activity. The first evidence is given by the fact that FAD linked mutations of presenilins shifted the preferred site of γ-cleavage from position 40 to 42 of Aβ. Secondly, γ-secretase activity is diminished in cells derived from PS1 knockout mouse (De Strooper et al., 1998). Thirdly, substitution of either of the two aspartate residues in the 6 and 7 transmembrane domains of PS1 (D257 and D385) abolished γ-secretase activity (Steiner et al., 1999a; Wolfe et al., 1999; Kimberly et al., 2000). Despite of the strong evidence, presenilin alone is not sufficient for the secretase activity as it's overexpression does not increase the γ-secretase activity. Other cofactors that were identified for γ-secretase activity are nicastrin, Aph-1 and PEN-2 (Yu et al., 2000b; Goutte et al., 2002; Francis et al., 2002). RNAi of each of the four fragments (PS, nicastrin, Aph-1 and PEN-2) in drosophila Schneider (S2) cells and in mammalian cells disrupts γ-secretase activity (Steiner et al., 2002; Edbauer et al., 2002b; Kimberly et al., 2003). Subsequently, it was also reconfirmed that expression of these four proteins in yeast, which lacks endogenous γ-secretase activity, reconstitute γ-secretase activity (Edbauer et al., 2003). However, recent studies by two independent groups show that all components of γ-secretase are assembled in early compartments of the secretory pathway and that this complex is transported to late compartments in which substrates (e.g. APP or Nicastrin) are encountered and subsequently processed within respective transmembrane segments (Kim et al., 2004; Capell et al., 2005).

2.4 Cellular Ca^{2+} homeostasis

Calcium (Ca^{2+}) is a ubiquitous intracellular signal responsible for controlling numerous cellular processes (Berridge, 1993; Berridge et al., 1998; Berridge et al., 2000). Cells at rest have a Ca^{2+} concentration of about 20-100 nM but when activated the Ca^{2+} concentration rises to roughly 10-200 µM. The Ca^{2+} concentration inside cells is regulated by the simultaneous interplay of multiple counteracting processes, which can be divided into "Ca^{2+} ON" and "Ca^{2+}OFF" mechanisms depending on whether they serve to increase or decrease cytosolic Ca^{2+} concentration (Berridge et al., 2000) (Fig 2.5).

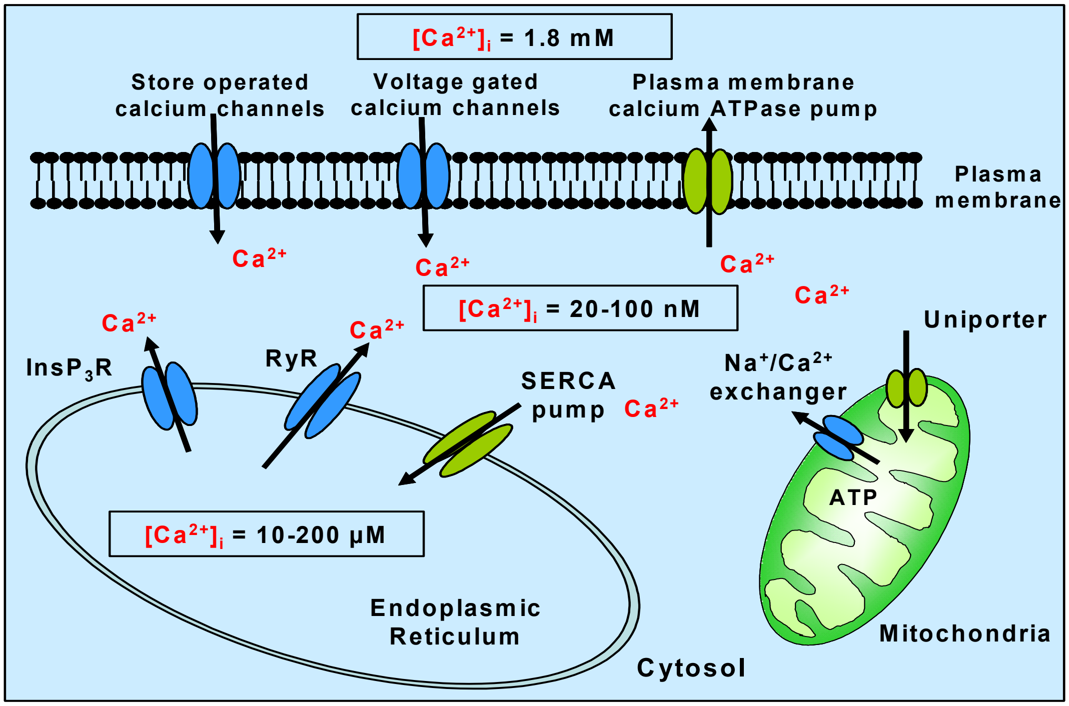
$[Ca^{2+}]_i$ = 1.8 mM
Store operated calcium channels
Voltage gated calcium channels
Plasma membrane calcium ATPase pump
Plasma membrane
Ca^{2+}
Ca^{2+}
Ca^{2+}
Ca^{2+}
$[Ca^{2+}]_i$ = 20-100 nM
Uniporter
Ca^{2+}
Ca^{2+}
$InsP_3R$
RyR
SERCA pump
Ca^{2+}
Na^+/Ca^{2+} exchanger
ATP
$[Ca^{2+}]_i$ = 10-200 µM
Endoplasmic Reticulum
Cytosol
Mitochondria

Fig 2.5: Cells maintain Ca^{2+} signaling by regulating influx of Ca^{2+} into the cell from the extracellular medium (1.8 mM) or by its release from the intracellular stores. At rest cytosolic Ca^{2+} levels are maintained at levels ranging between 20 to 100 nM. The Ca^{2+} concentration in the lumen of ER ranges between 10-200 µM. Ca^{2+} release from ER occurs through either IP_3 receptors or ryanodine receptors. On the other hand cell regulates Ca^{2+} entry from the extracellular medium through different type of channels on the plasma membrane; Voltage gated calcium channels or Store operated calcium channels. Ca^{2+} efflux from the cytosol occurs through plasma membrane calcium ATPase in an ATP dependent manner. The cytosolic Ca^{2+} load is also replenished back into the ER by ATP dependent sarco-endoplasmic Calcium ATPase pump (SERCA). Mitochondria are also known to buffer cytosolic Ca^{2+} in low amounts aided by a uniporter. The Ca^{2+} efflux from mitochondria occurs through Na^+/ Ca^{2+} exchanger.

2.4.1 “Ca^{2+} ON” mechanisms

The “Ca^{2+} ON“ mechanisms include channels that aid to increase cytosolic Ca^{2+}. Some of these channels are located at the plasma membrane and regulate the supply of Ca^{2+} from the extracellular space where Ca^{2+} concentration is about 1.8 mM. Other channels regulate the release of Ca^{2+} from intracellular stores into the cytosol, for instance channels on ER membrane.

Channels on the plasma membrane include *Voltage operated calcium channels* (VOCC), *receptor-operated calcium channels* (ROCCs) and *store operated calcium channel* (SOCCs) (Fig 2.5). VOCCs are largely expressed by excitable cell types such as neuronal and muscle cells, where they are activated by depolarization of the plasma membrane. ROCCs are activated by the binding of an agonist like glutamate, ATP or acetylcholine to the extracellular domain of the channel. SOCCs are activated in response to depletion of the intracellular Ca^{2+} store either by physiological Ca^{2+} mobilizing messengers or pharmacological agents. This mechanism is termed as "*Capacitative Calcium Entry (CCE)*" (Putney, Jr., 1986). CCE is a normal physiological phenomenon taking place predominantly in non-excitable cells. Recent reports have indicated that this phenomenon also plays an important physiological role in many, but not all excitable cells where it functions in the generation of cytoplasmic Ca^{2+} signals with cell specific functions (Antaramian et al., 2001). The mechanism by which the SOCCs sense the filling status of the intracellular pool is still unknown.

Ca^{2+} release from the ER occurs through two types of Ca^{2+} channels: inositol-1,4,5-triphosphate receptors (IP_3Rs) and ryanodine receptors (RyRs) (Fig 2.5). Release through IP_3Rs requires the activation of G protein on the cell surface that induce phospholipase C (PLC) to cleave phosphatidylinositol-4,5-biphosphate (PiP_2) into diacylglycerol and IP_3. IP_3 encounters with IP_3Rs and causes the channels to open, thus allowing the Ca^{2+} stored at high concentration in the ER/SR to enter the cytoplasm. Ryanodine receptors are structurally and functionally analogous to IP_3Rs and are activated by binding of ryanodine (Franzini-Armstrong and Protasi, 1997). As a result of these ON mechanism Ca^{2+} flows into the cytoplasm to produce the increase in concentration that constitutes a Ca^{2+} signal.

2.4.2 "Ca^{2+}OFF" mechanisms

Once Ca^{2+} has carried out its signaling functions, it is rapidly removed from the cytoplasm by various pumps and exchangers (Pozzan et al., 1994; Blaustein and

Lederer, 1999). The plasma membrane Ca^{2+}ATPase (PMCA) pump extrudes Ca^{2+} to the outside and sarco-endoplasmic Ca^{2+}ATPase (SERCA) pump returns Ca^{2+} to the internal stores (Fig 2.5). The Ca^{2+} concentration in ER and in extracellular space is much higher than in cytosol, therefore the Ca^{2+} extrusion by these pumps work against a high concentration gradient and is ATP dependent. In addition to it, there are also Na^+/Ca^{2+} exchangers that also extrude Ca^{2+} to the outside from the cytoplasm.

The mitochondria is another important component of OFF mechanism in that it sequesters Ca^{2+} under conditions of local elevated cytoplasmic Ca^{2+} and then releases it back slowly during the recovery phase (Fig 2.5). The uptake of Ca^{2+} by mitochondria is, in fact, not mediated by pumps or exchangers, but by a "uniporter" possibly a gated channel (Nicholls and Crompton, 1980). The molecular identity and nature of the uniporter is unknown. The uniporter provides a pathway for the accumulation of the Ca^{2+} into the mitochondrial matrix, driven by the electrochemical potential gradient across the inner mitochondrial membrane, usually estimated at 200 mV negative to the cytosol, and generated either by respiratory chain or ATP hydrolysis. However, the uniporter has a very low affinity for Ca^{2+} and has been demonstrated that mitochondria sequester only very low amounts of Ca^{2+} (Somlyo et al., 1979). The Ca^{2+} efflux from mitochondria back into the cytosol is mediated by two types of exchangers namely, Na^+/Ca^{2+} and H^+/Ca^{2+} exchangers (Nicholls and Crompton, 1980; Carafoli, 2003).

2.5 Alzheimer's disease and Ca^{2+} dyshomeostasis

Deregulation of intracellular Ca^{2+} signaling has been implicated in the pathogenesis of AD. The "Ca^{2+} hypothesis of Alzheimer's disease" was first proposed by Khachaturian (Khachaturian, 1989). Its basic tenet is that sustained disturbances in Ca^{2+} homeostasis are a proximal cause of neurodegeneration in Alzheimer's disease. One parameter of Ca^{2+} homeostasis in normally aged neurons is the enhanced value of resting intracellular Ca^{2+} values. Significant increase in resting cytosolic $[Ca^{2+}]_i$ with aging has been reported in synaptosomes obtained from the aged brains and in acutely dissociated neurons isolated from hippocampus or neocortex (MartInez et al., 1988; Villalba et al., 1995; Kirischuk and Verkhratsky, 1996). Similar increase has been reported for peripheral neurons and for cerebellar purkinje neurons recorded in brain slice (Kirischuk and Verkhratsky, 1996). The issue of the resting (or basal) intracellular Ca^{2+} values in the aged neurons is central for the "Ca^{2+} hypothesis" of neuronal aging. At steady state, the resting Ca^{2+} values represent the balance between the Ca^{2+} entry system (mainly Ca^{2+} permeable channels) and Ca^{2+} removal system (mainly Ca^{2+} pumps). Even a minimal dysfunction in any of these systems determine over a period of time a resetting of the steady state value of resting Ca^{2+} .

Studies of the pathogenic mutations in *PS1, PS2* and *APP* gene responsible for EOFAD have established central roles for perturbed cellular Ca^{2+} homeostasis. Ca^{2+} deregulation in AD includes APP processing regulation, ER dysfunction, mitochondrial changes and gene expression alterations.

2.5.1 Presenilins and Ca^{2+} dyshomeostasis

Presenilins contribute to neurodegeneration in AD mainly through the modulation of Ca^{2+} signaling in the ER. A pathological role for mutant PS1 in modulating IP_3 evoked Ca^{2+} release from the ER is shown by several groups in a variety of systems, including Xenopus oocyte, neural and non-neural cell lines, primary neurons and transgenic mice. For example, studies in fibroblast harbouring A246Q mutation of PS1 shows as enhanced IP_3 mediated Ca^{2+} liberation, therefore exhibiting an enhanced ER Ca^{2+} content, altered resting Ca^{2+} levels and altered mitochondrial functions (Peterson and Goldman, 1986; Gibson et al., 1996; Hirashima et al., 1996; Leissring et al., 1999b). Clinical mutation in the *PS2 gene* also enhances IP_3 evoked Ca^{2+} release from the ER. For instance, PS2 harboring FAD mutation (N141I , M239V) in *Xenopus* oocyte is reported to exhibit enhanced IP_3 mediated Ca^{2+} release (Leissring et al., 1999a). This finding reveals that a pathological pathway involving the destabilization of Ca^{2+} homeostasis is common to both PS1 and PS2. Studies in transgenic mice harboring M146L mutation in PS1 exhibits disruption of the control of intracellular Ca^{2+}, abnormal synaptic Ca^{2+} homeostasis and mitochondrial dysfunction (Begley et al., 1999; Barrow et al., 2000). Abrogation of functional PS1, by either knocking out PS1 or expressing inactive PS1 reduces ER Ca^{2+} storage (Yoo et al., 2000; Leissring et al., 2002) and potentiates Capacitative calcium entry (CCE) (Yoo et al., 2000). Likewise, the release of Ca^{2+} from ER stores after treatment with thapsigargin, an irreversible inhibitor of the SERCA pump, was also elevated in cells that expressed physiological levels of mutant PS1 (Leissring et al., 2000). Over expression of the *PS1* ΔE9 (exon 9 deleted *PS1*) mutation in neuroblastoma cells also increases Ca^{2+} stores (Smith et al., 2002). Conversely, Ca^{2+} stores are diminished in presenilin-deficient cells (Leissring et al., 2002). All these evidences show that presenilins play a very critical role in regulating Ca^{2+} homeostasis in the ER.

2.5.2 Amyloid Precursor Protein and Ca^{2+} dyshomeostasis

There have been considerable reports that link altered processing of APP to disruption of neuronal Ca^{2+} homeostasis and an excitotoxic mechanism of cell death in AD. Generally, secreted N-terminal molecules of APP (sAPPα or sAPPβ) normalize cytosolic Ca^{2+} levels and are regarded as neuroprotective (Goodman and Mattson, 1994). sAPPα or sAPPβ has been shown to moderate Ca^{2+} responses in hippocampal neurons after exposure to glutamate, and can protect neurons against excitotoxicity (Mattson et al., 1993a; Mattson, 1994; Koizumi et al., 1998). These molecules have also been shown to protect the cells against the pro-apoptotic effects of mutant PS1, and this effect is mediated by the stabilization of intracellular Ca^{2+} (Guo et al., 1998b).

Whereas sAPPα or sAPPβ is supposed to be neuroprotective and normalizes cytosolic Ca^{2+} levels, a series of studies yielded conflicting data concerning the possible neurotoxicity of Aβ. However, quite a number of reports have shown that, in fact, Aβ may or may not be neurotoxic depending upon whether or not it is in an aggregated state. For instance, it was shown that fresh unaggregated Aβ was not neurotoxic but if left for 2-4 days incubation prior to addition to the cultures resulted in aggregation and neurotoxicity (Pike et al., 1991). Subsequently, a direct relationship between peptide aggregation and neurotoxic potency was shown (Pike et al., 1991; Busciglio et al., 1993; Mattson et al., 1993b). These experimental studies are consistent with the observed AD pathology in which only plaques containing aggregated Aβ are associated with neuronal degeneration. The mechanism of Aβ toxicity was examined in a series of studies on cultured human cortical and rat hippocampal neurons. Chronic exposure of Aβ results in an elevation of resting Ca^{2+} values and increased Ca^{2+} responses to depolarization (Mattson et al., 1992; Mattson et al., 1993b).

As described in the preceding text, APP undergoes presenilin dependent γ-secretase cleavage generates Aβ peptides and AICD. Recently it has been shown that AICD regulates phosphoinositide mediated Ca^{2+} signaling through a γ-secretase dependent signaling pathway (Leissring et al., 2002). A recent report shows that elevated β-secretase (BACE1) expression in sporadic AD may induce the increase in β-CTF ($sAPP_{\beta}$) and Aβ but cause a reduction of AICD generation (Kume et al., 2004). This infers that as AICD has been shown to play a role in signal transduction, a decreased levels in sporadic AD brain may induce signal transduction failure (Cao and Sudhof, 2001; Scheinfeld et al., 2003), Interestingly, it has been reported that some *PS1* mutations causing EOFAD, inhibit the generation of AICD (Chen et al., 2002). Therefore, AICD may be a key molecule for the elucidation of AD pathology.

A large body of work shows that Ca^{2+} signaling can be disrupted by derivatives of APP but until now no definitive role for different cleavage products of APP playing role in Ca^{2+} homeostasis, has been ascribed.

2.5.3 Mitochondrial dysfunction and Ca^{2+} homeostasis

Mitochondria play a complex multifactorial role in the cell. In addition to their primary role in ATP generation, the organelles also sequester Ca^{2+} (Gunter et al., 1994) . These functions are intimately interlinked through the central bioenergetic parameter of the proton electrochemical gradient across the inner mitochondrial membrane which is generated as a result of oxidative phosphorylation. The NADH and $FADH_2$ formed in glycolysis, fatty acid oxidation and the citric acid cycle are energy rich molecules because each contains a pair of electrons having a high transfer potential. The flow of electrons from NADH or $FADH_2$ to O_2 through protein complexes (named as complex I-IV) located in the mitochondrial inner membrane leads to the pumping of protons out of the mitochondrial matrix (Fig 2.6). The resulting uneven distribution of protons generates a pH gradient and a transmembrane electrical potential ($\Delta\psi_m$), both of these components together constitutes a proton motive force (Δp). ATP is synthesized when proton flow back to the mitochondrial matrix through an enzyme complex named as ATP synthase (Fig 2.6). The proton motive force generated through this process is about 200 mV. Under most conditions $\Delta\psi_m$ is the dominant component of Δp which normally accounts for about 80% of Δp (Mitchell and Moyle, 1969; Nicholls, 1974). Therefore, mitochondrial membrane potential is usually used for a measure of mitochondrial activity and relative ATP production. Because the proton circuit is completed by the reentry of protons through the ATP synthase, which in turn is tightly coupled to ATP synthesis, it follows that the proton current responds automatically to the ATP demand. Tight coupling between electron flux and proton pumping in each respiratory chain complex means that electron flux (and hence respiration) is in turn controlled by ATP demand.

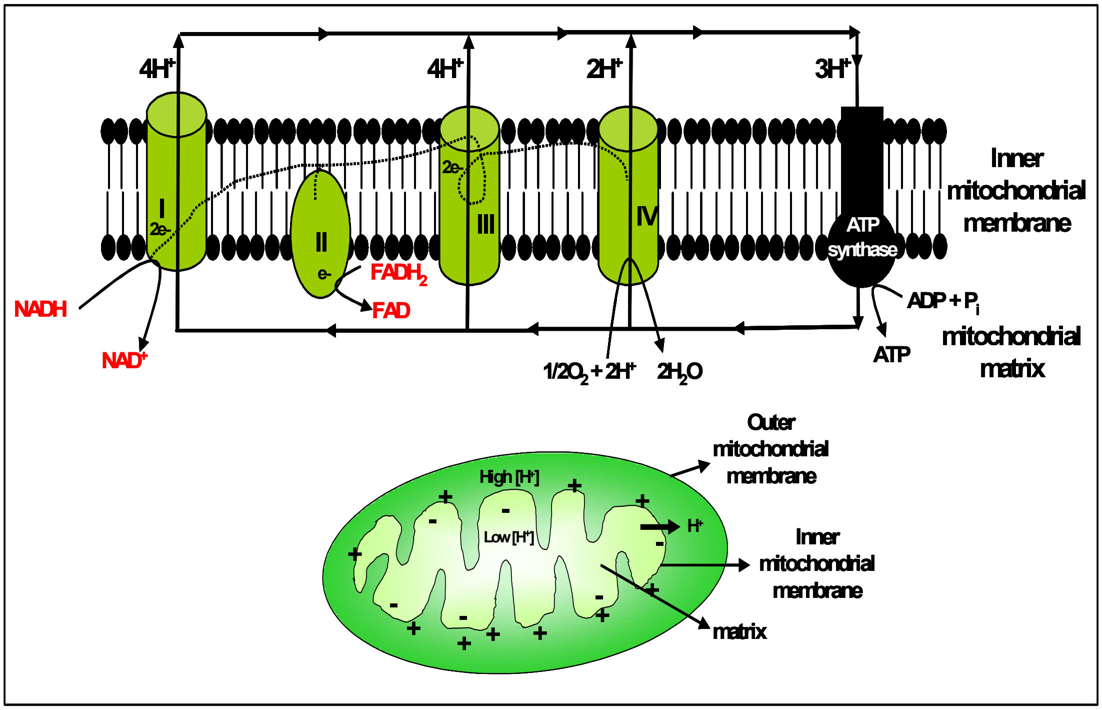
4H+
4H+
2H+
3H+
I
2e-
II
e-
III
2e-
IV
ATP synthase
Inner mitochondrial membrane
NADH
NAD+
FADH2
FAD
1/2O2 + 2H+
2H2O
ADP + Pi
ATP
mitochondrial matrix
Outer mitochondrial membrane
High [H+]
Low [H+]
H+
Inner mitochondrial membrane
matrix

Fig 2.6: NADH and $FADH_2$ are high energy electron carriers generated through citric acid cycle. Electrons from NADH and $FADH_2$ enters the electron transport chain at respectively complex I and complex II. The flow of electrons from complex I to IV leads to pumping of protons out of the mitochondrial matrix. Complex I, III and IV function as proton pumps. The resulting uneven distribution of protons generates a pH gradient and a transmembrane electrical potential that creates a proton motive force. ATP is synthesized when protons flow back to the mitochondrial matrix through an enzyme complex called ATP synthase that catalyses the synthesis of ATP. Due to this phenomenon, the mitochondrial membrane potential is negative on the matrix side and positive on the cytosolic side.

The mitochondrial membrane potential $\Delta\psi_{m,}$ not only serves as a key intermediate in the synthesis of ATP but can also be utilized to accumulate Ca^{2+} (Gunter and Gunter, 1994). Uptake of Ca^{2+} by mitochondria is mediated by a uniporter which is activated by elevated cytoplasmic Ca^{2+} and which allows Ca^{2+} to enter the matrix down the steep electrochemical gradient (composed mostly of a – 150 to – 180 mV mitochondrial membrane potential, ψ_m) that is maintained by selective pumps and conductances. Mitochondrial Ca^{2+} uptake increases the activity of several dehydrogenases (McCormack et al., 1990), which drives the operation of the electron transport chain and ATP synthesis, thereby matching energy production with demand (Duchen, 1999). Mitochondrial Ca^{2+} buffering is central to normal physiology and Ca^{2+} signaling. Therefore any alteration in any of these mitochondrial functions might be the underlying cause of disturbed Ca^{2+} homeostasis and altered energy metabolism, a characteristic of age related diseases like AD.

Subtle changes in respiratory chain capacity, substrate supply, cytoplasmic Ca^{2+} and membrane potential occur in aging. It has been shown that sustained elevation of cytoplasmic Ca^{2+} levels can promote mitochondrial oxyradical (superoxide) production, membrane depolarization and ATP depletion suggesting a contribution of altered Ca^{2+} homeostasis to mitochondrial dysfunction in AD (Guo et al., 1998a; Guo et al., 1999a). Conversely, impairment of mitochondrial function can result in increased cytoplasmic Ca^{2+} levels. Two independent reports on PC12 cells show that a rapid elevation of intracellular Ca^{2+}, was followed by caspase activation, accumulation of reactive oxygen species (ROS), and decrease in transmembrane potential (Kruman et al., 1998; Keller et al., 1998) . The Ca^{2+} chelator BAPTA-AM and agents that block Ca^{2+} release from ER and influx through voltage-dependent channels prevented mitochondrial ROS accumulation and membrane depolarization and apoptosis (Keller et al., 1998). Moreover, it was shown in rat cortical synaptosomes that ryanodine receptors were involved in ER-mediated mitochondrial Ca^{2+} changes in AD (Mungarro-Menchaca et al., 2002). Recent studies have suggested that Aβ may be directly toxic to mitochondria (Casley et al., 2002) and it also causes loss of cytochrome c oxidase activity in neurons in culture (Kim et al., 2002). The activities of key enzymes of glycolysis and the tricarboxylic acid cycle, pyruvate dehydrogenase complex and α-ketoglutarate dehydrogenase complex, was also found to be lower in brain taken post mortem from Alzheimer's patients compared with control (Sorbi et al., 1983; Butterworth and Besnard, 1990; Mastrogiacomo et al., 1993).

Taken together, the evidences described in the above sections strongly suggest that Ca^{2+} regulation employ PS1, PS2 and cleavage products of APP. The study of Ca^{2+} homeostasis therefore is the subject of key importance in aging and AD research and its fragmented knowledge attained until now deserves further consideration.

3 Aim of the study

Alzheimer's disease has a very complex and multifactorial etiology. The pathogenesis of AD is still not well understood and especially the precise cellular and molecular mechanisms that underlie the cause of disease. Lines of studies done on the pathogenic mutations in PS1, PS2 and APP in different cellular model have established central roles for disturbed Ca^{2+} homeostasis. But up to date no definitive mechanism have been described that underlie disturbances in Ca^{2+} homeostasis due to these mutations. The study done in this thesis is focused on the normal physiological role of APP and its cleavage products with regard to cellular Ca^{2+} homeostasis. The function of APP is unknown and ablation of *APP* gene does not lead to any substantial phenotype in gene targeted mice (Zheng et al., 1996). APP is a member of a gene family that includes Amyloid precursor like proteins APLP1 and APLP2, which might compensate for the loss of APP (Heber et al., 2000). In a previous study, it was revealed that ablation of all the three family members leads to early postnatal lethality (Herms et al., 2004), indicating the importance of these proteins in the cell.

Therefore the specific aims of the thesis are:

A. To understand the role of APP and its cleavage products in maintenance of Ca^{2+} homeostasis.
B. To study which cleavage product of APP processing is involved in ER Ca^{2+} storage and hence maintenance of Ca^{2+} homeostasis.
C. To study the underlying mechanism that control Ca^{2+} homeostasis via APP or its cleavage products.
D. To understand the disturbances in mechanisms caused as a result of altered APP processing.

4 Materials

4.1 Cell lines

4.1.1 Human embryonic kidney cells (HEK293 cells)

HEK293 cells were courteously provided by Prof.Christian Haass (Adolf Butenandt Institute, Munich). The following stable cells lines of HEK293 cells were used :

- Express human APP (wtAPP) (Haass et al., 1992a)
- Express APP with swedish mutation (APPsw) (Citron et al., 1992)
- Coexpress APPsw and PS1 with D385N mutation (PSD385N) (Capell et al., 2000)
- Coexpress APPsw and insulin degrading enzyme (IDE) (Edbauer et al., 2002a)

4.1.2 Human neuroglioma cells (H4 cells)

H4 cells were courteously provided by Ellen Kilger (Hertie Institut für Klinische Hirnforschung, Tübingen). The following stable cell lines under the control of “Tet-Off system” in H4 cells were used (Gossen and Bujard, 1992) :

- Express inducible allele of AICD fragment with VSV tag (H4-AICD-VSV)
- Express only regulator plasmid (H4-control)

4.1.3 Primary culture of mouse astrocytes

- *App* knockout mouse (*App*$^{0/0}$) (Muller et al., 1994)
- C57xSv129 mouse (Wt)

4.2 Bacterial strain

- E.*coli* DH5α (Hanahan, 1983)

4.3 Plasmids

- pEGFP-N1 was purchased from clontech.
- pcDNA3 (Invitrogen) encoding nucleotide sequence of AICD (pcDNA3-AICD). This construct was provided by Prof.Christian Haass. The AICD sequence was cloned between HindIII and XbaI restriction enzyme site in multiple cloning region.

4.4 Microscopes

- BX50WI upright microscope from Olympus (Germany) was used for imaging experiment. The 20X water immersion objective (UM plan FI) was also purchased from Olympus.
- Axiovert 40CFL from Zeiss (Germany) was used for normal visualization of cells.

4.5 Filter sets

- Fura-2 filter set (Till photonics, Germany)

Exciter filter	None
Dichroic mirror	DCLP410
Emission	LP470

Where, DC and LP are abbreviations used by the manufacturer for dichroic and long pass filters respectively.

- Fura-2/Rhodamine filter set (AHF analysen technik, Germany)

Exciter filter	None
Dichroic mirror	Dual band pass
Emission filter	Dual band pass

4.6 Antibodies

- Anti-VSV mouse antibody was purchased from Sigma, Germany.
- Anti-GSK-3β and Anti-GSK-3β (pY216) phospho specific mouse antibody was purchased from BD transduction laboratories, Germany.
- Anti-β-actin rabbit antibody was purchased from Santa Cruz Biotechnology INC., USA.
- Anti-Tim44 was courteously provided by Andreas Reichert (Adolf-Butenandt institut für physiologische chemie, Munich)
- Alkaline phosphatase conjugated anti-immunoglobulin mouse/rabbit antibody was purchased from DakoCytomation, Denmark.

4.7 Commercial kits

Ca^{2+} calibration buffer kit	Molecular probes, Germany.
Bioluminiscent somatic cell assay kit	Sigma, Germany.
DNeasy tissue kit	Qiagen, Germany.
Plasmid midi kit	Qiagen, Germany.
Effectene transfection kit	Qiagen, Germany.

4.8 Buffers

All buffers were prepared in deionized water.

4.8.1 Buffers for Ca^{2+} imaging

HBSS buffer

NaCl	145 mM
KCl	2.5 mM
$MgCl_2$	1 mM
HEPES	20 mM
Glucose	10 mM
$CaCl_2$	1.8 mM

pH was set to 7.2 before use.

HBSS buffer (Ca^{2+} free)

NaCl	145 mM
KCl	2.5 mM
$MgCl_2$	1 mM
HEPES	20 mM
Glucose	10 mM
EGTA	50 µM

pH was set to 7.2 before use.

Fura-2/AM and rhodamine-123 loading buffer

HBSS buffer	
Pluronic acid	0.08%
BSA	1% w/v

4.8.2 Buffers for crude mitochondrial extraction

Resuspension buffer (RSB buffer)

Tris-HCl (pH 7.5)	10 mM
EDTA	5 mM
$CaCl_2$	1.5 mM

Mannitol-Saccharose buffer (MS buffer)

Tris-HCl (pH 7.5)	10 mM
EDTA	5 mM
Mannitol	420 mM
Saccharose	140 mM

4.8.3 Buffers for western blotting

Lysis buffer

SDS	0.1% (w/v)
NP40	1% (v/v)
Deoxycholate	0.5% (w/v)
Tris (pH 8.0)	10 mM
NaCl	150 mM

Tricine-SDS running buffer

Tris-base	100 mM
Tricine	100 mM
SDS	0.1% (w/v)

pH was set to 7.3.

I–block

PBS	1 tablet per 1000 ml
I-block powder	0.2% (w/v)
Tween-20	0.1% (v/v)

Heated at 60^{o}C for 1 hour.

Blotting buffer

Tris-HCl (pH 7.4)	25 mM
Glycine	200 mM
SDS	0.1%
Methanol	20%

Laemmli buffer

EDTA (pH 8.0)	25 mM
SDS	7.5% (w/v)
Glycerin	50% (v/v)

Bromophenol blue	2.5% (w/v)
β-mercaptoethanol	7.5% (v/v)
Urea	4 M

TBS-Tween buffer

Tris-HCl	50 mM
Tween-20	0.1%
NaCl	100 mM

pH was set to 7.4.

Alkaline phosphatase buffer

Tris (pH 9.5)	100 mM
NaCl	100 mM
$MgCl_2$	5 mM

4.8.4 Buffer for agarose gel electrophoresis

TAE buffer

Tris-HCl (pH 8.2)	40 mM
Acetic acid	20 mM
EDTA (pH 7.6)	2 mM

4.8.5 Growth medium for bacterial cultures

Lurea-bertani medium (LB medium)

Trypton	1%
Yeast extract	0.5%
NaCl	1%

pH was set to 7.2.

Lurea-bertani agar plates

Lurea broth medium	
Agar	1.5%

4.9 Equipments

Centrifuge	5415 R, 5804 R, 5810 R Eppendorf, Germany.
Microplate reader (Luminometer)	BMG Labtech, Germany.
Gene pulser II (Electroporator)	Biorad, Germany.
Electroporation tubes (0.4 cm)	Gene pulser cuvette, Biorad, Germany.
Biophotometer	Eppendorf, Germany.
Vertical electrophoresis system	Invitrogen, Germany.
Horizontal electrophoresis system	Peqlab, Germany.
Blotting apparatus	Hoefer semiphor, Amersham pharmacia biotech., Germany.
pH meter	Heidolph instruments, Germany.
Incubators	Kendro, Germany.
PCR cycler	Eppendorf, Germany.
UV transilluminator	Vilber Lourmat, France.
Thermomixer	Eppendorf, Germany.
Water bath	GFL, England.
Pipetteman	Eppendorf, Germany.

4.10 Chemicals

Table 1: List of chemicals

No.	Chemical	Company
1.	10-20% tricine-SDS gels	Invitrogen, Germany
2.	Agar	Becton Dickinson, Germany
3.	Agarose	Peqlab, Germany
4.	Ampicillin	Roth, Germany
5.	BCIP	Roche, Germany
6.	Bovine serum albumin	Sigma, Germany
7.	Cyclopiazonic acid	Calbiochem, Germany
8.	Dimethyl malate	Sigma, Germany
9.	Dimethyl succinate	Sigma, Germany
10.	DMEM	PAN, Germany
11.	DPBS	PAN, Germany
12.	DTT	Roche, Germany
13.	Ethidium bromide	Sigma, Germany
14.	FCCP	Sigma, Germany
15.	FBS	PAA, Germany
16.	Fungizone	Gibco, Germany
17.	Fura-2/AM	Molecular probes, Germany
18.	G418	Sigma, Germany
19.	Gel loading solution	Sigma, Germany
20.	Gentamicin	Invitrogen, Germany
21.	Glutamax	Invitrogen, Germany
22.	Glycine	Sigma, Germany
23.	HBSS	Invitrogen, Germany
24.	HEPES	Sigma, Germany
25.	I-block	Tropix, Germany
26.	Methyl pyruvate	Sigma, Germany

27.	MITO	BD biosciences, Germany
28.	N2 supplement	Invitrogen, Germany
29.	NBT	Roche, Germany
30.	Oligomycin	Sigma, Germany
31.	PBS tablets	VWR, Germany
32.	Penicillin-streptomycin	Invitrogen, Germany
33.	Pluronic acid	Sigma, Germany
34.	Poly-d-lysine	Serva, Germany
35.	Rhodamine-123	Molecular probes, Germany
36.	See blue protein marker	Invitrogen, Germany
37.	SOC-medium	Peqlab, Germany
38.	Sodium dodecyl sulphate	Sigma, Germany
39.	Sodium-L-ascorbate	Sigma, Germany
40.	TMPD	Sigma, Germany
41.	Trypsin-EDTA	Invitrogen, Germany
42.	Trypton	Becton Dickinson, Germany
43.	Yeast extract	Becton Dickinson, Germany
44.	Zeocin	Invitrogen, Germany
45.	γ-IV	Calbiochem, Germany

Other general chemicals which are not mentioned in the table above were purchased from:

- Merck, Germany
- Sigma, Germany

4.11 Other materials

Plastic and related articles were purchased from:

- Nunc, Germany
- VWR, Germany
- Peqlab, Germany
- Abimed, Germany

4.12 Softwares

- Till vision 4.0 (Till photonics, Germany) was used for Ca^{2+} imaging.
- Fluostar optima (BMG Labtech, Germany) was used for luminescence.
- Sigma plot 7.0 (Systat software Inc., USA) was used for calculating area under the curve.
- Sigma stat 2.03 (Systat software Inc., USA) was used for statistical analysis.
- Reference manager 10 (ISI Research soft., USA) was used for generating the literature list.

5 Methods

5.1 Cell culture

HEK293 cell lines were cultured in DMEM supplemented with 10% foetal bovine serum (FBS), 1% penicillin/streptomycin (pen./strep.) and 1% Glutamax at 37^{o}C in 10% CO_2 atmosphere.

APPsw cells were cultured in DMEM supplemented with the selection antibiotic, G418 (0.2 mg/ml).

wtAPP cells were cultured in DMEM supplemented with the selection antibiotic, G418 (0.2 mg/ml).

APPsw/PSD385N cells were cultured in DMEM supplemented with the selection antibiotic G418 (0.2 mg/ml) and zeocin (0.2 mg/ml).

APPsw/IDE cells were cultured in DMEM supplemented with the selection antibiotic G418 (0.2 mg/ml) and zeocin (0.2 mg/ml).

H4 cells were cultured in DMEM supplemented with 10% FBS and 1% pen./strep. These cells express an inducible allele of AICD fragment with a C-terminal VSV-tag under the control of the “Tet-Off” system. The expression of AICD-VSV was turned off using doxycycline (100 ng/ml) in the growth medium.

5.2 Preparation of primary culture of mouse astrocytes

Primary cultures of astrocytes were prepared from homozygous *App* knockout mice (*App*$^{0/0}$) on a C57xSv129 background (Muller et al., 1994). C57xSv129 wild type mice were used as a control. Astrocytes were prepared from cortical hemisphere of new born (1-2 days old) mice. The brain was dissected out in HBSS medium supplemented with 0.25 µg/ml of fungizone, 50 µg/ml of gentamicin and 1% pen/strep. The meninges and both the hippocampi were removed. The cortical hemispheres were separated out and transferred into the mixture of HBSS and 20% trypsin for 5 min. Subsequently, prewarmed DMEM was added and centrifuged at 200 x g. The pellet was resuspended in DMEM and transferred to the culture flask. The cultures were maintained in DMEM supplemented with 5% FCS, 1% pen./strep., 1% N_2 supplement and 0.2% MITO at 37°C for nearly one week. After about 1 week, when astrocytes have reached 90-95% confluency, the flask was placed overnight on a laboratory shaker at fairly high agitation (agitation causes many of the process bearing cells like neurons to be shaken away) at 37°C. The medium was exchanged with fresh DMEM.

5.3 Freezing of mammalian cells

Cells were grown to 90-95% confluency in 100 mm petridishes, washed with warm PBS and trypsinized. Trypsinized cells were collected in falcon tubes and pelleted down at 700 x g for 5 min. The pellet was resuspended in FBS with 10% DMSO to a final volume of 1 ml per plate. Aliquots were transferred to cryovials and were stored in freezing containers at -70°C. The cryovials were later transferred to liquid nitrogen for long term storage.

5.4 Thawing of mammalian cells

Frozen cryovials were transferred in water bath at 37°C for rapid thawing. The contents of the cryovials were transferred to 10 ml growth medium and centrifuged at 100 x g for 3 min. The media was removed and the pellet was washed similarly two times to remove DMSO. Finally, the pellet was resuspended in suitable growth medium, transferred to culture flasks and grown under requisite culture conditions.

5.5 DNA isolation from rodent tails

Tail of about 6 mm was cut from the mouse into a microcentrifuge tube. DNA isolation was done using DNeasy tissue kit according to the manufacturer's protocol. Briefly, this procedure involves steps in which samples were lysed using proteinaseK and the lysate was loaded onto a DNeasy spin column. During centrifugation, DNA was selectively bound to the DNeasy membrane and contaminants were washed through. The DNA was eluted in TE buffer later on.

5.6 Genotyping

App$^{0/0}$ mice were genotyped routinely using DNA extracted from tail biopsies. The primers used are mentioned below:

Primers:

Primer	**Sequence**
App$^{0/0}$ 1	5‘ CGA GAT CAG CCT CTG TTC CAC A 3‘
App$^{0/0}$ 2	5‘ ATC ACC TGG TTC TAA TCA GAG GCC C 3‘
App$^{0/0}$ 3	5‘ GAG ACG AGG ACG CTC AGT CCT AGG G 3‘

App$^{0/0}$ 1 and App$^{0/0}$ 2 primers were used for analyzing wild type allele and App$^{0/0}$ 2 and App$^{0/0}$ 3 primers were used for amplifying knockout allele using the following PCR conditions.

For a 50 µl reaction volume, the following components were pipetted into a PCR tube:

Reaction mixture:

	For 1 sample
Mastermix (purchased from Eppendorf)	25 µl
Primer 1 (25 pmol)	0.5 µl
Primer 2 (25 pmol)	0.5 µl
Water	22 µl
DNA	2 µl

PCR programme:

96ºC	2 min	
94ºC	1 min	35 X
60ºC	1 min	
72ºC	1 min	
72ºC	10 min	

The PCR product was analyzed using agarose gel electrophoresis.

5.7 Agarose gel electrophoresis

The agarose gel was prepared by dissolving an appropriate amount of agarose (usually 1% final concentration) in 1X TAE buffer and ethidium bromide (1 µg/ml). The mixture was cooked and poured into precast agarose gel chambers. The DNA was mixed with the loading buffer (1:5) and loaded into spurs on the gel. The DNA was separated electrophoretically at 100 volts using 1X TAE as a running buffer. Finally, the DNA was visualized on a UV transilluminator.

5.8 Ca^{2+} Imaging

Real time measurements for intracellular Ca^{2+} concentration were done using Ca^{2+} indicator fura-2/AM (Fig 5.1).

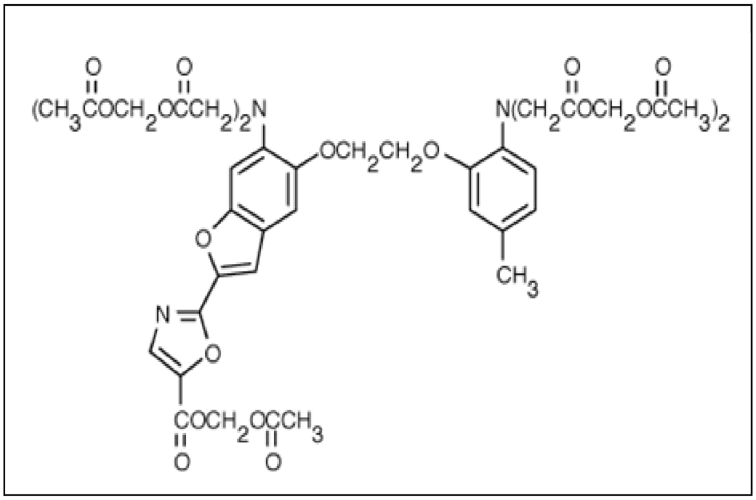

Fig. 5.1: Structure of Ca^{2+} indicator Fura-2 ($C_{44}H_{47}N_3O_{24}$). Its molecular weight is 1001.86

Fura-2 can be used to measure intracellular Ca^{2+} concentration changes for two reasons: First, it has an affinity to bind Ca^{2+} ions in a reversible manner. Secondly, the spectroscopic properties of fura-2.Ca^{2+} complex differ from that of the free fura-2. The fluorescence excitation maximum of fura-2 shifts to a lower wavelength on Ca^{2+} binding with negligible shift in the emission maximum. This allows fura-2 to be utilized as a dual excitation indicator. For optimal separation of fluorescence due to the two forms of the indicator, Ca^{2+} free fura-2 is usually monitored at 380 nm and Ca^{2+} bound dye at 340 nm. At an excitation wavelength of 340 nm, an increase in fluorescence emission indicates an increase in free intracellular Ca^{2+} concentration which can also be measured at an excitation wavelength of 380 nm as a decrease in fluorescence emission. Fura-2 has an iso-fluorescence point at 360 nm which is useful for monitoring Ca^{2+} independent fluorescence or for following quenching by heavy metal ions (Fig. 5.2).

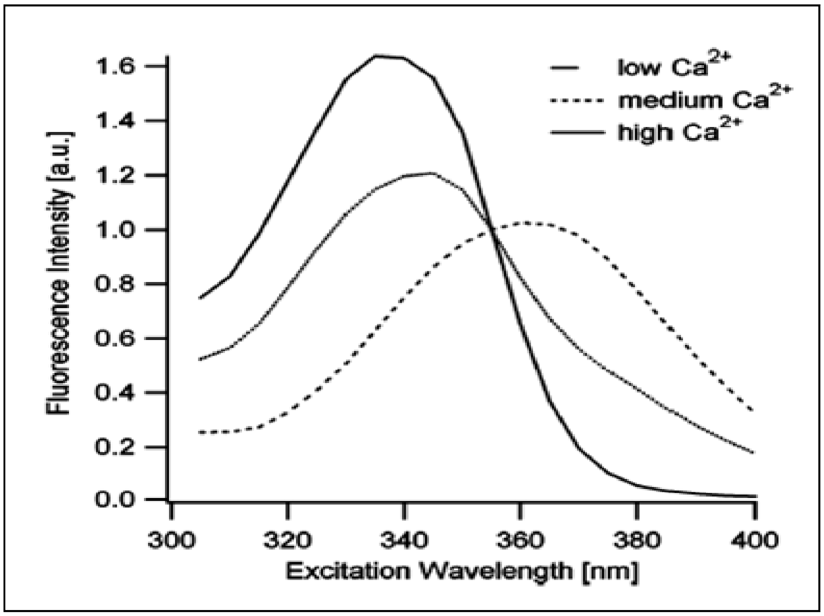

Fig. 5.2: Excitation spectra of Fura-2 solutions with different Ca^{2+} concentration are shown.

Fura-2 is used as an acetoxymethyl (AM) ester form to achieve penetration through the lipophilic cell membrane and AM form is then readily activated by cellular esterases. Cells were viewed by upright epifluorescence microscope using 20X water immersion objective (Fig 5.3).

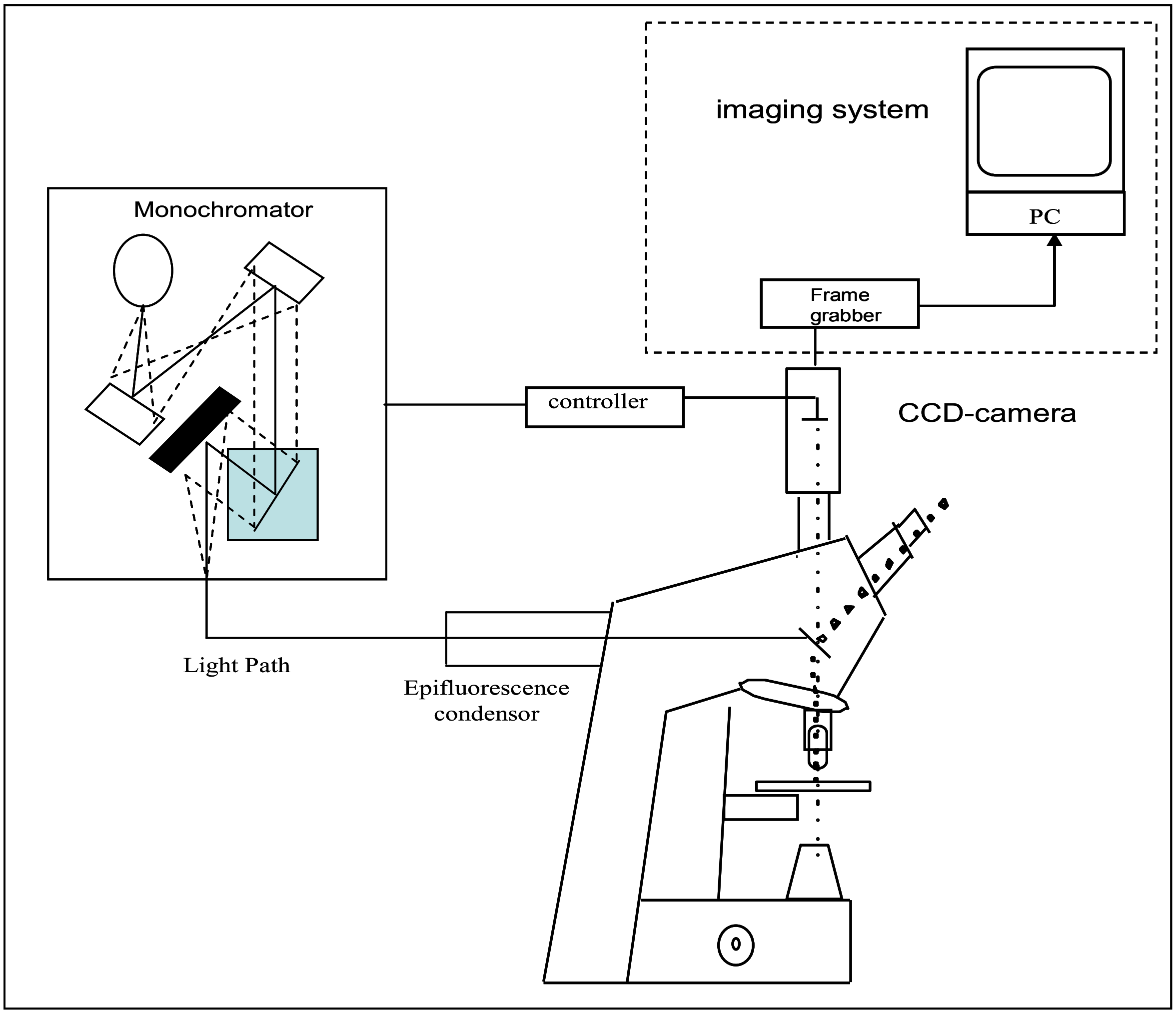
imaging system
PC
Monochromator
Frame grabber
controller
CCD-camera
Light Path
Epifluorescence condensor

Fig. 5.3: Schematic representation of imaging system. The monochromator sets the wavelength sent by the computer via imaging system controller. The monochromatic light is linked to the microscope via a specially designed epifluorescence condenser. The fluorescence image is detected by a CCD camera. The frame grabber is the interface between the imaging computer and the CCD camera. It grabs the digitized images from the camera at 12.5 MHz (12.5 million pixels per second). The digitized images are then displayed by the computer as pseudocolor images.

Microscope designed for epifluoroscence allows measurements of fluorescence from a region of cells selected specifically by the operator. The microscope contains the optical components necessary to deliver the excitation beam to the sample, isolate the fluorescence emission signal, and focus it as an image at the detector.

Excitation of the cells was performed at 340 nm and 380 nm and the ratio of the emissions was obtained using digital imaging system. Digital fluorescence images were acquired and displayed as pseudocolor images and subsequently analyzed by choosing defined region of interest so as to exclude any area not covered by a cell. Values were acquired at 3 sec intervals at both excitation wavelengths (340 and 380 nm). Ca^{2+} concentration were calculated from fluorescence intensities ratio using the following equation (Grynkiewicz et al., 1985):

$$[Ca^{2+}] = K_d \, [(R - R_{min}) / (R_{max} - R)] \, {*}\beta$$

Where, R is the ratio of emission intensity, exciting at 340 nm to emission intensity exciting at 380 nm; R_{min} is the ratio at zero free Ca^{2+}; R_{max} is the ratio at saturating Ca^{2+}; β is the ratio of fluorescence intensity exciting at 380 nm for zero free Ca^{2+} to fluorescence intensity exciting at 380 nm at saturating Ca^{2+}. K_d of an indicator or chelator is defined as the concentration at which it reaches the half saturation point. The dissociation constant (K_d) of Fura-2 is 224 nm. Values for R_{min} and R_{max} were computed using Ca^{2+} calibration buffer kit.

Cell loading with Fura-2/AM:

Fura-2/AM was dissolved in HBSS buffer to 5 µM final concentration containing 1% BSA to improve solublization of the ester form of the dye and pluronic acid (0.08%) to serve as an additional dispersion aid. Cells were grown on glass coverslips, precoated with poly-d-lysine (PDL, 1:5). Cells on coverslips were then loaded with fura-2 at 37°C for 30 min and then washed 2-3 times with normal HBSS buffer before starting the measurements.

5.9 *In vitro* Ca^{2+} calibration

Solutions of free Ca^{2+} concentrations 0 µM and 39 µM were used for calculating R_{min} and R_{max}. These solutions contain 50 µM Ca^{2+} indicator fura-2. In addition the solutions contain 15 µm diameter polystyrene beads in suspension at 16,000 beads per ml. These beads serve as focusing aid. A third buffer which do not contain fura-2 was used as a control to calculate background fluorescence. A 5 µl of each solution was pipetted on a clean dry microscope slide. The droplet was then covered with 18 x 18 mm coverslips. Using transmitted light polystyrene beads in the field of view was focused up and down through until the largest diameter was found. After focusing in this plane, the slide was moved on the stage to find a field of view without beads visible. A defined area was then selected to acquire fluorescence data excited at 340 nm and 380 nm, measuring emission at 510 nm. The average of three determinations was made. The emission intensity for background fluorescence was corrected by substracting the fluorescence value of control buffer (lacking fura-2) obtained at 340 nm excitation from each 340 nm excitation value and fluorescence value obtained with 380 nm excitation from each 380 nm excitation value. R_{min} is the ratio of the emission intensity obtained at 340 nm excitation and 380 nm excitation at 0 µM Ca^{2+}. R_{max} is the ratio of the emission intensity obtained at 340 nm excitation and 380 nm excitation at 39 µM Ca^{2+} (saturating Ca^{2+}).

5.10 Analysis of mitochondrial membrane potential

Rhodamine-123 was used to monitor the membrane potential of mitochondria. The lipohilic nature of rhodamine-123 allows it to diffuse through the mitochondrial membrane and accumulate in the mitochondrial matrix in response to the electrical gradient. The higher the membrane potential, more is the rhodamine-123 taken up into the matrix. Respiring mitochondria generate a proton gradient across the inner membrane and this proton gradient was assessed by monitoring fluorescence quenching of rhodamine-123. The membrane potential can be completely depolarized by an uncoupler like FCCP (carbonyl cyanide 4-trifluoro-methoxyphenylhydrazone), that dissipates the potential across the mitochondrial membrane, consequently releasing rhodamine-123 producing maximum fluorescence.

Cells cultured on coverslips, were analyzed for mitochondrial membrane potential using the similar microscope and software as described above. Cells were loaded with rhodamine-123 at a final concentration of 10 µM in HBSS buffer (supplemented with 1% BSA and 0.08% pluronic acid) for 20 min at 37°C, and then washed once with normal HBSS buffer. For measurements, cells were excited at 470 nm and fluorescence data was acquired at 3 sec intervals. At the end of each experiment, mitochondrial membrane potential was completely depolarized by FCCP (2 µM) to attain maximal fluorescence. The data presented here was normalized to the maximal increase in rhodamine-123 signal in response to complete mitochondrial depolarization by FCCP.

5.11 Bioluminescent ATP assay

ATP was determined luminometrically using ATP bioluminescent somatic cell assay kit (Sigma-Aldrich, Germany) according to manufacturer's protocol. This kit is based on the luminometric method employing the luciferin-luciferase reaction. This reaction involves the ATP dependent oxidation of luciferin catalyzed by firefly luciferase yielding oxyluciferin, AMP, CO_2, and pyrophosphate (PPi) as products. This is accompanied by emission of light which is linearly related to ATP concentration and is measured using luminometer. ATP content was measured using internal standards.

5.12 Isolation of mitochondria from cultured cells

The method for isolation of mitochondria is based on slight modification to the method described previously (Schneider et al., 1948). Cells were washed once with PBS, trypsinized and pelleted down at 700 x g for 12 min at 4°C. The cell pellet was resuspended in 700 µl of RSB buffer and incubated on ice for 10 min. The cells were then homogenized on ice in glass teflon homogenizer using

20 strokes. This was followed by addition of 700 µl of MS buffer ① and the homogenized cells were pelleted down at 700 x g for 12 min at 4°C. This centrifugation step was repeated twice. The pellet contains broken cell membranes and nuclei (nuclear pellet). Subsequently, the supernatant (post-nuclear supernatant) was centrifuged at 16,500 x g for 12 min at 4°C. The pellet obtained is the crude mitochondrial fraction ② (mitochondrial pellet) and the supernatant is the post-mitochondrial supernatant. The mitochondrial pellet was finally resuspended in 100 µl mixture of RSB and MS buffer (1:1). The nuclear pellet, mitochondrial pellet, post-nuclear supernatant and post-mitochondrial supernatant were frozen at -80 °C for western blot analysis.

5.13 Bradford method of protein estimation

Bradford method is a commonly used method for protein estimation (Bradford, 1976). The method is based on the principle that the absorption maxima of an acidic solution of commasive brilliant blue G-250 shifts from 465 nm to 595 nm when binding to protein occurs with a concomitant color change from brown to blue.

Serial dilutions of IgG ③ (standard) were prepared starting from 4 µg/µl to 0.5 µg/µl and 10 µl of samples of unknown protein concentration were taken in separate polystyrene cuvettes. 1 ml of bradford reagent was added to both samples and standards, mixed well and incubated for 5 min at room temperature. The absorbance was taken in spectrophotometer set at 595 nm. Absorbance of 1 ml bradford reagent without protein was used as a blank and was substracted from the absorbance values of both samples and standards. A standard curve

---

① Instead of isotonic sucrose used in the original method, the buffer used consists of mannitol and saccharose as described earlier (Bogenhagen and Clayton, 1974).

② The crude mitochondrial fraction also consists of ER membranes and golgi membranes. Purification of mitochondria, if necessary, can be carried out using discontinuous gradients (Magalhaes et al., 1998)

③ Linear working range of IgG is 125 – 1.5 µg/ml.

was later prepared by plotting the blank corrected absorbance values of standards vs. its concentration in µg/µl. This standard curve was used to determine the protein concentration of each unknown sample.

5.14 Western Blotting

Cells were cultured to about 80-90% confluency, washed with cold PBS and lysed with RIPA lysis buffer. Viscous lysate was sonicated and then mixed with laemmli buffer followed by heating at 95°C for 10 min. Samples were then loaded on 10-20 % tricine-SDS gels and were allowed to separate at a constant voltage of 100 volts. Following this, proteins were electrophoretically transferred to a PVDF membrane. The membrane was washed in blocking solution (I-block or TBS tween buffer) for 30 minutes on a shaker. Subsequently, the membrane was incubated with the primary antibody (diluted in I-block or TBS tween buffer) directed against the protein of interest overnight at 4°C, following which the blot was washed with I-block buffer three times for 15 min each. The other set of same samples were incubated with β-actin, diluted 1:2000, as a control protein. The secondary antibody conjugated with alkaline phosphatase was then added at 1:5000 dilution and incubated for 1 hour. After the incubation, membrane was washed with I-block and developed using the BCIP/NBT④ substrate in alkaline phosphatase buffer.

5.15 Preparation of electrocompetent cells

Bacterial strain, DH5α was inoculated in 5 ml Lurea Bertani (LB) medium (preinoculum) and grown overnight at 37°C under constant shaking. 250 ml LB medium was inoculated with 75 µl of the preinoculum and grown under constant

---

④ The working principle of this method is that alkaline phosphatase cleaves the phosphatase group from BCIP to produce precipitating indoxyl group. This group then dimerizes resulting in the reduction of the NBT to produce a dark blue insoluble formazan product.

shaking at 37°C until the O.D reaches between 0.6-0.8 at 560 nm. Subsequently, the flasks were kept on ice for 15-30 min. The culture was then centrifuged at 4900 rpm (rotor JLA 10500) at 4°C for 15 min. The pellet was resuspended in 250 ml of autoclaved cold distilled water and centrifuged at 4900 rpm (rotor JLA 10500) at 4°C for 15 min. This step of resuspension in water and centrifugation was repeated twice in order to wash the cells. The pellet was resuspended in 10 ml of 10% glycerol and centrifuged again at 4900 rpm (rotor JLA 10500) at 4°C for 15 min. The supernatant was discarded and the pellet was finally resuspended in 2-3 ml of 10% glycerol. Aliquots were directly frozen in liquid nitrogen and later stored at -80°C.

5.16 Electrotransformation

Electrotransformation is a method of transferring DNA into the bacterial or yeast strain by applying high voltage electric field pulses of short duration (Dower et al., 1988). The electric field pulses create temporary pores in the membrane of the cells. These pores are large enough to allow DNA to diffuse into the cells. Upon removal of the electric field these pores reseal and the DNA is free to replicate and transcribe within the cell.

The DH5α electrocompetent cells were thawed on ice. A mixture of 80 µl of electrocompetent cells and 5 ng of plasmid was transferred to a precooled sterile electroporation tube and was then incubated on ice for 20 min. The electroporation tube was placed in the electroporator shock pod and a pulse was given for few seconds with resistance of 200 ohm, capacitance of 25 µF and voltage of 1.6 kV. Following this, 500 µl of SOC medium⑤ was added to it and carefully pipetted up and down. The mixture was incubated for 1-2 hrs at 37°C. Subsequently, the mixture was centrifuged at 800 x g for 3 min at room temperature. The pellet was resuspended in 50 µl of LB medium and was

---

⑤ During electrotransformation, electrolysis of the medium drastically affects the pH which might lead to death of many cells if fresh medium is not immediately added for recovery. SOC medium works as a recovery medium for bacterial cells.

spreaded on LB-agar plates with ampicillin (100 µg/ml) as a selection antibiotic. The plates were then incubated overnight at 37^{o}C.

5.17 Plasmid isolation (Midi prep)

A single colony was picked from the LB-agar plate and inoculated in 2.5 ml of LB medium (starter culture) containing the selective antibiotic (ampicillin). The culture was incubated for nearly 8 hrs at 37^{o}C with vigorous shaking. The starter culture was diluted to 1:500 and 25 ml of selective LB medium was inoculated. The culture was grown at 37^{o}C for 12-16 hrs with vigorous shaking. The bacterial pellet was harvested at 6000 x g for 15 min at 4^{o}C. The plasmid isolation was then carried out using Qiagen plasmid midi kit according to the manufacturer's protocol. The working principle of this kit is based on the modified alkaline lysis procedure of plasmid isolation (Birnboim and Doly, 1979). The DNA concentration was determined photometrically at 260 nm using spectrophotometer.

5.18 Transient transfection

Transient transfection in HEK293 cells was carried out using Qiagen effectene transfection reagent. The working principle of this method is that the DNA is condensed by enhancer in a defined buffer system. The subsequent addition of effectene reagent spontaneously forms micelles around the condensed DNA. Such micelles effectively transfer DNA into the eukaryotic cells.

Cells were seeded at density of $2x10^{5}$ per well in 12 well plate, a day before transfection. On the day of transfection, 0.3 µg of DNA was diluted with buffer EC (condensation buffer) to a total volume of 75 µl. Subsequently, 2.4 µl of enhancer was added, mixed and incubated for 5 min at room temperature. 6 µl of effectene transfection reagent was then added to DNA-enhancer mixture and incubated for 10 min at room temperature. Cells were washed with PBS and fresh medium was added. Following this, 400 µl of growth medium mixed with transfection complex was immediately added onto the cells. The cells were then incubated under normal growth conditions for 48 hrs before analysis.

5.19 Statistical analysis

Data analysis was performed offline using Microsoft excel 2003. Area under curve was calculated using Sigma Plot.7. All results were expressed as mean ± SEM. Statistical data was assessed by the unpaired student's t-test using sigma stat 2.03 program. Values less than 0.001 were considered as highly significant and values less than 0.05 were considered as significant values.

6 Results

Several studies that have been done till date indicate a link between pathogenic mutation in the *APP* gene and deregulation of Ca^{2+} homeostasis in AD. To identify the cleavage product of APP that is involved in regulating Ca^{2+} homeostasis, basal cytosolic Ca^{2+} levels and ER Ca^{2+} content was studied by Ca^{2+} imaging experiments.

6.1 An enhanced cytosolic concentration of Ca^{2+} was observed in cells lacking APP or its C-terminal cleavage products.

To elucidate the effect of APP or its cleavage product on basal (or resting) cytosolic Ca^{2+} levels, these levels were analyzed in untransfected wild type HEK293 cells (Wt), in HEK293 cells that overexpress *APP* with Swedish mutation ⑥ (APPsw) and in HEK293 cells that overexpress wild type *APP* (wtAPP). These cell lines were studied as a model to study effect of cleavage products of APP on Ca^{2+} homeostasis. In addition, similar studies were also done in HEK293 cells that co-express *APPsw* and a dominant negative D385N ⑦ mutation in *PS1* (PSD385N) or in HEK293 cells that co-express *APPsw* and the gene encoding the insulin degrading enzyme ⑧(IDE). These two cell lines (PSD385N and *IDE* expressing) served as a model to study the effect of loss of γ-secretase cleavage products of APP on Ca^{2+} homeostasis. In addition to it, APPsw cells were also studied after treatment with the γ-secretase inhibitor, γ-IV⑨.

Fig. 6.1 shows mean values of Ca^{2+} measurements by ratiometric imaging using fura-2/AM in HEK293 cells. The basal (or resting) cytosolic Ca^{2+} was calculated in the presence of 1.8 mM (physiological Ca^{2+} concentration) extracellular Ca^{2+}

---

⑥ This mutation dramatically increases β-secretase activity and Aβ42 production (for details see page 17).

⑦ This mutation abolishes γ-secretase activity and therefore has no γ-secretase cleavage products of APP.

⑧ This enzyme efficiently degrades cytoplasmic AICD.

⑨ This is a peptide aldehyde inhibitor that has been shown to potently inhibit γ-secretase cleavage of β-CTF in HEK293 cells expressing APPsw (Sinha and Lieberburg, 1999) from the fluorescence ratio (340/380 nm) of the first 10 cycles (30 sec) (refer fig. 6.6).

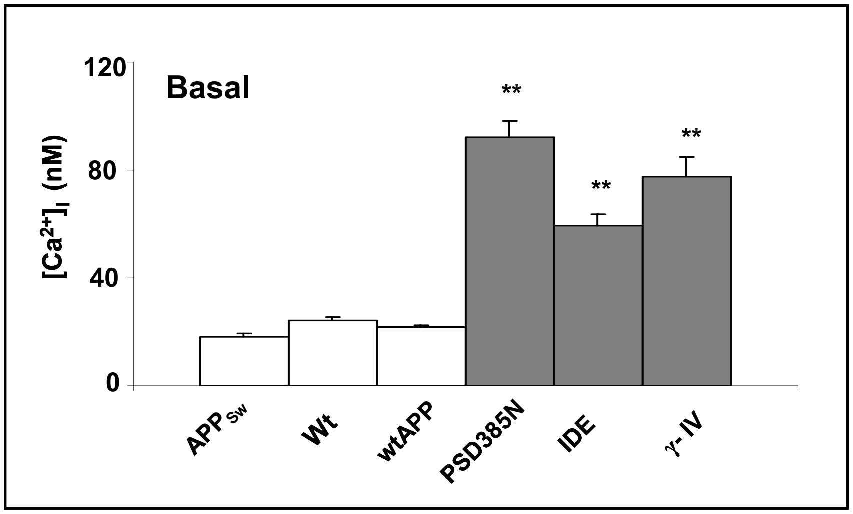

Fig. 6.1: Data represented here shows the mean of basal (or resting) cytoplasmic Ca^{2+} measured by fluorescence ratio imaging with fura-2/AM in different stably transfected HEK293 cell lines. Cells were loaded with 5 µM fura-2/AM for 30 min at 37°C. Ca^{2+} ion concentration in individual cell was calculated from the 340/380 nm ratio obtained using digital imaging system (for details see material and methods). Bars shown in white represents mean values obtained in HEK293 cells expressing *APPsw* (APPsw), untransfected HEK293 cells (Wt) and HEK293 cells expressing wild type *APP* (wtAPP). Bars shown in grey represents mean values obtained in HEK293 cells co-expressing APPsw and PS1 mutation with a D385N mutation (PSD385N), HEK293 cells co-expressing APPsw and the insulin degrading enzyme gene (IDE) and APPsw cells treated with γ-secretase inhibitor, γ-IV (10 µM for 24 hours). The statistical significance in PSD385N cells, IDE cells or γ-IV treated APPsw cells was determined compared to APPsw cells. The figure depicts that basal (or resting) cytosolic Ca^{2+} level is enhanced as a result of loss of APP C-terminal fragments in HEK293 cells. The data represented here is mean ± SEM for 4 to 6 independent experiments. Number of cells selected for each experiment range between 50 to 80 cells. Statistical significance **, $p < 0.001$.

Resting cytosolic Ca^{2+} levels in wild type HEK293 cells (Wt), *APPsw* cells or *wtAPP* cells exhibited non-significant differences and showed on an average a free cytosolic Ca^{2+} of around 20 nM (Fig. 6.1). On the other hand, PSD385N cells exhibited more than four times higher resting cytoplasmic Ca^{2+} values i.e. 92 ± 6 nM. Similar observations were obtained in *IDE* cells (60 ± 4 nM). Moreover, HEK293 cells that express *APPsw* when treated with a potent γ-secretase inhibitor, γ-IV (10 µM for 24 hours), also showed an enhanced cytosolic Ca^{2+} levels i.e. 77± 7 nM (Fig. 6.1).

In order to prove that the enhanced cytosolic Ca^{2+} levels observed in PSD385N or IDE cells were indeed due to an alteration in production of APP cleavage products and not due to other γ-secretase cleavage products, for instance Notch, similar measurements were performed in primary cultures of 1-2 days old *App* knockout mouse astrocytes ($App^{0/0}$) as compared to wild type C57xSv129 astrocytes (Wt). The mice were routinely genotyped for $App^{0/0}$ gene before measurements. The amplified fragment obtained was around 430 base pairs for $App^{0/0}$ and around 650 base pairs for Wt (Fig. 6.2).

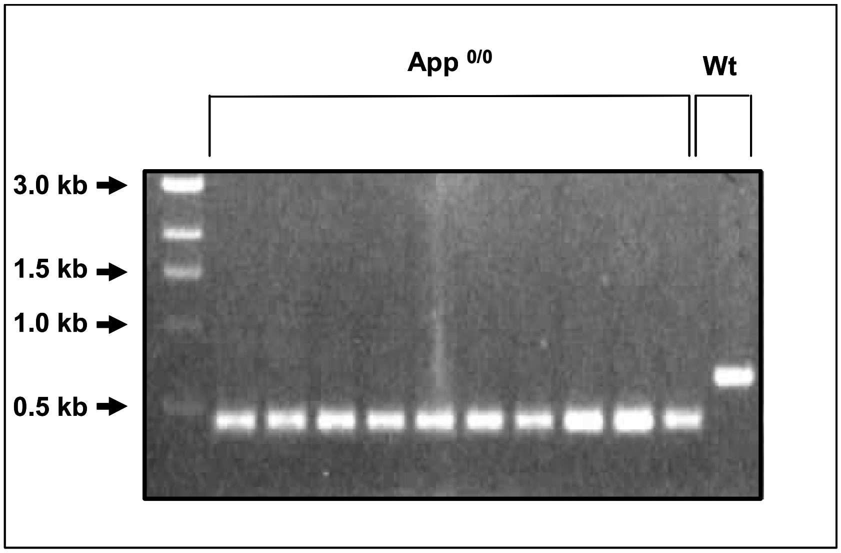

Fig. 6.2: PCR showing the amplified fragments of *App* knockout ($App^{0/0}$) and C57xSv129 mice (Wt). The amplified PCR products were separated by 1% agarose gel electrophoresis and was obtained about 430 bp for $App^{0/0}$ and about 650 bp for Wt mice.

A significantly enhanced resting Ca^{2+} levels in $App^{0/0}$ astrocytes (50 ± 7 nM) as compared to Wt astrocytes (30 ± 1 nM) was obtained (Fig. 6.3). Furthermore, to evaluate the role of other γ-secretase cleavage products produced for example by the two other members of the APP protein family, namely, the amyloid precursor like protein 1 and 2 (APLP1 and APLP2), additional experiments were performed in the presence of a γ-secretase inhibitor, DAPT⑩. Treatment of $App^{0/0}$

---

⑩ DAPT is known to acutely lower Aβ and AICD levels (Dovey et al., 2001).

astrocytes with γ-secretase inhibitor further enhanced the cytosolic Ca^{2+} to 74 ± 7 nM (Fig. 6.3). This experiment indicated that AICD might be the causal cleavage product of APP that modulates resting cytosolic Ca^{2+} levels.

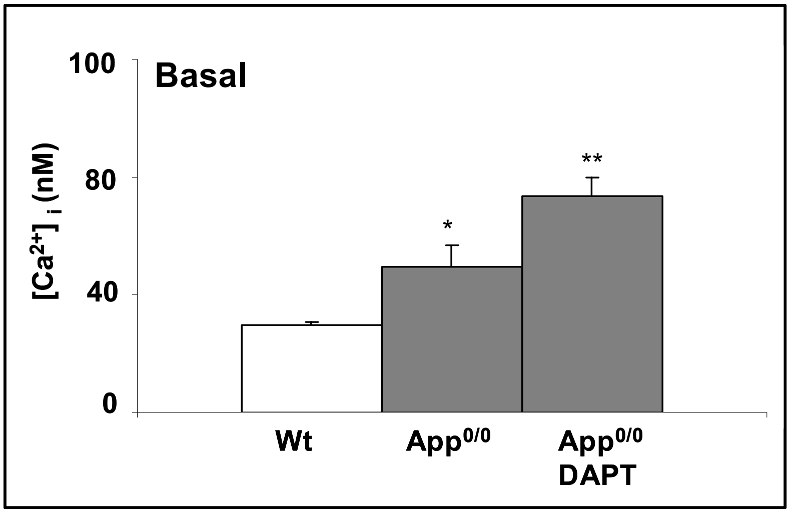

Fig. 6.3: Data represented here shows basal cytosolic Ca^{2+} measured by fluorescence ratio imaging in fura-2/AM loaded mouse astrocytes. Cytosolic Ca^{2+} values were calculated from 340/380 nm ratio obtained during the measurements. Bar shown in white represents mean values of basal Ca^{2+} in wild type C57xSv129 astrocytes (Wt). Bars shown in grey show mean values of basal Ca^{2+} in *App* knockout astrocytes (*$App^{0/0}$*) and *$App^{0/0}$* astrocytes treated with γ-secretase inhibitor, DAPT (1µM for 24 hours). *$App^{0/0}$* astrocytes were treated with DAPT in order to exclude the effect of AICD produced by APLP1 and APLP2 cleavage. The statistical significance in *$App^{0/0}$* and *$App^{0/0}$* treated with DAPT was determined compared to Wt astrocytes.The figure depicts that cells lacking *App* exhibit an enhanced basal Ca^{2+} level which was further enhanced on treatment of *$App^{0/0}$* astrocytes with DAPT. The data represented here is mean ± SEM for 6 to 9 independent experiments. Number of cells selected for each experiment range between 25 to 35 cells. Statistical significance *, $p< 0.05$ and **, $p< 0.001$.

To ascertain which further γ-secretase cleavage fragment of APP, AICD or Aβ, is responsible for modulating the responses observed above, another set of experiments were performed to analyze the effects of γ-secretase derived intracellular fragment, AICD, using human neuroglioma cells (H4 cells) expressing AICD with a VSV tag (AICD-VSV) under the control of the tetracycline inducible promotor (Tet-Off system). Ca^{2+} imaging experiments were made in the cells that express *AICD-VSV* in the absence of doxycycline compared to cells in which its expression was turned off by using doxycycline

(Fig. 6.4). These experiments were performed in presence of DAPT (1 µM) to exclude any effect of Aβ or AICD produced endogenously.

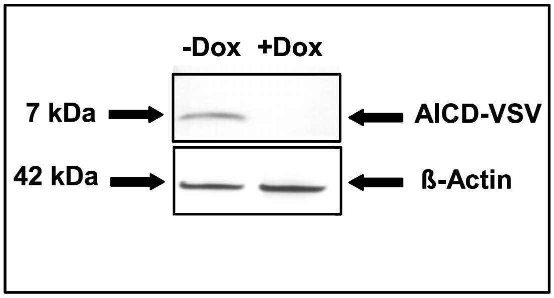

Fig. 6.4: Western blot showing AICD-VSV protein expression (-Dox) and non-expression (+Dox) in H4 cells. Cells were equally plated and cultured for two days in the presence and absence of doxycycline (100 ng/ml). Equal volume of lysates was loaded on 10-20% tricine-SDS gel. AICD-VSV fragment was detected by monoclonal mouse anti-VSV antibody (1:10,000). Equal sample loading was analyzed by mouse anti β-actin antibody (1:2000). The AICD-VSV fragment was detected at around 7 kDa.

As illustrated in fig 6.5, cells lacking AICD-VSV fragments markedly enhanced the cytosolic Ca^{2+} levels to 93 ± 13 nM as compared to *AICD-VSV* expressing cells that showed 28 ± 2 nM of cytosolic Ca^{2+} levels. This response was analogous to the data obtained in the HEK293 cells and in astrocytes. In order to confirm that the differences in cytosolic Ca^{2+} was due to AICD-VSV only and not the effect of doxycycline, another control experiment was made under similar experimental conditions in H4 cells that express only the regulator plasmid and not the response plasmid (H4-Control). The cells were measured both in presence and absence of doxycycline and in the presence of DAPT. There was no significant difference in resting cytosolic Ca^{2+} levels (Fig. 6.5). In order to determine the extent of the effect produced by endogenous AICD, H4 cells expressing only regulator plasmid were also measured without γ-secretase inhibitor (DAPT). In absence of DAPT, H4 cells exhibited resting Ca^{2+} of 33 ± 6 nM, a level almost equal to AICD-VSV overexpressing cells (Fig. 6.5). This experiment suggests that the endogenous AICD is sufficient to maintain a normal Ca^{2+} balance. The main observation that emerged out of these measurements was that the ablation of AICD enhances resting cytosolic Ca^{2+} levels independent of the cell types used.

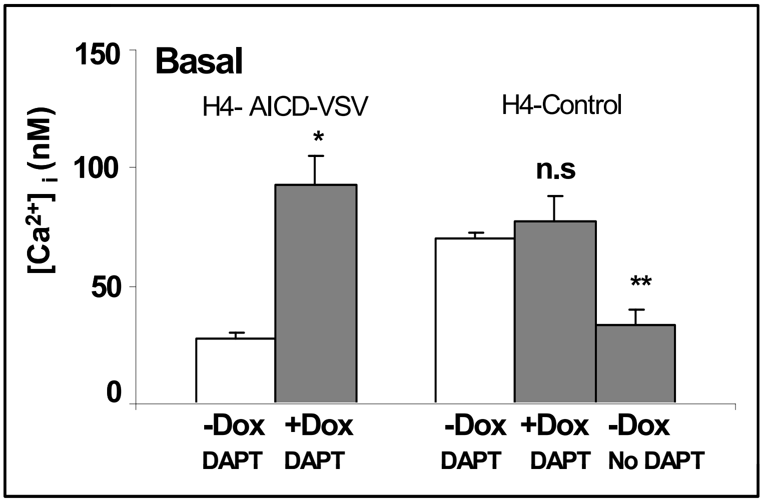

Fig. 6.5: Data illustrated here shows basal cytosolic Ca^{2+} measured by fluorescence ratio imaging in fura-2/AM loaded H4 cells with Tet-off system for AICD and in H4 cells expressing only the regulator plasmid for Tet-off system (H4-control). AICD was expressed with a VSV tag (AICD-VSV). The expression of AICD-VSV was suppressed by administration of doxycycline (100 ng/ml for 48 hrs). Both *AICD-VSV* expressing (-Dox) and non-expressing (+Dox) cells were pretreated with DAPT for 24 hrs in order to exclude any effects of endogenous AICD. The data shown here for H4-AICD-VSV (+/- Dox) cells is mean ± SEM for 5 to 7 independent experiments. Number of cells selected for determination of Ca^{2+} values range between 40 to 55 cells per experiment. Statistical significance *, $p < 0.05$. H4 cells expressing only the regulator plasmid (H4-control) were also measured under similar experimental conditions. To check for the effect of endogenous AICD, experiments were also performed in absence of γ-secretase inhibitor, DAPT, in H4-control cells. The data represented here for H4-control cells is mean ± SEM for 3 to 4 independent experiments and number of cells determined for Ca^{2+} values were 55 to 65 cells per experiment. Statistical significance *,$p<0.05$ and **, $p < 0.001$.

6.2 ER Ca^{2+} storage is modulated in cells lacking *APP* or its C-terminal cleavage products.

Inside the cell, Ca^{2+} load in the cytoplasm is replenished back into the ER predominantly by sarco-endoplasmic Ca^{2+}ATPases (SERCA) which work in an ATP dependent manner. To investigate if ER Ca^{2+} level was also affected as a consequence of loss of γ-secretase cleavage products of APP, the level of Ca^{2+}

inside the ER was subsequently determined. This was analyzed by the application of cyclopiazonic acid (CPA)⑪.

As shown in fig 6.6 and 6.7, the application of CPA caused a strong rise in cytosolic Ca^{2+} in APPsw cells (570 ± 40 nM) but not in PSD385N mutant cells (150 ± 1 nM) (indicated by c).

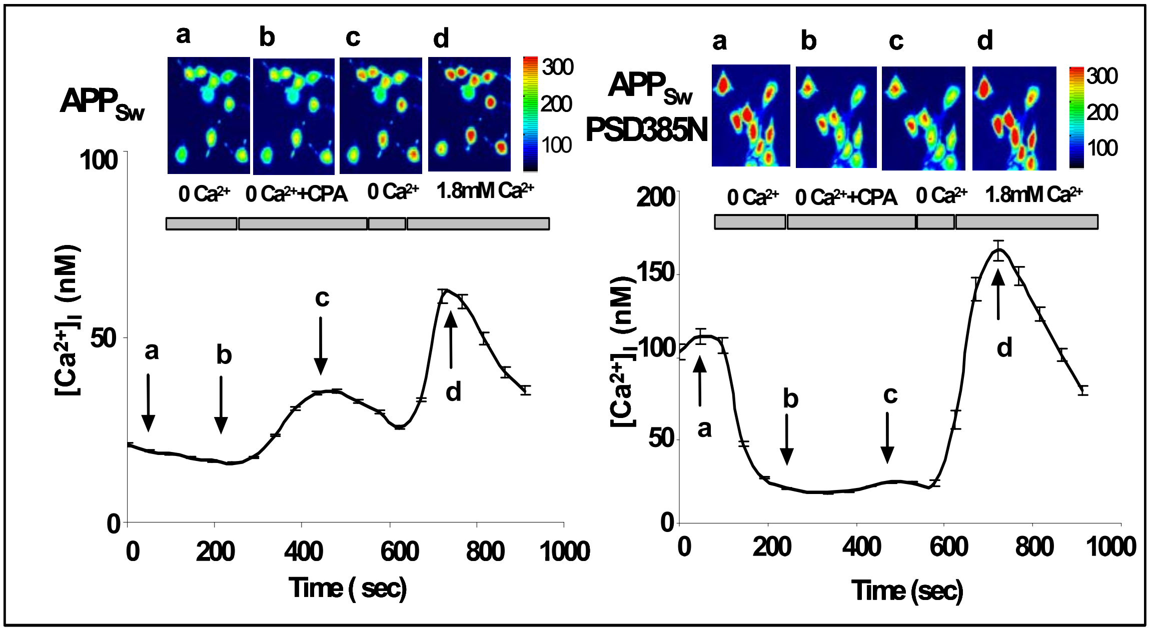

Fig. 6.6: Representative traces of Ca^{2+} measurements in HEK293 cells expressing APPsw mutation (left panel) and HEK293 cells co-expressing APPsw with dominant negative D385N mutation in PS1 (PSD385N) (right panel). Note the different scales. The horizontal bars indicate the time of the application of extracellular fluid with Ca^{2+} (1.8 mM Ca^{2+}) or without Ca^{2+} (0 mM Ca^{2+}) or cyclopiazonic acid (CPA). Ratiometric images (a-d) show fura-2/AM loaded cells which correspond to time points indicated (a-d) in the curve. Scale represents the fluorescence intensity of fura-2/AM loaded cells which increases on increase of cytosolic Ca^{2+}. Experiments were started when cells were in normal physiological Ca^{2+} concentration (1.8 mM) in extracellular medium (0-60 sec). Values at this time period were taken to calculate resting cytosolic Ca^{2+} levels. Subsequently, extracellular medium with 0 mM Ca^{2+} was applied. This was followed by addition of CPA (10 µM) which causes an increase in cytosolic Ca^{2+} and then drops down due to buffering. The Ca^{2+} released from ER was calculated as area under the curve. This step was followed by a short washing with 0 mM Ca^{2+} medium and then readdition of 1.8 mM Ca^{2+}. The rise in cytosolic Ca^{2+} by readdition of Ca^{2+} shows capacitative Ca^{2+} entry (CCE) and this Ca^{2+} influx was also calculated as area under the curve. The curves represent the mean ± SEM of 75 cells with APPsw and 65 cells with PSD385N mutation taken from one single experiment.

---

⑪ CPA is known to release Ca^{2+} from the ER by blocking the Ca^{2+}ATPase present within the ER membrane, which maintains a high Ca^{2+}gradient between the cytosol and the ER lumen (Schaefer et al., 1994; Mason et al., 1991)

In addition to PSD385N mutant cells, a reduced ER Ca^{2+} release was also observed in *IDE* expressing cells (179 ± 9 nM) and APPsw cells pretreated with γ-secretase inhibitor, γ-IV (345 ± 11 nM) as compared to APPsw cells (Fig. 6.7). Such reduced ER Ca^{2+} stores promote the influx of Ca^{2+} from the extracellular medium. This process is termed as capacitative calcium entry (CCE). To show further that this is indeed a reduction in the ER Ca^{2+} levels, CCE was analyzed at the end of the experiment by the readdition of 1.8 mM Ca^{2+} into the extracellular medium. Application of 1.8 mM extracellular Ca^{2+} results in a strong Ca^{2+} influx in PSD385N cells owing to the reduced ER stores as compared to APPsw cells (indicated by d in fig. 6.6). Analysis of CCE in *IDE* expressing cells and APPsw cells treated with γ-IV also exhibited the same phenomenon. All these results indicated that loss of γ-secretase cleavage products reduce ER Ca^{2+} storage capacity.

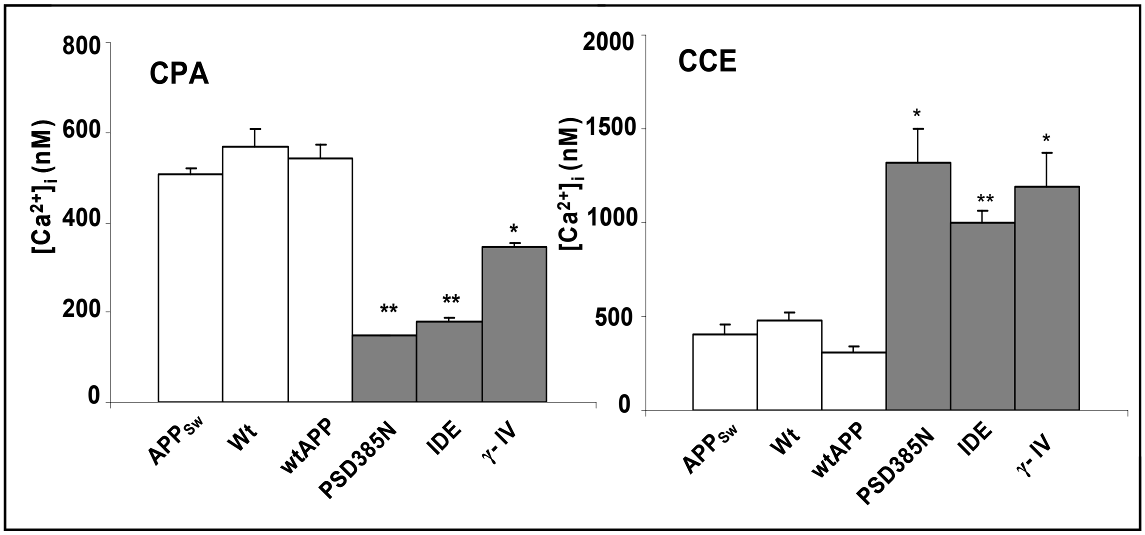

Fig. 6.7: The left panel shows the level of Ca^{2+} released from the ER on application of CPA (10 µM). The Ca^{2+} values were calculated from the 340/380 nm ratio obtained by Ca^{2+} imaging of fura-2/AM loaded cells. The Ca^{2+} released from the ER was calculated as area under the curve. The right panel shows values for Ca^{2+} influx by capacitative Ca^{2+} entry and were also deduced as area under the curve. The statistical significance in PSD385N cells, IDE cells or γ-IV treated APPsw cells was determined compared to APPsw cells. The figure depicts a lower CPA induced ER Ca^{2+} release and a higher CCE in cells that lack APP C-terminal cleavage products. The data represented here is mean ± SEM for 4 to 6 independent experiments. Number of cells selected for each experiment range between 50 to 80 cells. Statistical significance *, $p < 0.05$ and **, $p < 0.001$.

The reduced ER Ca^{2+} levels observed above in PSD385N and *IDE* expressing cells could be a consequence of γ-secretase activity on other substrates rather than APP. To exclude this possibility and to establish that the effects observed were due to APP cleavage product/s only, similar studies were done on primary cultures of *App*$^{0/0}$ astrocytes. Fig. 6.8 shows representative curves of changes in cytosolic Ca^{2+} levels on different treatments during the course of the measurement.

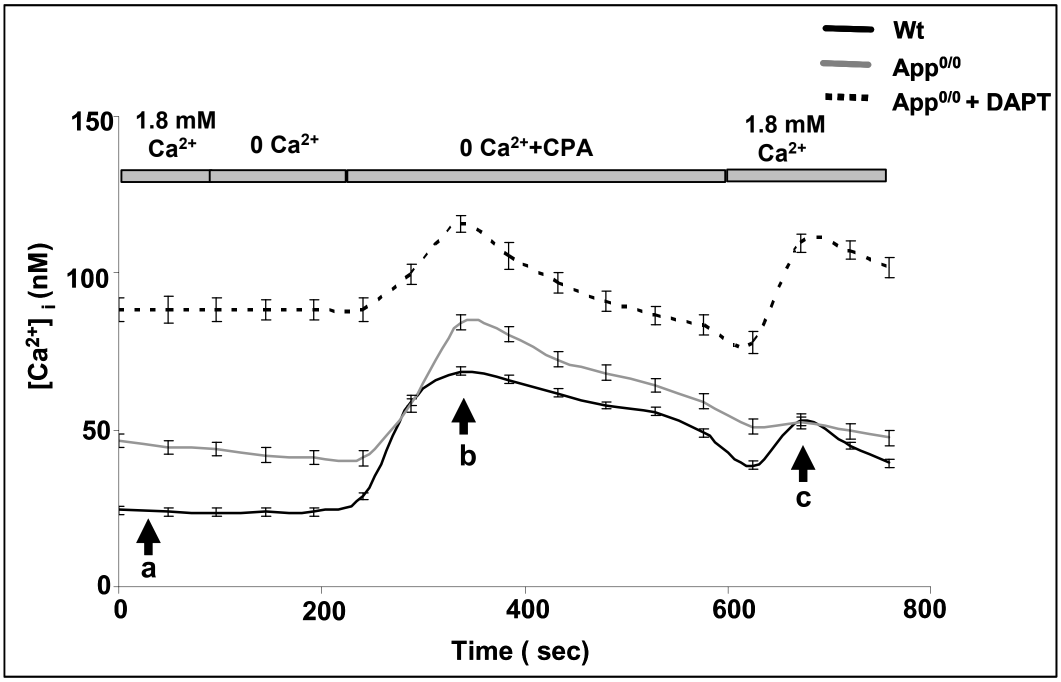

Fig. 6.8: Representative traces of Ca^{2+} measurements in primary cultures of Wt astrocytes, *App*$^{0/0}$ astrocytes and *App*$^{0/0}$ astrocytes treated with DAPT (1 µM for 24 hrs). The horizontal bars indicate the time of the application of extracellular fluid with Ca^{2+} (1.8 mM Ca^{2+}) or without Ca^{2+} (0 mM Ca^{2+}) or 10 µM cyclopiazonic acid (CPA). The region indicated by ‘a’ shows the basal cytosolic Ca^{2+} levels in the presence of 1.8 mM extracellular Ca^{2+}, arrow indicated by ‘b’ shows the region of CPA induced ER Ca^{2+} release and the arrow indicated by ‘c’ shows the region of capacitative Ca^{2+} entry on readdition of 1.8 mM Ca^{2+}. The Ca^{2+} values were deduced from the 340/380 nm ratio obtained from fura-2/AM loaded cells. The curves represent the mean ± SEM of 10 cells taken from one single experiment.

As shown in fig. 6.8 and 6.9, CPA induced Ca^{2+} release from intracellular stores was found to be reduced in *App*$^{0/0}$ (459 ± 12 nM) as compared to control astrocytes (532 ± 14 nM). To further evaluate the role of other γ-secretase cleavage products produced by APLP1 and APLP2, similar measurements were performed on *App*$^{0/0}$ astrocytes pretreated with γ-secretase inhibitor (DAPT). Consistent with the results described in HEK293 cells the CPA induced Ca^{2+} release from the ER was further reduced to 364 ± 10 nM as compared to Wt astrocytes (Fig 6.9). However CCE on the other hand was not found to be significantly affected as compared to the controls (Fig 6.9).

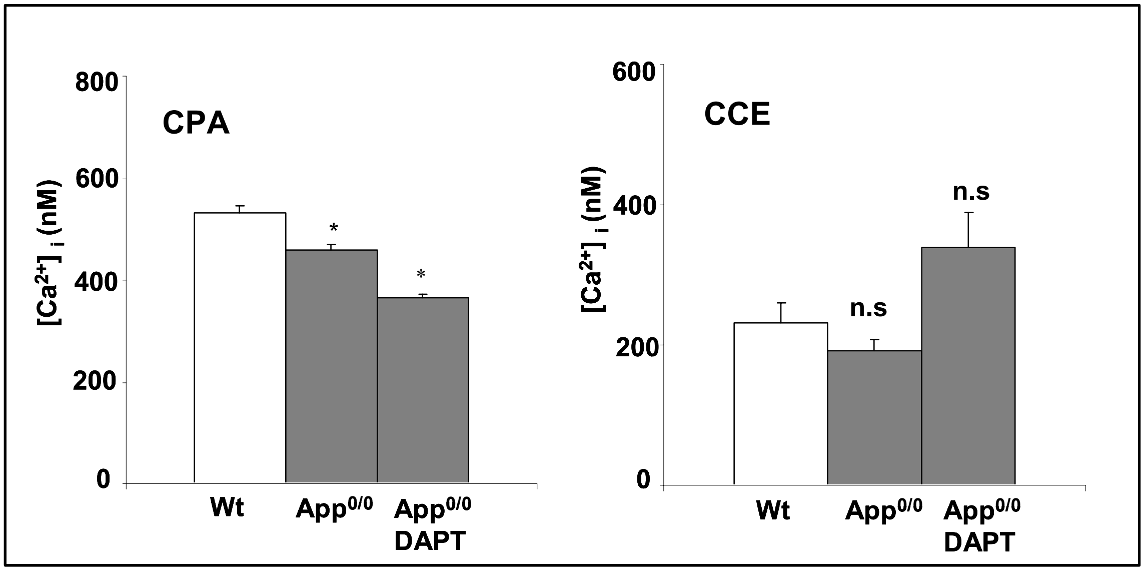

Fig. 6.9: Bar graph shows CPA induced Ca^{2+} release from ER (left panel) and CCE on readdition of 1.8 mM Ca^{2+} (right panel) in *APP* knock out astrocytes (*App*$^{0/0}$) compared to Wt astrocytes. In addition, *App*$^{0/0}$ astrocytes were also analyzed after pretreatment with γ-secretase inhibitor, DAPT (1 µM for 24 hours). The data represented here are values of area under the curve for ER Ca^{2+} release by CPA and Ca^{2+} influx. The data represented here is mean ± SEM for 6 to 9 independent experiments. Number of cells selected for each experiment range between 25 to 35 cells. Statistical significance *, $p < 0.05$.

The enhanced cytosolic basal Ca^{2+} levels and reduced ER Ca^{2+} release observed in *IDE* expressing HEK293 cells and in *App*$^{0/0}$ astrocytes treated with DAPT strongly indicated that this phenomenon is attributable to AICD.

To ascertain that modulation in cellular Ca^{2+} was due to AICD, HEK293 cells expressing PSD385N mutation were transiently cotransfected with cDNA encoding AICD together with enhanced green fluorescent protein (pEGFP) as an expression control. Ca^{2+} imaging was performed on the transfected cells 48 hrs later. As shown in fig. 6.10, basal cytosolic Ca^{2+} was reduced and ER Ca^{2+} was enhanced in cells cotransfected with pEGFP and AICD and also in cells transfected with pEGFP alone. These results showed that transfection with pEGFP produce non-specific effect on Ca^{2+} measurements. Therefore this strategy could not be followed up further to study the role of AICD on Ca^{2+}.

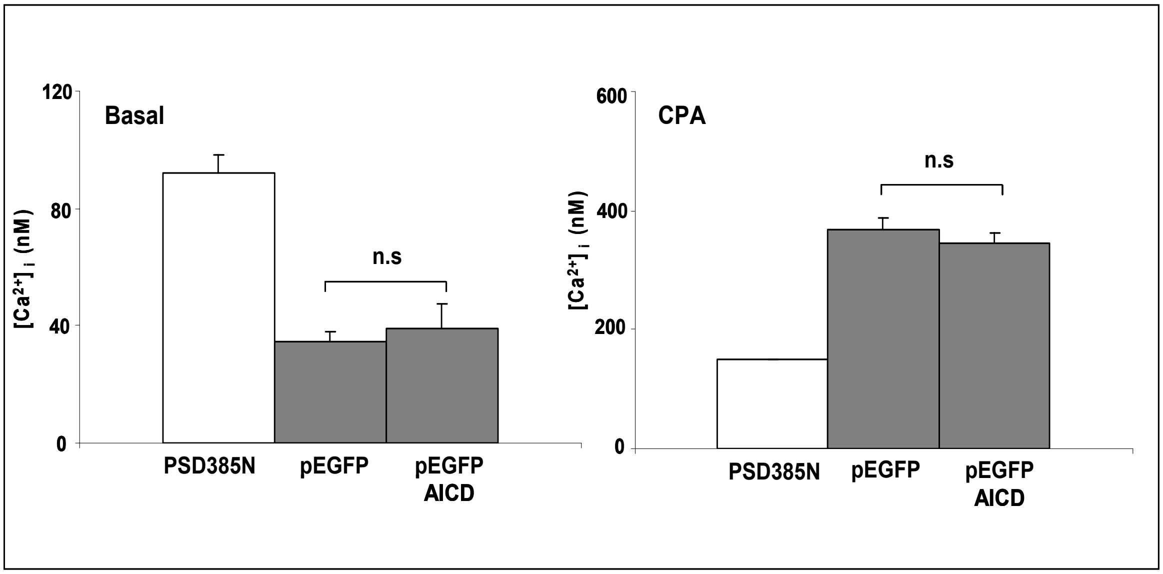

Fig. 6.10 Data illustrated here represents the mean values of basal cytosolic Ca^{2+} (left panel) and CPA induced ER Ca^{2+} release (right panel) in HEK293 cells stably expressing PSD385N and transiently cotransfected with pEGFP and AICD constructs. To quantify for the effect of pEGFP on Ca^{2+}, PSD385N cells transiently transfected with pEGFP alone were also analyzed as a control. Transient transfection was carried out with effectene reagent and Ca^{2+} imaging was performed 48 hrs later. As depicted in the figure, pEGFP transfected and cotransfected cells showed a non-significant difference in both basal cytosolic Ca^{2+} and CPA induced ER Ca^{2+} release, indicating that pEGFP transfection causes non-specific effects on Ca^{2+} responses. Ca^{2+} values were deduced from the 340/380 nm ratio obtained by Ca^{2+} imaging of fura-2/AM loaded cells. Data shown here is mean ± SEM of 6 experiments per condition. The number of cells determined were 40 to 50 cells per experiment. Statistical non-significance , n.s, when $p > 0.05$.

To establish which γ-secretase cleavage product of APP, AICD or Aβ, is responsible for reducing ER Ca^{2+} storage, H4 cells under the control of Tet-Off system were analyzed for AICD expression. Experiments for both doxycycline treated and non-treated cells were performed in the presence of DAPT to exclude the effect of endogenous AICD and Aβ. Fig. 6.11 shows representative curves of changes in cytosolic Ca^{2+} levels on different treatments during the course of the measurement.

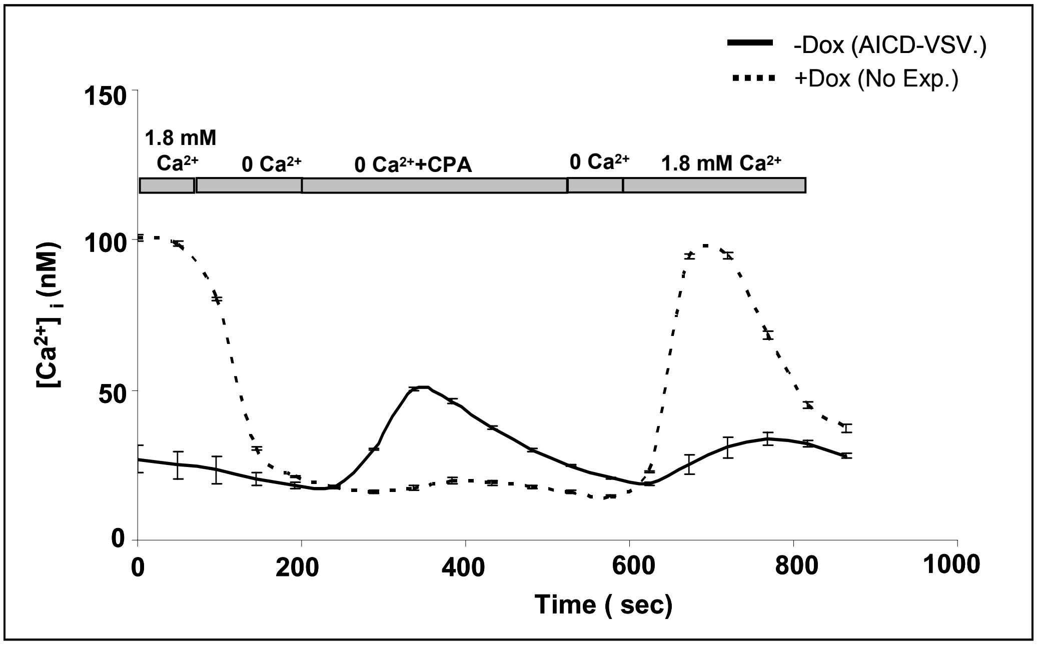

Fig. 6.11: Representative curve of Ca^{2+} measurements done on H4 cells expressing *AICD-VSV* under the control of Tet-off system. *AICD-VSV* expression (-Dox) curve is shown in black while curve with suppressed *AICD-VSV* expression (+Dox) is shown in grey. The horizontal bars indicate the time of the application of extracellular fluid with Ca^{2+} (1.8 mM) or without Ca^{2+} (0 Ca^{2+}) or CPA (10 µM). The Ca^{2+} values were calculated from the 340/380 nm ratio obtained from Ca^{2+} imaging of fura-2/AM loaded cells. Each curve represents the mean ± SEM of 40 cells from one single experiment.

As illustrated in fig 6.11 and 6.12, cells lacking the AICD-VSV fragment (+Dox) significantly reduced CPA induced ER Ca^{2+} release to 312 ± 15 nM as compared to cells that express AICD-VSV (-Dox) i.e. 511 ± 40 nM. Furthermore, to prove that the reduced CPA induced ER Ca^{2+} release in doxycycline treated H4 cells was not due to any unspecific effect of doxycycline, H4 cells expressing only the regulator plasmid (H4-Control) for the Tet-Off system were analyzed. As shown in fig 6.12, there was non-significant difference in the CPA induced Ca^{2+} release in both doxycycline treated and untreated cells. All of the experiments described above in H4 cells were performed in the presence of DAPT. However, to determine the extent of the effect produced by endogenous AICD, additional experiments in H4 cells expressing only regulator plasmid were performed in the absence of DAPT. As shown in fig. 6.12, H4-control cells without DAPT pretreatment had an enhanced CPA induced ER Ca^{2+} release to almost comparable levels as in *AICD-VSV* expressing H4 cells.

These results strongly indicated that the γ-secretase derived C-terminal cleavage product of APP, known as AICD, mediates the regulation of resting cytosolic free Ca^{2+} concentration via ER Ca^{2+} storage.

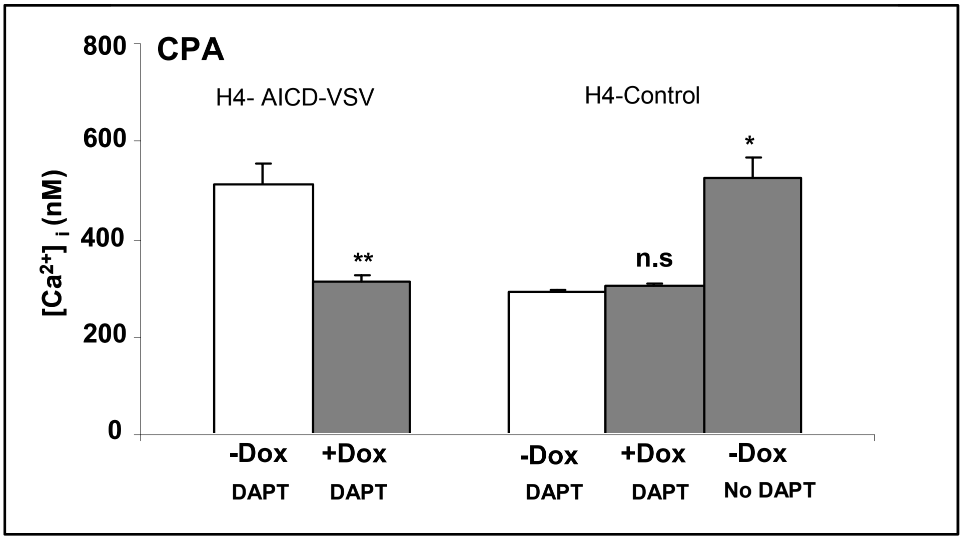

Fig. 6.12: Data represented here shows CPA induced ER Ca^{2+} release both in *AICD-VSV* expressing (-Dox) and non-expressing (+Dox) H4 cells. H4 cells without regulator plasmid (H4-Control) were also studied under similar conditions as for H4-AICD-VSV. All cells, where indicated, were pretreated with 1 µM DAPT for 24 hrs. Ca^{2+} values were deduced from the 340/380 nm ratio obtained from the fura-2/AM loaded cells by Ca^{2+} imaging. The data shown here is the CPA induced Ca^{2+} release from the ER calculated as area under the curve and is mean ± SEM for 3 to 4 independent experiments. The figure depicts that the CPA induced ER Ca^{2+} release is reduced in cells lacking AICD. The number of cells determined were 55 to 65 cells per experiment. Statistical significance *, $p < 0.05$ and **, $p<0.001$.

6.3 Cells lacking AICD have decreased ATP production and enhanced mitochondrial membrane potential.

The above results strongly indicated that the loss of AICD consequently enhanced the resting cytosolic Ca^{2+} levels and reduced ER Ca^{2+} storage. It can be inferred from the combination of enhanced resting cytosolic Ca^{2+} and reduced ER Ca^{2+} that Ca^{2+} removal mechanisms are probably affected as a loss of AICD. The removal of resting cytosolic free Ca^{2+} is tightly regulated and mainly controlled by the Ca^{2+}ATPase that is located within the ER membrane. It pumps Ca^{2+} against a strong gradient into the ER lumen in an ATP dependent fashion. Maintenance of a normal level of resting Ca^{2+} therefore is acutely dependent on the continuous energy support provided predominantly by mitochondria. Therefore, it became relevant to study the efficiency of cell to meet the energy demand as a result of the AICD ablation. To assess this hypothesis, direct ATP measurements were made using ATP bioluminescent assay.

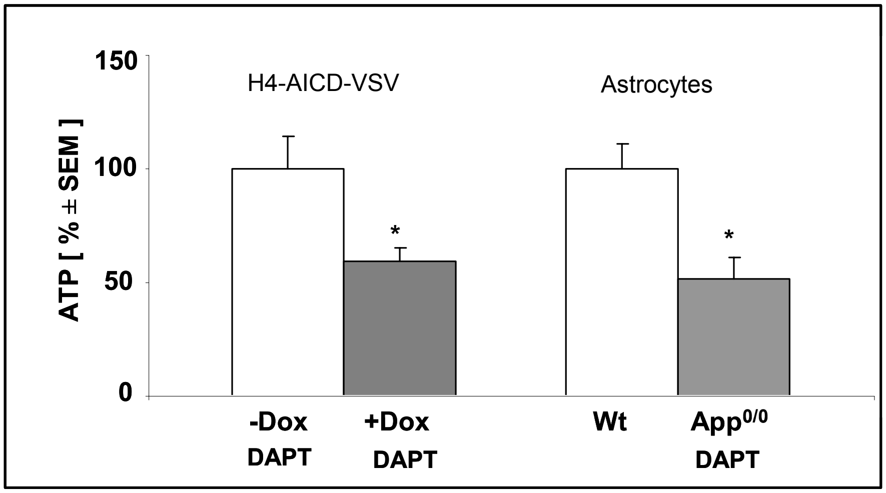

Fig. 6.13: Data shown here represents the levels of ATP (nM) per 10^6 cells represented as percentages of the control conditions. ATP levels were calculated using ATP bioluminescent assay in H4 cells with suppressed *AICD-VSV* expression (+Dox) and *AICD-VSV* expression (-Dox). Similar assay was also performed in *App*$^{0/0}$ astrocytes and in Wt astrocytes. H4 cells and *App*$^{0/0}$ astrocytes were pretreated with DAPT (1 µM, 24 hrs). The data represented here is mean ± SEM for four independent determinations. Statistical significance *, $p < 0.05$.

As shown in fig 6.13, the ATP levels were reduced to 56% in *AICD-VSV* non-expressing cells (+Dox) as compared to *AICD-VSV* expressing cells (-Dox). Consistently, *App*$^{0/0}$ astrocytes pretreated with DAPT also showed 53% reduced ATP generation as compared to Wt astrocytes.

As discussed in the preceding text (see introduction), the major factor determining the level of mitochondrial ATP production is the mitochondrial membrane potential (ψ_m). In light of the reduced ATP generation found in cells lacking AICD, the mitochondrial membrane potential was also analyzed. Here this parameter was monitored using rhodamine-123 (Nicholls and Budd, 2000). Respiring mitochondria generate a proton gradient across the inner membrane, producing a pH gradient and a membrane potential ($\Delta\psi_m$). The membrane potential represents most of the energy of the proton gradient. Rhodamine-123 is a nerstian dye that distributes itself preferentially across the mitochondrial membrane strictly as a function of mitochondrial membrane potential (Nicholls and Budd, 2000; Toescu and Verkhratsky, 2000). The lipohilic nature of rhodamine-123 allows it to diffuse through the mitochondrial membrane in response to potential gradients. The higher the $\Delta\psi_m$, more is the rhodamine-123 taken up into the matrix. Carbonyl cyanide 4-trifluoro-methoxyphenylhydrazone (FCCP), an uncoupler of oxidative phosphorylation, was used as a control for maximal increase in rhodamine-123 fluorescence. FCCP carry protons across the inner mitochondrial membrane and causes the mitochondrial membrane potential to dissipate. Due to the dissipation of membrane potential, rhodamine-123 is released from mitochondria producing maximal fluorescence (Fmax).

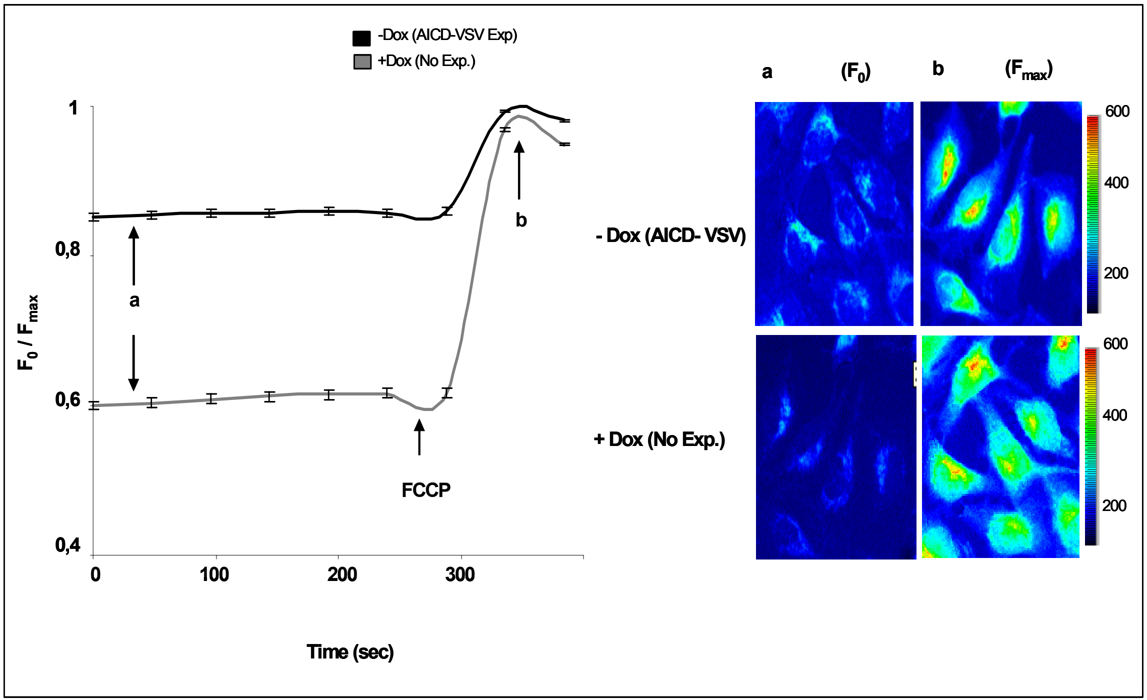

Fig. 6.14: Left panel shows traces of mitochondrial membrane potential studied in H4 cells with *AICD-VSV* expression (-Dox, shown in black) and *AICD-VSV* non-expression (+Dox, shown in grey), pretreated with DAPT (1 µM). The membrane potential shown here is normalized to maximal fluorescence on complete depolarization by an uncoupler of oxidative phosphorylation, FCCP (Fmax, 1µM), indicated by arrow b. The figure depicts a higher mitochondrial membrane potential in cells lacking AICD-VSV. Each trace represents the mean ± SEM of 50 cells from one single experiment. Right panel shows fluorescent images of rhodamine-123 (incubated with 10 µM for 20 min) loaded cells at time points indicated by arrows in the traces. The fluorescence values were acquired at 470 nm excitation wavelength at an interval of every 3 sec. The scale in the right panel represents fluorescence intensity.

As shown in fig. 6.14 and 6.15, the membrane potential was dissipated more on FCCP application in *AICD-VSV* non-expressing cells (+Dox) as compared to *AICD-VSV* expressing (-Dox) H4 cells. Therefore, the F_0/F_{max} value was lower in *AICD-VSV* non-expressing cells. Similar analysis was also made in *App*$^{0/0}$ astrocytes as compared to Wt astrocytes. As shown in fig. 6.15, consistent with the results obtained with H4 cells, dissipation through FCCP was higher in *App*$^{0/0}$ astrocytes as compared to Wt astrocytes. These results imply that the mitochondrial membrane is hyperpolarized in cells lacking AICD.

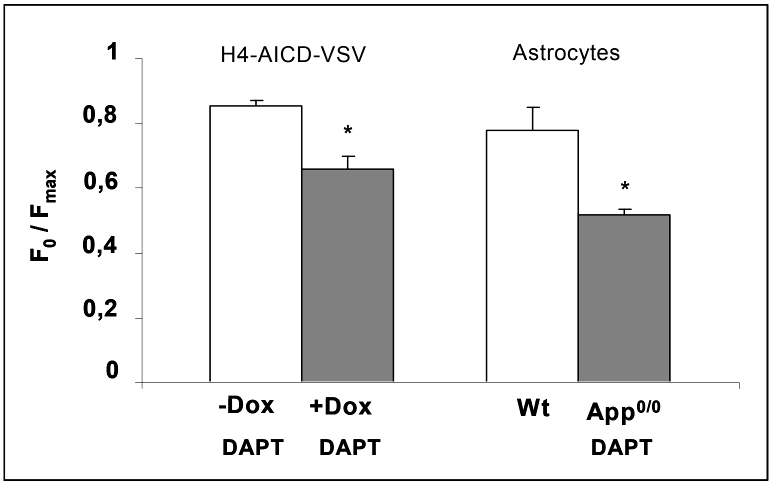

Fig. 6.15: Data represented here shows the mean value of the mitochondrial membrane potential in H4 cells with (-Dox) or without (+Dox) *AICD-VSV* expression and in primary cultures of 1-2 *App*$^{0/0}$ astrocytes as compared to Wt astrocytes. All experiments in H4 cells and *App*$^{0/0}$ astrocytes were performed after pretreatment with γ-secretase inhibitor, DAPT (1 µM for 24 hours). The fluorescence values in rhodamine-123 loaded cells were acquired at an interval of 3 sec at 470 nm excitation wavelength. These values were normalized to maximum fluorescence produced on FCCP (1 µM) application and are shown here as F_0 / F_{max}. The figure depicts that the mitochondrial membrane is hyperpolarized in cells lacking AICD. The data represented here is mean ± SEM for 4 independent experiments. The number of cells determined were 45 to 55 cells per experiment for H4 cells and 25 to 35 cells per experiment for astrocytes. Statistical significance *, $p < 0.05$.

6.4 The basal cytosolic free Ca^{2+} level was enhanced and ER Ca^{2+} was reduced on inhibition of oxidative phosphorylation

Maintenance of basal cytosolic Ca^{2+} level is highly dependent upon cytoplasmic ATP, either generated by oxidative phosphorylation or glycolysis (Nicholls and Budd, 2000; Xiong et al., 2002; Nicholls et al., 2003). Mostly active glycolysis suffices to supply ATP in the absence of mitochondrial ATP synthesis. In view of the reduced ATP production obtained in cells lacking AICD, the next objective was to analyze if the reduced ATP production was indeed due to a mitochondrial dysfunction. Also it was aimed to ascertain whether the alterations in the Ca^{2+} homeostasis observed in cells lacking AICD was due to a reduced ATP generation. Therefore, pyruvate was substituted for glucose as a substrate for the glycolysis, which means that the cells were entirely dependent on ATP generation by oxidative phosphorylation. These experiments were performed in *AICD-VSV* expressing cells and in wild type astrocytes. The cells were cultured in glucose depleted conditions for 24 hours and the effect of oligomycin (inhibitor of ATP synthase)⑫ and NaCN (inhibitor of complex IV) ⑬ was studied. In addition to it, experiments were also performed in glucose depleted conditions in order to distinguish between the effect of glucose depletion and mitochondrial toxins.

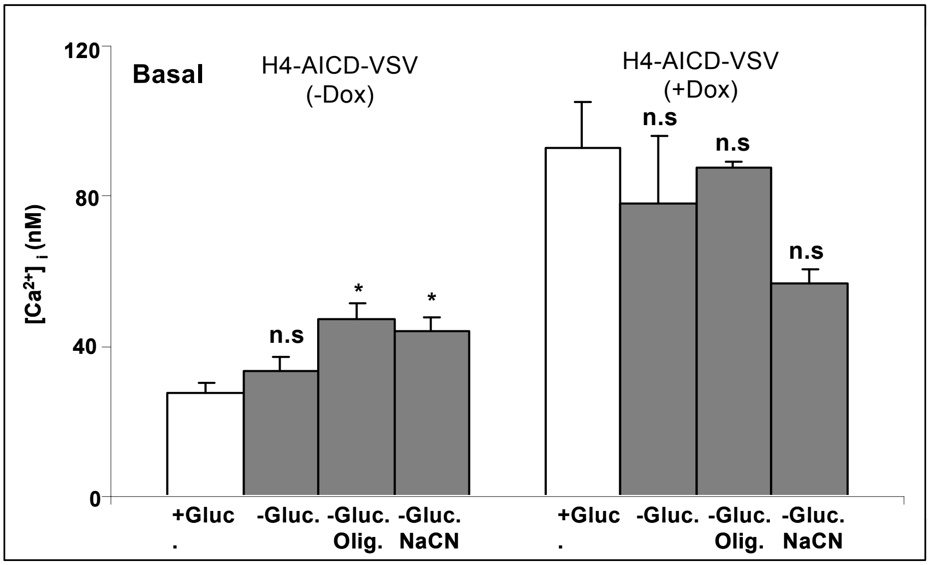

Fig. 6.16: Left panel, represents the mean values of resting cytosolic Ca^{2+} in *AICD-VSV* expressing (-Dox) H4 cells on sodium cyanide (inhibitor of complex IV) and oligomycin (inhibitor of ATP synthase) treatment. The inhibition by cyanide and oligomycin was studied in cells after glucose was substituted with pyruvate for 24 hours to preclude any effect of ATP produced by glycolysis. Cells were treated with 10 µM oligomycin for 1 hr and with 2 mM sodium cyanide for 1 hr in growth medium before measurement. Right panel represents mean values of basal cytosolic Ca^{2+} in *AICD-VSV* non-expressing cells (+Dox) were also analyzed in order to show that these effects were attributable to AICD and not due to non-specific effects of mitochondrial toxins. Ca^{2+} values were deduced from the 340/380 nm ratio obtained by imaging of fura-2/AM loaded cells. Data represented here is mean ± SEM for 3-6 independent experiments. The number of cells determined were 40 to 50 cells per experiment for *AICD-VSV* expressing cells and 60 to 70 cells per experiment for *AICD-VSV* non-expressing cells. Statistical significance *, $p < 0.05$.

---

⑫ Oligomycin prevent the influx of protons through ATP synthase due to which electron transport chain ceases to operate and consequently inhibits ATP generation.

⑬ NaCN inhibits electron flow through the complex IV (cytochrome oxidase) due to which proton motive force (or membrane potential) can no longer be sufficiently generated, consequently causing inhibition of ATP production.

As shown in fig. 6.16, on treatment of AICD-VSV expressing cells with oligomycin and NaCN, the resting cytosolic Ca^{2+} was enhanced to 47 ± 5 nM and 44 ± 4 nM respectively. In addition, in order to ascertain that the Ca^{2+} disturbances were attributable to AICD only and not due to non-specific effects of mitochondrial toxins, similar analysis was also made in AICD-VSV non-expressing cells (+Dox). A non-significant difference was found on treatment of oligomycin, NaCN and glucose depletion in these cells (Fig. 6.16). As shown in fig. 6.17, CPA induced ER Ca^{2+} release on the other hand was reduced to 338 ± 16 nM and 288 ± 20 nM in oligomycin and NaCN treated cells respectively. Assesment of ER Ca^{2+} release on similar treatments in AICD-VSV non-expressing cells (+Dox) showed non-significant differences (Fig. 6.17).

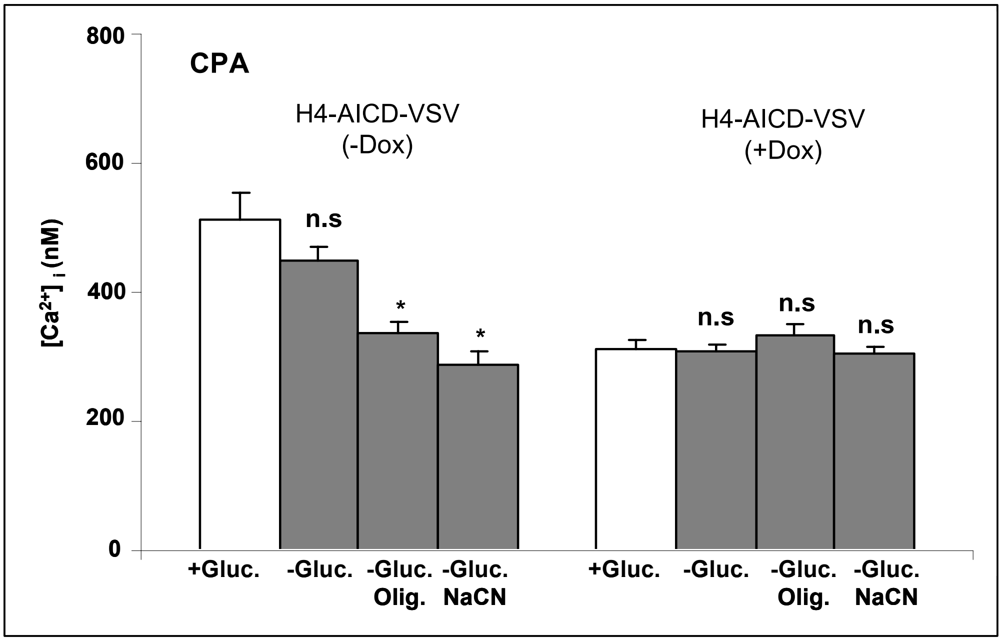

Fig. 6.17: The figure represents the mean value of CPA induced ER Ca^{2+} release in *AICD-VSV* expressing (-Dox) and non-expressing cells (+Dox) on NaCN (10 µM for 1 hr) and oligomycin (2 mM for 1 hr) treatment. The cells were grown in glucose depleted medium for 24 hrs. CPA induced ER Ca^{2+} release was determined as area under the curve. Ca^{2+} values were deduced from the 340/380 nm ratio obtained by Ca^{2+} imaging of fura-2/AM loaded cells. Data represented here is mean ± SEM for 3-6 independent experiments. The number of cells determined were 40 to 50 cells per experiment. Statistical significance *, $p < 0.05$.

However, cells cultured in glucose depleted conditions for 24 hrs showed non-significant differences in both basal cytosolic Ca^{2+} levels and CPA induced ER Ca^{2+} release (Fig. 6.16 and 6.17).

Similar observations were obtained in Wt astrocytes that showed enhanced basal cytosolic Ca^{2+} levels on oligomycin and NaCN treatment i.e. 64 ± 7 nM and 51 ± 6 nM respectively as compared to 29 ± 1 nM in non-treated astrocytes (Fig 6.18). A reduced CPA induced ER Ca^{2+} release was also observed in oligomycin and NaCN treated Wt astrocytes i.e. 271 ± 7 nM and 345 ± 41 nM as compared to non-treated 531 ± 14 nM (Fig. 6.18). However, glucose depletion exhibited non-significant differences in resting cytosolic Ca^{2+} and ER Ca^{2+} release (Fig 6.18).

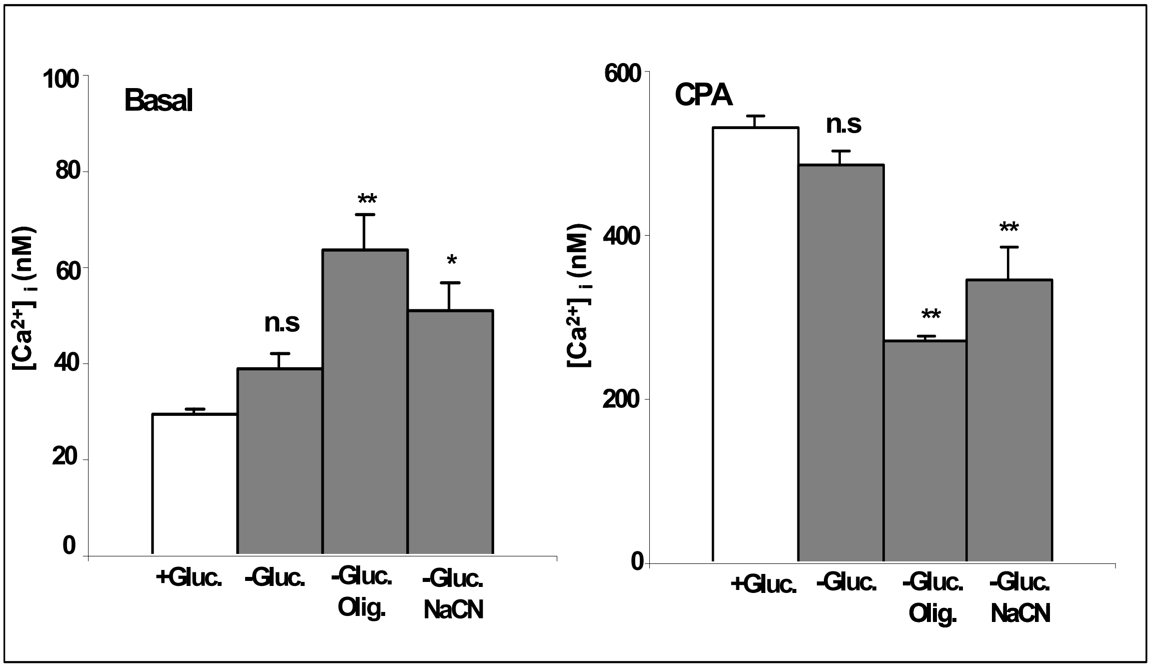

Fig. 6.18 The figure represents the mean value of basal cytosolic Ca^{2+} and CPA induced ER Ca^{2+} release in Wt astrocytes on NaCN (10 µM for 1 hr) and oligomycin (2 mM for 1 hr) treatment. The cells were grown in glucose depleted medium for 24 hrs and Ca^{2+} values were deduced from the 340/380 nm ratio obtained by imaging of fura-2/AM loaded cells. Data represented here is mean ± SEM for 4-6 independent experiments. The number of cells determined were 25 to 30 cells per experiment. Statistical significance *, $p < 0.05$ and **, $p < 0.001$.

6.5 Responses of cells lacking AICD were reversed on the application of Complex I and II substrates.

As shown in the above experiments, inhibition of mitochondrial respiratory chain mimics the Ca^{2+} responses from cells lacking AICD or APP. These results led to explore if the action of substrates for mitochondrial complexes on cells lacking AICD also mimics the phenotype shown by cells expressing AICD. To study this, another set of experiment was carried out in which substrates for complex I, complex II and complex IV were applied on AICD-VSV non-expressing cells and *App*$^{0/0}$ astrocytes. Citric acid cycle oxidizes different substrates and forms electrons carrying high energy compounds i.e. NADH and $FADH_2$. NADH and $FADH_2$ are then oxidized by electron transport chain. Electrons released by these compounds flow through a series of complexes in the electron transport chain (complex I to complex IV) to generate a proton gradient across the inner mitochondrial membrane leading to ATP generation.

As shown in fig. 6.19, substrates for complex I (pyruvate and malate⑭) and substrates for complex II (succinate⑮) significantly reduced the basal cytosolic Ca^{2+} levels to 52 ± 1 nM and 40 ± 1 nM as compared to untreated AICD-VSV non-expressing (+Dox) cells i.e. 93 ± 13 nM. However, there was non-significant difference in basal Ca^{2+} levels on treatment with substrates for complex IV (TMPD and ascorbate⑯)

---

⑭ Oxidation of pyruvate and malate in citric acid cycle forms NADH. The electrons of NADH enter the oxidative phosphorylation chain at complex I.

⑮ Oxidation of succinate in citric acid cycle forms $FADH_2$. The electrons of $FADH_2$ enter the oxidative phosphorylation chain at complex II.

⑯ Tetra methyl phenylene diamine (TMPD) is an artificial redox mediator which assists transfer of electrons from ascorbate to cytochrome c.

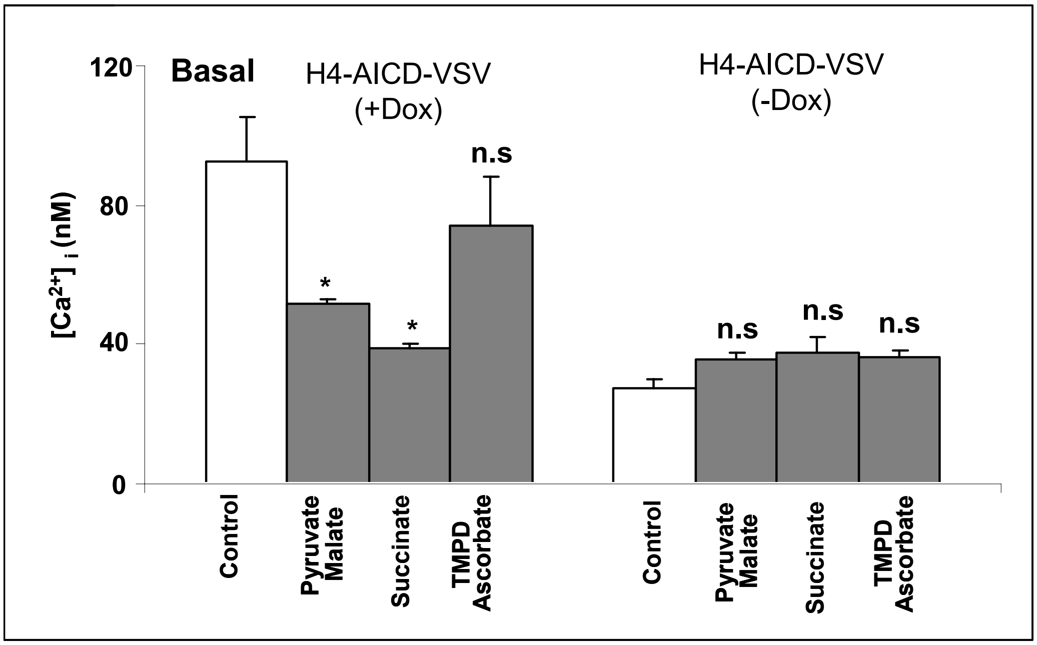

Fig. 6.19 Data shown here represents the mean values of basal (or resting) cytosolic Ca^{2+} concentration on treatment of *AICD-VSV* non-expressing (+Dox) cells. Pyruvate and malate (5 mM each for 1 hr in growth medium) was used as a substrate for complex I; methyl succinate (10 mM for 1 hr in growth medium) was used as a substrate for complex II; TMPD and ascorbate (200 µM and 1 mM respectively for 1 hr in growth medium) was used as a substrate for complex IV. *AICD-VSV* expressing cells (-Dox) were also analyzed in order to show that these responses were not due to non-specific effects of mitochondrial substrates. Ca^{2+} values were deduced from 340/380 nm ratio obtained by Ca^{2+} imaging of fura-2/AM loaded cells. The data represented here is mean ± SEM for 4 to 7 independent experiments. The number of cells analyzed were 55 to 65 cells per experiment. Statistical significance *, $p < 0.05$.

The CPA induced ER Ca^{2+} release was also found to be enhanced by succinate treatment to 455 ± 9 nM as compared to untreated AICD-VSV non-expressing (+Dox) H4 cells (312 ± 15 nM) (Fig 6.20). However, non-significant reversal was seen by the application of complex I and complex IV substrates (Fig 6.20). As a control, mitochondrial substrate treatment was also made on AICD-VSV expressing cells in order to examine that the application of substrates do not produce any non-specific effects. As shown in fig 6.19 and 6.20, a non-significant difference was found in these cells on substrate treatment.

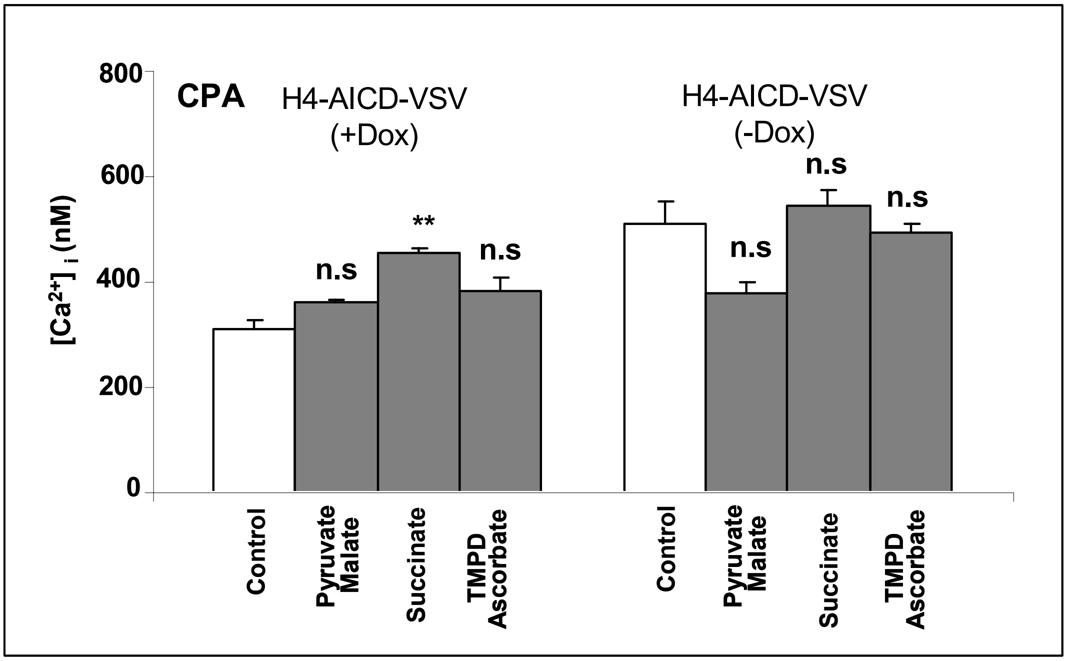

Fig. 6.20 Data shown here represents the mean values of CPA induced ER Ca^{2+} release on treatment of *AICD-VSV* non-expressing (+ Dox) and *AICD-VSV* expressing H4 cells. Pyruvate and malate (5 mM each for 1 hr in growth medium) was used as a substrate for complex I; methyl succinate (10 mM for 1 hr in growth medium) was used as a substrate for complex II; TMPD and ascorbate (200 µM and 1 mM respectively for 1 hr in growth medium) was used as a substrate for complex IV. Ca^{2+} values were deduced from 340/380 nm ratio obtained by Ca^{2+} imaging of fura-2/AM loaded cells. The data represented here is mean ± SEM for 4 to 7 independent experiments. The number of cells analyzed were 55 to 65 cells per experiment. Statistical significance *, $p < 0.05$.

Similar treatment of substrates were also made on *App*$^{0/0}$ astrocytes but only the succinate was found to reduce the basal Ca^{2+} to 56 ± 3 nM as compared to Wt astrocytes (74 ± 6 nM) (Fig. 6.21). The CPA induced Ca^{2+} release was also found to be enhanced to 460 ± 12 nM only by succinate treatment on *App*$^{0/0}$ astrocytes as compared to Wt astrocytes which showed 363 ± 10 nM of CPA induced Ca^{2+} release. Administration of pyruvate and malate (complex I substrates) and TMPD (complex IV substrates) on *App*$^{0/0}$ astrocytes showed non-significant differences in basal cytosolic Ca^{2+} levels as well as CPA induced ER Ca^{2+} release (Fig. 6.21).

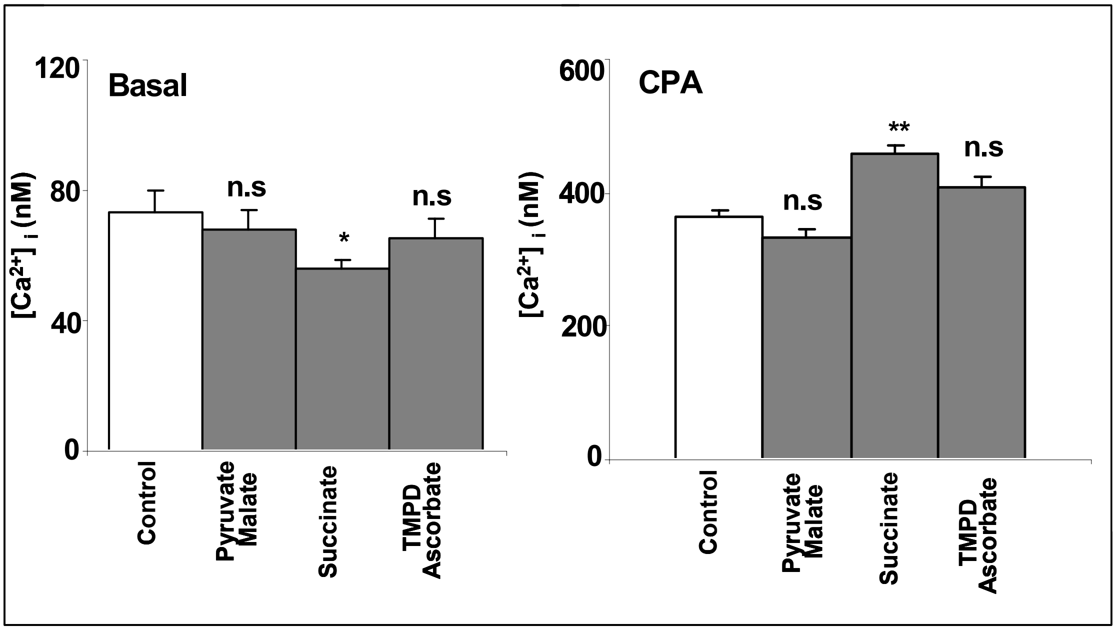

Fig 6.21: Left panel represents the mean value of basal cytosolic Ca^{2+} and right panel represents the CPA induced ER Ca^{2+} release in *App*$^{0/0}$ astrocytes on treatment with mitochondrial substrates analyzed by Ca^{2+} imaging. *App*$^{0/0}$ astrocytes were treated with pyruvate and malate (5 mM each for 1 hr in growth medium) as a substrate for complex I; methyl succinate (10 mM for 1 hr in growth medium) as a substrate for complex II; TMPD and ascorbate (200 µM and 1 mM respectively for 1 hr in growth medium) as a substrate for complex IV. The data represented here is mean ± SEM for 5 to 7 independent experiments. The number of cells analyzed were 35 to 40 cells per experiment. Statistical significance *, $p < 0.05$ and **, $p < 0.001$.

It is of interest to note here is that the alteration in Ca^{2+} recovered almost completely by substrates of complex II both in H4 cells lacking AICD-VSV and in *App*$^{0/0}$ astrocytes.

6.6 AICD was not detected in isolated mitochondria.

To gain insight into the control mechanisms by which AICD might affect mitochondrial function, the isolated mitochondria were analyzed for AICD by western blotting. As shown in fig. 6.22, no AICD-VSV was not detected in the

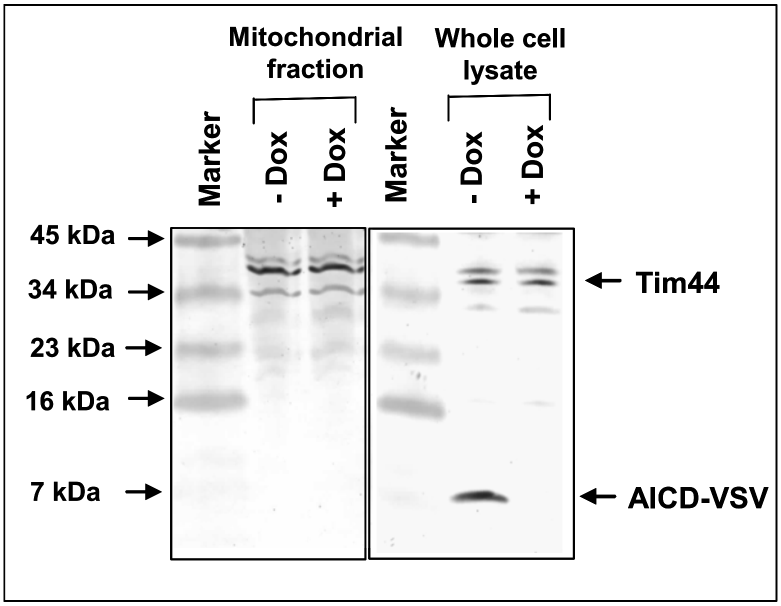

Fig. 6. 22: Western blot analysis of AICD-VSV in mitochondrial fraction and whole cell lysates of AICD-VSV expressing (-Dox) and non-expressing cells (+Dox). Cells were cultured to equal confluency under both conditions. Equal volume of mitochondrial fraction and whole cell lysates were loaded on 10-20% tricine-SDS gradient gel. AICD-VSV was detected by monoclonal anti-VSV antibody (1:10,000). Equal loading of sample was detected by anti-Tim44⑰ antibody (1:500). AICD-VSV was detected around 7 kDa and Tim-44 was detected around 42 kDa.

crude mitochondrial fraction while it was detected in the whole cell lysates of *AICD-VSV* expressing cells (-Dox).

In addition, subcellular fractions were also investigated for AICD-VSV by western blotting. As shown in fig. 6.23, a high amount of AICD-VSV was detected in nuclear pellet while it was not detected in post-nuclear supernatant (PNS) and post-mitochondrial supernatant (PMS). These results indicated that AICD is located in nucleus and might affect mitochondrial functioning via transcriptional regulation rather than its direct interaction.

---

⑰ Transport across the mitochondrial membrane requires translocation machinery. Such translocation complex in the inner membrane is called Tim complex (Translocator inner membrane) while on the outer membrane is called Tom complex (Translocator outer membrane) (Rapaport and Neupert, 1999; Davis et al., 2000)

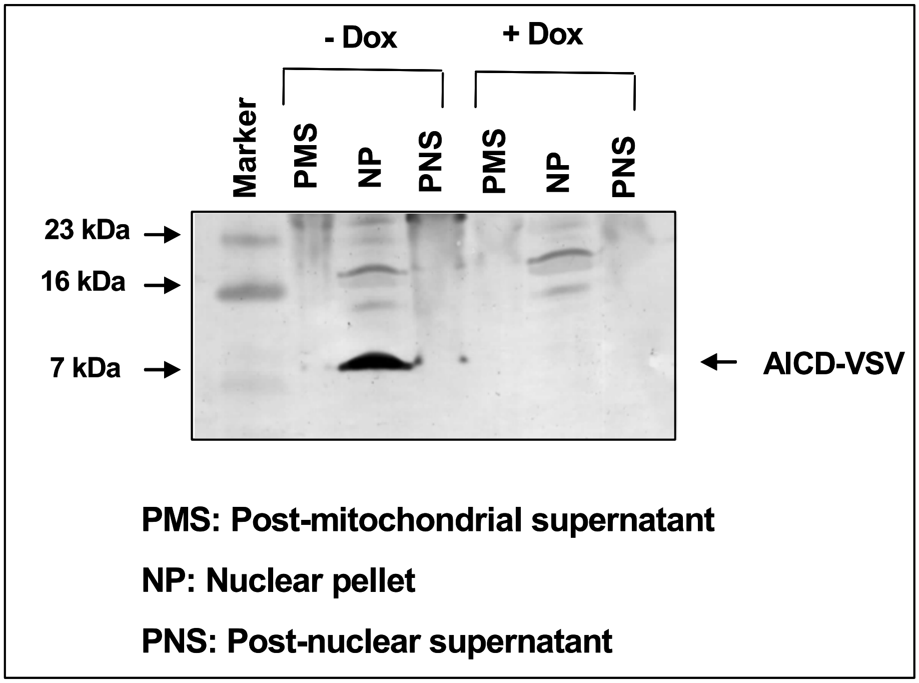
- Dox
+ Dox
Marker
PMS
NP
PNS
PMS
NP
PNS
23 kDa
16 kDa
7 kDa
AICD-VSV
PMS: Post-mitochondrial supernatant
NP: Nuclear pellet
PNS: Post-nuclear supernatant

Fig. 6.23: Western blot analysis of subcellular fractions of *AICD-VSV* expressing (-Dox) and non-expressing (+Dox) H4 cells. Protein estimation of each subcellular fraction was done by Bradford method and 60 µg protein was loaded on 10-20% tricine-SDS gel. AICD-VSV was detected by monoclonal anti-VSV antibody (1:10,000). The AICD-VSV was detected around 7 kDa.

6.7 Responses of cells lacking AICD was reversed on application of Li^{2+}

A recent study using an inducible expression system reveal that the AICD expression modulates expression of *GSK-3β* (von Rotz et al., 2004). The role of AICD in transcription of *GSK-3β* has also been observed in a study done in nuclear extracts of AICD transfected PC12 cells (Kim et al., 2003). Interestingly, the active form of GSK-3β has been found in mitochondria (Bijur and Jope, 2003) and is known to be an important modulator of mitochondrial function (Hoshi et al., 1996). Activation of GSK-3β is also known to decrease the transcription of

IP_3 receptor⑱ genes (Beals et al., 1997; Graef et al., 1999). All these reports prompted us to investigate if suppression of AICD modulates Ca^{2+} homeostasis through activation of GSK-3β⑲.

GSK-3β activity is regulated by its phosphorylation at Ser-9 or Tyr-216 residues. Phosphorylation of GSK-3β at Ser-9 position reduces its activity (Plyte et al., 1992) while phosphorylation at Tyr-216 residues enhances its activity (Hughes et al., 1993). Li^{2+} has been shown to be a direct, reversible inhibitor of GSK-3 with an IC_{50} value of nearly 2 mM (Klein and Melton, 1996), acting as a competitive inhibitor of Mg^{2+} (Ryves and Harwood, 2001). The principle of interaction between Li^{2+} and GSK-3 is that GSK-3 catalyses the phosphorylation of many protein substrates in the presence of Mg^{2+}- ATP.

As shown in fig. 6.24, administration of 5 mM Li^{2+} for 24 hours on AICD non-expressing (+Dox) H4 cells reduce the basal cytosolic Ca^{2+} levels to 47 ± 5 nM as compared to untreated cells (93 ± 13 nM). An enhanced CPA induced ER Ca^{2+} release (417 ± 15 nM) was also observed in these cells on treatment with 5 mM Li^{2+}. Treatment with 0.5 mM Li^{2+} and 2 mM Li^{2+} showed non-significant changes both in basal Ca^{2+} levels and in CPA induced ER Ca^{2+} release.

---

⑱ Inositol 1,4,5-triphosphate (IP_3) receptors are present on the ER membrane, the opening of which is regulated by both IP_3 and Ca^{2+}. These receptors allow rapid and regulated release of Ca^{2+} from the intracellular stores (Taylor and Laude, 2002).

⑲ Glycogen synthase kinase-3β (GSK-3β) is a serine/threonine kinase that phosphorylates glycogen synthase and downregulate its activity. Apart from glycogen synthase, GSK-3β has been shown to phosphorylate several other proteins *in vitro.* These include pyruvate dehydrogenase, β-catenin, ATP citrate lyase etc. (Frame and Cohen, 2001). Factors that promote cell survival, for instance growth factors, activate Akt which in turn phosphorylates GSK-3β at Ser-9, that leads to inactivation of its kinase activity. On the otherhand, mechanisms that promote cell death, for instance growth factor removal increase phosphorylation within the catalytic domain at Tyr-216 and stimulate kinase activity (Bhat et al., 2000).

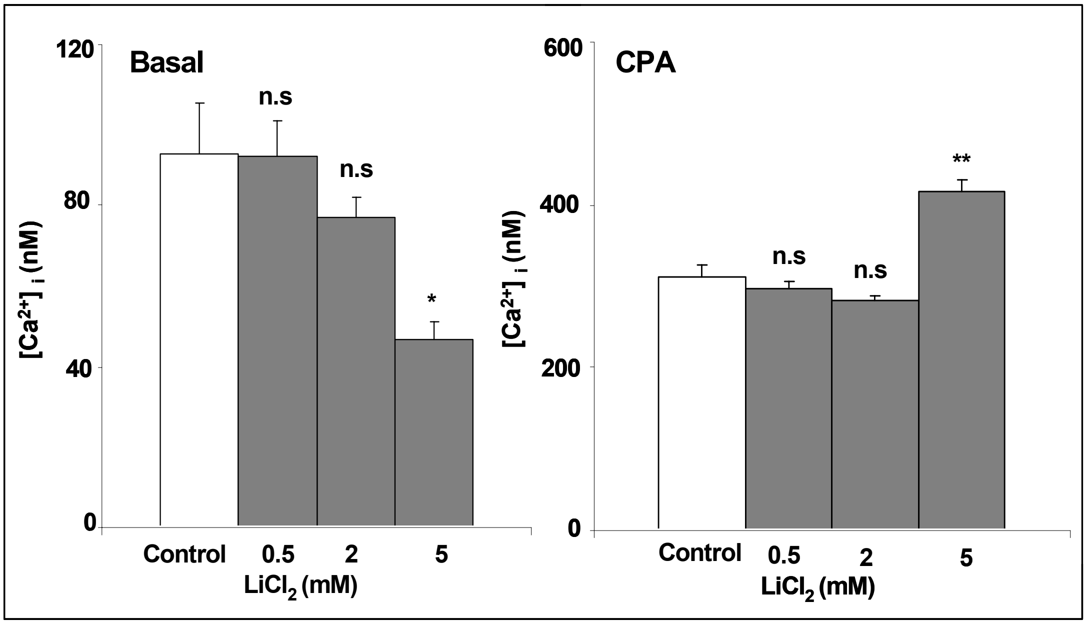

Fig. 6.24: Left panel shows basal cytosolic Ca^{2+} levels and right panel shows CPA induced ER Ca^{2+} release in *AICD-VSV* non-expressing cells (+ Dox) on treatment with $LiCl_2$ for 24 hrs. Cells were treated with 0.5, 2 and 5 mM $LiCl_2$ for 24 hrs in growth medium. Ca^{2+} values were deduced from 340/380 nm ratio obtained by fluorescence imaging of fura-2/AM loaded cells. CPA induced Ca^{2+} release is determined as area under the curve. The data represented here is mean ± SEM for 6 independent experiments. The number of cells determined were 65 to 75 cells per experiment. Statistical significance *, $p < 0.05$ and **, $p < 0.001$.

In addition, to investigate if GSK-3β expression or its phosphorylation at Tyr216 is dependent on AICD, the expression for both phosphorylated and total GSK-3β was analyzed by western blot in *AICD-VSV* expressing (-Dox) and non-expressing (+Dox) H4 cells (Fig. 6.25). As shown in fig 6.25, there were no differences observed in expression of both phosphorylated and non-phosphorylated forms of GSK-3β, indicating that its expression in either form is not dependent on AICD.

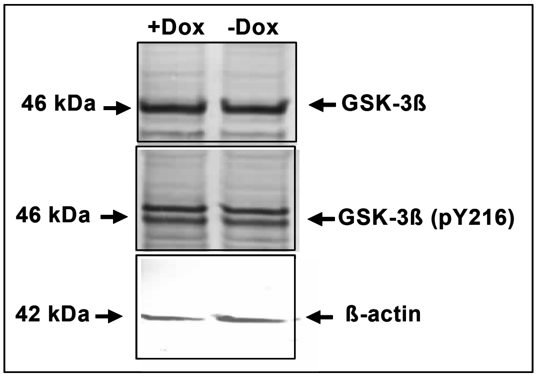

Fig. 6.23: Western blot showing GSK-3β (Upper) and phosphorylated GSK-3β (lower) expression in *AICD-VSV* expressing (-Dox) and non-expressing (+Dox) H4 cells. Cells were equally plated and cultured for two days in presence and absence of doxycycline (100 ng/ml). Equal volume of lysates was loaded on 10-20% tricine-SDS gel. Total GSK-3β and phosphorylated GSK-3β (pY216) was detected by mouse anti GSK-3β and phosphospecific GSK-3β (pY216) antibody (1:3000). Equal sample loading was analyzed by mouse anti β-actin antibody (1:2000). The GSK-3β fragment was detected at around 46 kDa. The band detected above the phosphorylated form (pY216) is the double phosphorylated GSK-3β i.e phosphorylated at both pY216 and pS9.

7 Discussion

7.1 AICD regulates cellular Ca^{2+} homeostasis

Genetic ablation of the presenilins or pharmacological inhibition of γ-secretase activity have been shown to attenuate phosphoinositide mediated Ca^{2+} signaling (Leissring et al., 2002). Such Ca^{2+} deficits were also observed in cells deficient in *APP*, and these deficits could be rescued by transfection with cDNA encoding either full length APP or other C-terminal deletion mutant containing an intact AICD domain (Leissring et al., 2002). The results reported in this thesis further confirm the critical role of AICD in modulating ER Ca^{2+} storage. Moreover, this work shows for the first time that the resting cytosolic Ca^{2+} is affected as a consequence of loss of AICD in addition to the previously described report which shows that ER Ca^{2+} storage is modulated (Leissring et al., 2002). This phenomenon was consistently observed in HEK293 cells that express *PS1* with the D385N mutation, in HEK293 cells that over express Insulin degrading enzyme (IDE) and in HEK293 cells that express APPsw treated with a potent γ-secretase inhibitor (Wolfe et al., 1999; Kimberly et al., 2000; Edbauer et al., 2002a). Similar observations were obtained in primary culture of *App* knock out astrocytes (*App*$^{0/0}$). As the AICD domain is also produced by the γ-secretase cleavage of other APP family members APLP1 and APLP2, therefore *App*$^{0/0}$ astrocytes were also analyzed in the presence of the γ-secretase inhibitor (DAPT) in addition (Scheinfeld et al., 2002). Treatment with DAPT further enhanced resting cytosolic Ca^{2+} levels and reduced CPA induced ER Ca^{2+} transients, strongly indicating the involvement of AICD as a crucial cleavage product of APP. Furthermore, to ascertain that the modulation observed in resting Ca^{2+} and ER Ca^{2+} storage was attributable to AICD, a “Tet-Off” system in H4 cells was used for the regulated expression of AICD with a VSV tag (AICD-VSV). Consistent with the results obtained in HEK293 cells and in astrocytes, strongly enhanced resting cytosolic Ca^{2+} levels and reduced ER Ca^{2+} release was observed in H4 cells where *AICD-VSV* expression was suppressed by doxycycline. However, H4 cells expressing only the regulator plasmid showed non-significant differences in the resting cytosolic Ca^{2+} levels in the presence or absence of doxycycline, both measured in the presence of DAPT. These cells, when analyzed in the absence of DAPT, exhibited normal basal Ca^{2+} levels and CPA induced ER Ca^{2+} release. This indicates that AICD produced endogenously is sufficient to maintain normal resting Ca^{2+} levels and ER storage. Moreover, these results suggest that the alteration of the Ca^{2+} storage by ER is not merely due to the alterations in the mechanism involved in ER Ca^{2+} release through the phosphoinositol cascade (evaluated by bradykinin induced Ca^{2+} release) as suggested previously (Leissring et al., 2002). Our study using CPA mediated induction of ER Ca^{2+} release by inhibiting Ca^{2+}ATPase shows a remarkably strong correlation of enhanced resting cytosolic Ca^{2+} and reduced ER Ca^{2+} release in AICD ablated cells . This supports the idea that there might be an alteration in the refilling mechanism of Ca^{2+} from the cytosol into the ER. In other words, these results favor the hypothesis that AICD affects Ca^{2+} uptake by the ER, possibly due to a modulation of activity of the Ca^{2+}ATPase located within the ER membrane.

7.2 AICD regulates Ca^{2+} buffering by ER through mitochondrial ATP generation

Ca^{2+} removal mechanism including Ca^{2+} reuptake by the ER from the cytosol is predominantly dependent on the ATP generation by mitochondria. To account for an enhanced cytosolic Ca^{2+} in cells lacking AICD, a direct measurement of ATP was carried out using bioluminescent ATP assay. This assay revealed that AICD-VSV non-expressing H4 cells and *App*$^{0/0}$ generate significantly lower amounts of ATP.

To confirm the hypothesis that the Ca^{2+} disturbances seen in cells lacking AICD are due to lower ATP generation, another set of experiments were carried out in which AICD-VSV expressing cells and wild type astrocytes were treated with oligomycin and sodium cyanide (NaCN). Both the conditions inhibit ATP generation. Oligomycin inhibits ATP synthase and NaCN inhibits electron transport through complex IV (cytochrome oxidase). Altering mitochondrial function by oligomycin and NaCN was found to alter the Ca^{2+} homeostasis in a similar manner as the depletion of AICD. However lack of AICD was found to have a stronger effect on the Ca^{2+} homeostasis than the total inhibition of mitochondrial function. This may be due to the fact that the action of the mitochondrial blocker was analyzed after an interval of one hour whereas the effect of a downregulation of AICD expression was analyzed after 48 hours.

Since cellular ATP generation is driven by mitochondrial membrane potential, therefore it was also analyzed in both AICD expressing H4 cells and in astrocytes. It was found that H4 cells that do not express *AICD-VSV* (+Dox) and $App^{0/0}$ exhibited a higher membrane potential or in other words the mitochondrial membrane was hyperpolarized. One possible explanation for this phenomenon is that the ATP synthase activity is reduced as a consequence of lack of AICD. A reduced ATP synthase activity and hyperpolarized mitochondrial membrane is a condition analogous to inhibition of ATP synthase by oligomycin. Oligomycin inhibits flow of protons through F_0 particle of ATP synthase eventually increasing mitochondrial membrane potential (Baracca et al., 2003).

Another point worth noting is that the application of substrate for complex II i.e. succinate efficiently normalizes Ca^{2+} disturbances. In general, substrates for complex II generate a significantly higher membrane potential than substrates for complex I (Nicholls, 1974). Complex II, also called succinate dehydrogenase, is the only enzyme of the respiratory complex that functions in two ways, one as a part of electron transport chain and second as a component of citric acid cycle. It oxidizes succinate to fumarate and generates $FADH_{2,}$ which serves to feed electrons to the respiratory chain. Application of high amounts of succinate might therefore enforce the ATP synthase to function in direction of ATP synthesis by further increasing mitochondrial membrane potential. However, further studies are required to reveal if lack of AICD indeed affects the mitochondrial ATP synthase.

7.3 AICD might regulate Ca^{2+} homeostasis and mitochondrial function through gene transcription.

AICD being a highly labile product of APP have been shown to be stabilized by binding of nuclear adaptor protein, Fe65 and translocate to nucleus. Fe65, in turn, interacts with the transcription factors CP2/LSF/LBP1 and a histone acetyltransferase, Tip60 (Fiore et al., 1995; Cao and Sudhof, 2001; Kimberly et al., 2001; Minopoli et al., 2001; Walsh et al., 2003). AICD complexed with Fe65 and Tip60 has been shown to potently regulate the expression of artificial expression constructs (minigenes) in transfected cells (Cao and Sudhof, 2001).

There could be several possible mechanisms by which AICD might modulate Ca^{2+} signaling and mitochondrial function. Numerous compelling evidences about the role of AICD in gene transcription add support to the hypothesis that AICD might affect Ca^{2+} signaling by regulating the expression of genes involved in Ca^{2+} homeostasis and energy production. Leissring et al. suggested that CP2/LSF/LBP1 response elements are present in the regulatory region of an ER Ca^{2+}ATPase, as revealed by BLAST search (Leissring et al., 2002). AICD has also been shown to induce the expression of GSK-3β at both mRNA and protein levels in neuronal cells (Kim et al., 2003). The active form of GSK-3β is also known to be an important modulator of mitochondrial function (Hoshi et al., 1996). To our surprise, administration of 5 mM Li^{2+} (a reversible inhibitor of GSK-3) for 24 hrs lowered the resting cytosolic Ca^{2+} levels and elevated the ER Ca^{2+} release in *AICD-VSV* non-expressing cells. However, in contrast to the results described by Kim et al., we found no differences both in total levels of GSK-3β and active form of GSK-3β (phosphorylated at Tyr216), between AICD-VSV expressing (-Dox) and non-expressing (+Dox) H4 cells at protein levels. This indicates that Li^{2+} produces a downstream effect that normalizes the resting cytosolic Ca^{2+} and ER Ca^{2+} release in cells lacking AICD, independent of GSK-3β.

Cloning and sequencing the *APP* gene revealed a -GYENPTY- motif in the cytoplasmic tail. Multiple sequence alignment of the cytoplasmic tail of APP reveals that only the -GYENPTY- motif is 100% conserved from C.*elegans* to human, suggesting a significant role of this domain. Subsequent mutational analysis defined the -YENP- sequence as the critical tetrapeptide motif for APP internalization (Perez et al., 1999). The -GYENPTY- sequence is also a consensus motif for the binding of adaptor proteins that possess a phosphotyrosine binding (PTB) domain, such as those in the Fe65, X11 and JIP families. A recent report provides strong evidence in favour of nuclear signaling functions of AICD and shows that these functions are regulated by the APP adaptor proteins Fe65, Jip1b and X11-α as well as the nuclear docking protein Tip60. This report also shows that AICD regulates the expression of *APP* gene in a positive feedback mechanism. In otherwords, endoproteolysis of APP upregulates its own expression eventually replenishing full length APP (von Rotz et al., 2004). It has also been reported that Fe65 on binding with the NPTY domain of AICD interacts with Mena (Ermekova et al., 1997). Mena is a cytoskeletal protein involved in microfilament assembly and cell motility. It is also found in areas of dynamic actin remodeling such as axonal growth cones (Gertler et al., 1996). Interestingly, hippocampal neurons derived from *App* knockout mice have reduced neuritic branching and outgrowth (Perez et al., 1997), suggesting an involvement of the APP/Fe65/Mena protein complex. In addition, the cytoplasmic domain of APP (AICD) interacts with other adaptor proteins like X11, BP1 (APP binding protein 1), ShcA (SH2 domain containing transforming protein 1), SHcC, PAT1 (protein that interacts with APP tail 1), JNK interacting protein, and disabled 1 (Fiore et al., 1995; Chow et al., 1996; Borg et al., 1996; Tanahashi and Tabira, 1999; Homayouni et al., 1999; Gao and Pimplikar, 2001; Matsuda et al., 2001). All of these evidences suggest a critical role for AICD in gene regulation and intracellular signaling pathways.

However, identifying which genes are regulated by AICD is another major question of future research. In view of AICD controlling gene expression, it is possible to envision that signaling through APP could influence Ca^{2+} dependent processes such as cellular differentiation, neurite outgrowth and synaptic plasticity.

7.4 AICD might regulate mitochondrial function directly

In support of direct interaction of AICD with mitochondria, recent reports indicate the location of APP, its cleavage and its degradation components in mitochondria. Full length APP has been shown to be targeted to the mitochondria in a transmembrane arrested topology in neuronal cells. The C-terminal domain of APP faces the cytoplasmic side and causes the transmembrane arrest. The transmembrane arrested APP is either in direct contact with, or traversing through the TOM40 translocase (a translocator of mitochondrial protein) (Anandatheerthavarada et al., 2003). In addition to APP, active γ-secretase complex and IDE are also reported to be present in mitochondria (Leissring et al., 2004; Hansson et al., 2004). On the contrary, our study in subcellular fractions in AICD-VSV expression system indicates that AICD is not present in mitochondria. Its detection in nuclear pellet supports the previously described report indicating its role in gene transcription (Cao and Sudhof, 2001). Whether or not AICD regulates mitochondrial function by transcriptional regulation needs to be further investigated. Since all components i.e. APP, active γ-secretase complex and IDE have been shown to be present in the mitochondria, one cannot completely rule out the possibility of its direct involvement.

7.5 AICD and Alzheimer’s Disease

Alzheimer’s disease is characterized by synaptic dysfunction and excitotoxicity leading to the death of neurons. Several evidences suggest that these neurodegenerative processes involve mechanisms that alter cellular Ca^{2+} homeostasis (Harkany et al., 2000). Mitochondrial based energy deficits have also been implicated in the pathophysiology of AD (Sullivan and Brown, 2005).

It is a well described fact that pathogenic mutations in presenilin, which cause FAD enhance the production of the highly amyloidogenic Aβ42. FAD mutations in PS1 have also been shown to modulate Ca^{2+} signaling in a variety of systems, including fibroblasts from FAD patients, mutant presenilin “knock in“ mice, transgenic mice, transfected PC12 cells and xenopus oocyte (Ito et al., 1994;

Guo et al., 1996; Guo et al., 1997; Gibson et al., 1997; Etcheberrigaray et al., 1998; Begley et al., 1999; Leissring et al., 1999b; Guo et al., 1999b; Herms et al., 2003). A report by Chen et al. shows that although presenilin mutations augment γ-secretase cleavage at residue 42 (generating Aβ42), they infact suppress ε-cleavage ⑳ of APP generating AICD (Chen et al., 2002). This report supports the notion that PS1 mutation causing early onset of familial Alzheimer's disease (EOFAD) and disturbances in Ca^{2+} homeostasis might be a consequence of loss of AICD. An increased BACE1 (β-secretase) expression and activity has also been shown in the sporadic AD brain (Holsinger et al., 2002; Yang et al., 2003). Recently it has been shown that elevated β-secretase (BACE) levels induced the increase of C99 and Aβ generation but reduced C83 and AICD generation *in vitro* (Kume et al., 2004). These reports link decreased AICD levels also to sporadic AD. All these evidences lead to speculate that AICD might be the underlying cleavage product of APP, suppression of which cause cellular disturbances in AD. In addition to Ca^{2+} disturbances found in AD, the disease is also characterized by mitochondrial defect and deficits in energy production. Our results revealed that *AICD-VSV* non-expressing cells (+Dox) and *App*$^{0/0}$ astrocytes exhibits 56% and 53% reduced ATP generation, respectively, as evaluated by bioluminescent ATP assay. These results link to a previously described report by Hoyer et al. showing a decrease in ATP production from glucose by around 50% in the first stages of sporadic AD. The oxidative utilization of substrates other than glucose restores ATP formation to 80% of normal, but thereafter ATP levels decrease throughout the course of the disease (Hoyer, 1992). A fall in ATP formation in the sporadic AD brain has also been demonstrated by other investigators (Sims et al., 1983b; Brown et al., 1989). This energy deficit may compromise ATP dependent processes. For instance, a depletion of cellular ATP levels prevents the dissociation of chaperons/protein complexes and thus blocks secretion of these

---

⑳ Weidemann et al. have referred to the cleavages of APP C-terminal domain at residues 40-42 as γ-secretase cleavage and the cleavages at residues 49-52 as ε-cleavage (Wiedemann et al., 2002). The authors Chen et al. have retained the same terminology. However, the relation between γ- and ε-cleavage is unknown till date.

proteins (Dorner et al., 1990). Misfolded or malfolded protein complexes accumulate in the ER and are indicative of “endoplasmatic reticulum stress” (Kaufman, 1999). Alternatively, deficits in ATP production due to the loss of AICD can be transiently balanced by the cell by the utilization of endogenous substrates like amino acids and fatty acids to meet the energy demand. However, it has been described earlier that in EOFAD, glucoplastic amino acids, in particular glutamate, are used for energy formation to maintain ATP concentrations at a normal level. As a side effect of glutamate utilization, neurotoxic ammonia is formed in the brain and inhibits mitochondrial dehydrogenases such as α-ketoglutarate dehydrogenase, isocitrate dehydrogenase and malate dehydrogenase (Hoyer et al., 1990; Lai and Cooper, 1991). In addition to this, a reduced activity of pyruvate dehydrogenase (the enzyme that converts pyruvate to acetyl-CoA in mitochondria) has been found in the brain of AD patients (Perry et al., 1980; Sorbi et al., 1983). This effect can be related to other major symptoms of AD, as reduced pyruvate dehydrogenase activity results in a decreased level of acetyl-CoA, and together with a diminished activity of choline acetyl transferase, the synthesis of acetylcholine in the presynaptic neuron is markedly reduced (Sims et al., 1983a). In this respect, it is noteworthy that the degradation of the cholinergic system correlates with the progression of mental disturbances in patients with AD (Baskin et al., 1999). A decreased concentration of acetyl-CoA may also decrease the formation of intracellular cholesterol (Michikawa and Yanagisawa, 1999). Cholesterol is the main sterol in membranes and is important for the normal cell function. Cholesterol levels are markedly decreased in brain membranes and in the cerebrospinal fluid (CSF) of patients with AD (Svennerholm and Gottfries, 1994; Mulder et al., 1998; Eckert et al., 2000). Another study done in brain samples of AD patients shows a 50%-60% decrease in mRNA levels of nuclear DNA that encodes subunit IV of cytochrome oxidase and the beta-subunit of the F_0F_1-ATP synthase (Chandrasekaran et al., 1997).

Based on earlier studies described in the discussion and the results obtained in this thesis work, a hypothetical model is drawn that illustrate a possible link of reduced AICD generation to AD (Fig. 7.1).

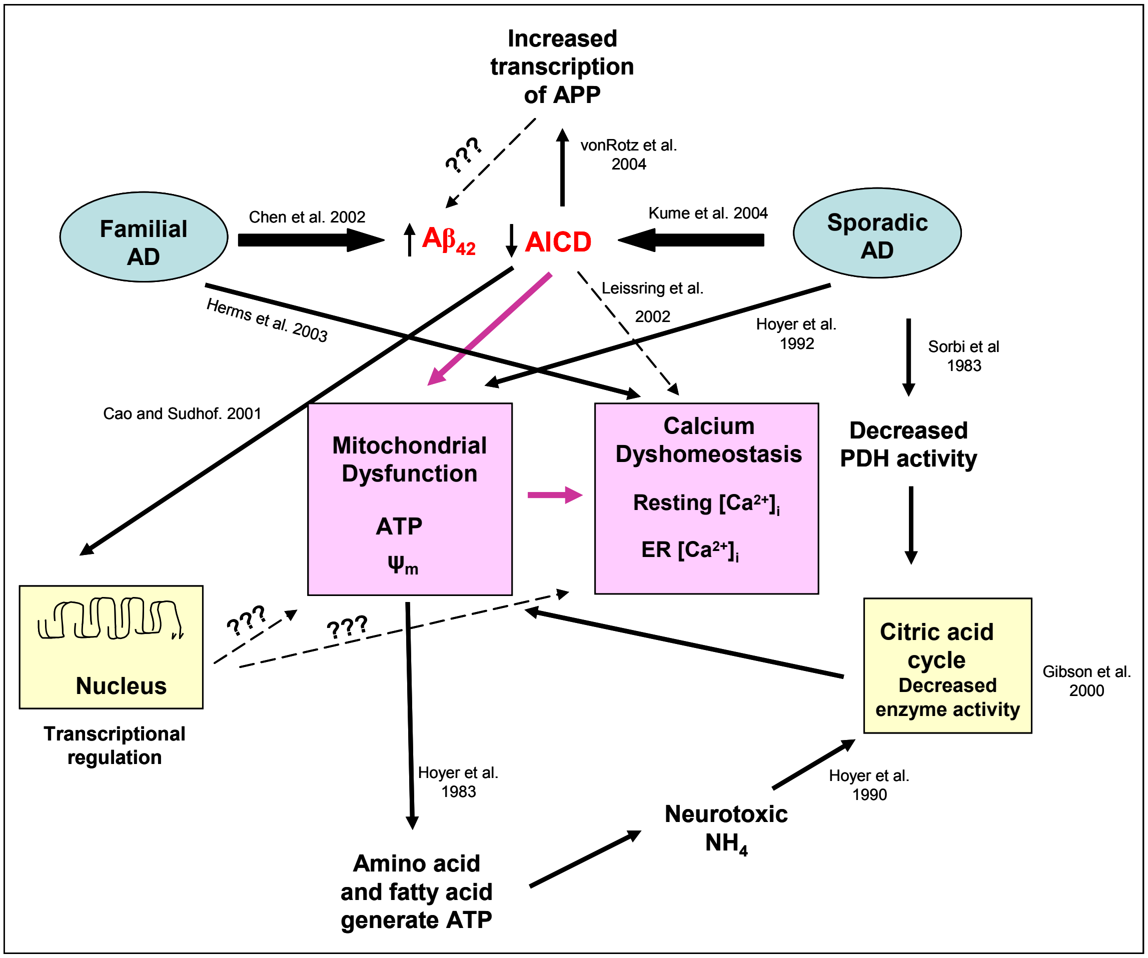
Increased transcription of APP
???
vonRotz et al. 2004
Familial AD
Chen et al. 2002
↑ Aβ42
↓ AICD
Kume et al. 2004
Sporadic AD
Herms et al. 2003
Leissring et al. 2002
Hoyer et al. 1992
Sorbi et al 1983
Cao and Sudhof. 2001
Mitochondrial Dysfunction
ATP
Ψm
Calcium Dyshomeostasis
Resting [Ca2+]i
ER [Ca2+]i
Decreased PDH activity
Nucleus
Transcriptional regulation
???
???
Citric acid cycle
Decreased enzyme activity
Gibson et al. 2000
Hoyer et al. 1983
Hoyer et al. 1990
Neurotoxic NH4
Amino acid and fatty acid generate ATP

Fig 7.1: Hypothetical model of the etiological role of AICD in AD. Both familial and sporadic forms of AD have been shown to produce decreased levels of AICD. Suppression of AICD leads to disturbed Ca^{2+} homeostasis which is proposed to be due to mitochondrial dysfunction and deficits in ATP production. Progress of sporadic AD leads to reduced ATP levels either due to decreased activity of pyruvate dehydrogenase (PDH) or decrease in the activity of other enzymes of the citric acid cycle. Reduced ATP generation through oxidation of glucose leads to oxidation of non-carbohydrate precursors as an alternate source of ATP. Oxidation of amino acids produce toxic ammonia which also reduces enzymatic activity of citric acid cycle enzymes. The energy deficits due to mitochondrial dysfunction might lead to perturbances in Ca^{2+} homeostasis. AICD also regulates the expression of APP in a positive feedback mechanism and might lead to enhanced production of Aβ42 in diseased condition. Alternatively, AICD might transcriptionally regulate certain genes that are vital for mitochondrial functioning and Ca^{2+} homeostasis.

7.6 Consequences of gamma secretase inhibitors as therapeutic drug targets for Alzheimer's disease

The existence of pathogenic mutations in *APP* and *PS* genes provides a strong support that Aβ production and deposition contribute to the etiology of AD. The most direct approach to reduce the amyloid levels is to control the production by inhibiting γ-secretase that liberates the Aβ peptide from the precursor. It should be noted that γ-secretase appears to have more substrates and cleavage products, for instance the production of AICD besides producing Aβ. Studies done in this thesis work implicate an important function of AICD in maintaining cellular Ca^{2+} homeostasis and energy production. Therefore, discovery of drugs that can selectively inhibit Aβ without disrupting the production of AICD or inhibit the generation of Aβ42 rather than Aβ40 needs to be developed.

In the light of these functions of AICD and the universal importance of Ca^{2+} as the major intracellular signaling cation, the therapeutic use of γ-secretase inhibitors for prevention of AD needs to be carefully evaluated.

8 Literature

Alzheimer, A. (1907). Über eine eigenartige Erkrankung der Hirnrinde. Allg. Zeitschr. Psychiatr. Psychiatr-Gerichtl. Med. *109*, 146-148.

Alzheimer, A., Stelzmann, R.A., Schnitzlein, H.N., and Murtagh, F.R. (1995). An English translation of Alzheimer's 1907 paper, "Uber eine eigenartige Erkankung der Hirnrinde". Clin. Anat. *8*, 429-431.

Anandatheerthavarada, H.K., Biswas, G., Robin, M.A., and Avadhani, N.G. (2003). Mitochondrial targeting and a novel transmembrane arrest of Alzheimer's amyloid precursor protein impairs mitochondrial function in neuronal cells. J. Cell Biol. *161*, 41-54.

Anderson, J.P., Esch, F.S., Keim, P.S., Sambamurti, K., Lieberburg, I., and Robakis, N.K. (1991). Exact cleavage site of Alzheimer amyloid precursor in neuronal PC-12 cells. Neurosci. Lett. *128*, 126-128.

Annaert, W.G., Levesque, L., Craessaerts, K., Dierinck, I., Snellings, G., Westaway, D., George-Hyslop, P.S., Cordell, B., Fraser, P., and De Strooper, B. (1999). Presenilin 1 controls gamma-secretase processing of amyloid precursor protein in pre-golgi compartments of hippocampal neurons. J. Cell Biol. *147*, 277-294.

Antaramian, A., Butanda-Ochoa, A., Vazquez-Martinez, O., Diaz-Munoz, M., and Vaca, L. (2001). Functional expression of recombinant type 1 ryanodine receptor in insect cells. Cell Calcium *30*, 9-17.

Arai, H., Lee, V.M., Messinger, M.L., Greenberg, B.D., Lowery, D.E., and Trojanowski, J.Q. (1991). Expression patterns of beta-amyloid precursor protein (beta-APP) in neural and nonneural human tissues from Alzheimer's disease and control subjects. Ann. Neurol. *30*, 686-693.

Baracca, A., Sgarbi, G., Solaini, G., and Lenaz, G. (2003). Rhodamine 123 as a probe of mitochondrial membrane potential: evaluation of proton flux through F(0) during ATP synthesis. Biochim. Biophys. Acta *1606*, 137-146.

Barrow, P.A., Empson, R.M., Gladwell, S.J., Anderson, C.M., Killick, R., Yu, X., Jefferys, J.G., and Duff, K. (2000). Functional phenotype in transgenic mice expressing mutant human presenilin-1. Neurobiol. Dis. *7*, 119-126.

Baskin, D.S., Browning, J.L., Pirozzolo, F.J., Korporaal, S., Baskin, J.A., and Appel, S.H. (1999). Brain choline acetyltransferase and mental function in Alzheimer disease. Arch. Neurol. *56*, 1121-1123.

Beals, C.R., Sheridan, C.M., Turck, C.W., Gardner, P., and Crabtree, G.R. (1997). Nuclear export of NF-ATc enhanced by glycogen synthase kinase-3. Science *275*, 1930-1934.

Begley, J.G., Duan, W., Chan, S., Duff, K., and Mattson, M.P. (1999). Altered calcium homeostasis and mitochondrial dysfunction in cortical synaptic compartments of presenilin-1 mutant mice. J. Neurochem. *72*, 1030-1039.

Berridge, M.J. (1993). Cell signalling. A tale of two messengers. Nature *365*, 388-389.

Berridge, M.J., Bootman, M.D., and Lipp, P. (1998). Calcium--a life and death signal. Nature *395*, 645-648.

Berridge, M.J., Lipp, P., and Bootman, M.D. (2000). The versatility and universality of calcium signalling. Nat. Rev. Mol. Cell Biol. *1*, 11-21.

Bhat, R.V., Shanley, J., Correll, M.P., Fieles, W.E., Keith, R.A., Scott, C.W., and Lee, C.M. (2000). Regulation and localization of tyrosine216 phosphorylation of glycogen synthase kinase-3beta in cellular and animal models of neuronal degeneration. Proc. Natl. Acad. Sci. U. S. A *97*, 11074-11079.

Bijur, G.N. and Jope, R.S. (2003). Glycogen synthase kinase-3 beta is highly activated in nuclei and mitochondria. Neuroreport *14*, 2415-2419.

Birnboim, H.C. and Doly, J. (1979). A rapid alkaline extraction procedure for screening recombinant plasmid DNA. Nucleic acids Res. 7, 1513-1523.

Blaustein, M.P. and Lederer, W.J. (1999). Sodium/calcium exchange: its physiological implications. Physiol. Rev. *79*, 763-854.

Bogenhagen, D., and Clayton, D.A. (1974). The number of mitochondrial deoxyribonucleic acid genomes in mouse L and human HeLa cells: Quantitative isolation of mitochondrial deoxyribonucleic acid. J. Biol. Chem. *249*, 7991-7995.

Borg, J.P., Ooi, J., Levy, E., and Margolis, B. (1996). The phosphotyrosine interaction domains of X11 and FE65 bind to distinct sites on the YENPTY motif of amyloid precursor protein. Mol. Cell. Biol. *16*, 6229-6241.

Bradford, M.M. (1976). A rapid and sensitive method for the quantitation of microgram quantities of protein utilizing the principle of protein-dye binding. Anal. Biochem. *72*, 248-254.

Bronfman, F.C., Garrido, J., Alvarez, A., Morgan, C., and Inestrosa, N.C. (1996). Laminin inhibits amyloid-beta-peptide fibrillation. Neurosci. Lett. *218*, 201-203.

Brown, G.G., Levine, S.R., Gorell, J.M., Pettegrew, J.W., Gdowski, J.W., Bueri, J.A., Helpern, J.A., and Welch, K.M. (1989). In vivo 31P NMR profiles of Alzheimer's disease and multiple subcortical infarct dementia. Neurology *39*, 1423-1427.

Busciglio, J., Gabuzda, D.H., Matsudaira, P., and Yankner, B.A. (1993). Generation of beta-amyloid in the secretory pathway in neuronal and nonneuronal cells. Proc. Natl. Acad. Sci. U. S. A *90*, 2092-2096.

Butterworth, R.F. and Besnard, A.M. (1990). Thiamine-dependent enzyme changes in temporal cortex of patients with Alzheimer's disease. Metabolic Brain Dis. *5*, 179-184.

Buxbaum, J.D., Liu, K.N., Luo, Y., Slack, J.L., Stocking, K.L., Peschon, J.J., Johnson, R.S., Castner, B.J., Cerretti, D.P., and Black, R.A. (1998). Evidence that tumor necrosis factor alpha converting enzyme is involved in regulated alpha-secretase cleavage of the Alzheimer amyloid protein precursor. J. Biol. Chem. *273*, 27765-27767.

Cai, H., Wang, Y., McCarthy, D., Wen, H., Borchelt, D.R., Price, D.L., and Wong, P.C. (2001). BACE1 is the major beta-secretase for generation of Abeta peptides by neurons. Nat. Neurosci. *4*, 233-234.

Cai, X.D., Golde, T.E., and Younkin, S.G. (1993). Release of excess amyloid beta protein from a mutant amyloid beta protein precursor. Science *259*, 514-516.

Cao, X. and Sudhof, T.C. (2001). A transcriptionally [correction of transcriptively] active complex of APP with Fe65 and histone acetyltransferase Tip60. Science *293*, 115-120.

Capell, A., Steiner, H., Romig, H., Keck, S., Baader, M., Grim, M.G., Baumeister, R., and Haass, C. (2000). Presenilin-1 differentially facilitates endoproteolysis of the beta-amyloid precursor protein and Notch. Nat. Cell Biol. *2*, 205-211.

Capell, A., Beher, D., Prokop, S., Steiner, H., Kaether, C., Shearman, M.S., and Haass, C. (2005). Gamma-secretase complex assembly within the early secretory pathway. J. Biol. Chem. *280*, 6471-6478.

Carafoli, E. (2003). Historical review: mitochondria and calcium: ups and downs of an unusual relationship. Trends Biochem. Sci. *28*, 175-181.

Casley, C.S., Land, J.M., Sharpe, M.A., Clark, J.B., Duchen, M.R., and Canevari, L. (2002). Beta-amyloid fragment 25-35 causes mitochondrial dysfunction in primary cortical neurons. Neurobiol. Dis. *10*, 258-267.

Chandrasekaran, K., Hatanpaa, K., Rapoport, S.I., and Brady, D.R. (1997). Decreased expression of nuclear and mitochondrial DNA-encoded genes of oxidative phosphorylation in association neocortex in Alzheimer disease. Brain Res. Mol. Brain Res. *44*, 99-104.

Checler, F. (1995). Processing of the beta-amyloid precursor protein and its regulation in Alzheimer's disease. J. Neurochem. *65*, 1431-1444.

Chen, F., Gu, Y., Hasegawa, H., Ruan, X., Arawaka, S., Fraser, P., Westaway, D., Mount, H., and George-Hyslop, P. (2002). Presenilin 1 mutations activate gamma 42-secretase but reciprocally inhibit epsilon-secretase cleavage of amyloid precursor protein (APP) and S3-cleavage of notch. J. Biol. Chem. *277*, 36521-36526.

Chow, N., Korenberg, J.R., Chen, X.N., and Neve, R.L. (1996). APP-BP1, a novel protein that binds to the carboxyl-terminal region of the amyloid precursor protein. J. Biol. Chem. *271*, 11339-11346.

Citron, M., Oltersdorf, T., Haass, C., McConlogue, L., Hung, A.Y., Seubert, P., Vigo-Pelfrey, C., Lieberburg, I., and Selkoe, D.J. (1992). Mutation of the beta-amyloid precursor protein in familial Alzheimer's disease increases beta-protein production. Nature *360*, 672-674.

Citron, M., Teplow, D.B., and Selkoe, D.J. (1995). Generation of amyloid beta protein from its precursor is sequence specific. Neuron *14*, 661-670.

Cook, D.G., Forman, M.S., Sung, J.C., Leight, S., Kolson, D.L., Iwatsubo, T., Lee, V.M., and Doms, R.W. (1997). Alzheimer's A beta(1-42) is generated in the endoplasmic reticulum/intermediate compartment of NT2N cells. Nat. Med. *3*, 1021-1023.

Daigle, I. and Li, C. (1993). apl-1, a Caenorhabditis elegans gene encoding a protein related to the human beta-amyloid protein precursor. Proc. Natl. Acad. Sci. U. S. A *90*, 12045-12049.

De Strooper, B., Saftig, P., Craessaerts, K., Vanderstichele, H., Guhde, G., Annaert, W., Von Figura, K., and Van Leuven, F. (1998). Deficiency of presenilin-1 inhibits the normal cleavage of amyloid precursor protein. Nature *391*, 387-390.

De Strooper, B. and Annaert, W. (2000). Proteolytic processing and cell biological functions of the amyloid precursor protein. J. Cell Sci. *113 (Pt 11)*, 1857-1870.

Dickson, D.W. (1997). The pathogenesis of senile plaques. J. Neuropathol. Exp. Neurol. *56*, 321-339.

Dorner, A.J., Wasley, L.C., and Kaufman, R.J. (1990). Protein dissociation from GRP78 and secretion are blocked by depletion of cellular ATP levels. Proc. Natl. Acad. Sci. U. S. A *87*, 7429-7432.

Dovey, H.F., John, V., Anderson, J.P., Chen, L.Z., de Saint, A.P., Fang, L.Y., Freedman, S.B., Folmer, B., Goldbach, E., Holsztynska, E.J., Hu, K.L., Johnson-Wood, K.L., Kennedy, S.L., Kholodenko, D., Knops, J.E., Latimer, L.H., Lee, M., Liao, Z., Lieberburg, I.M., Motter, R.N., Mutter, L.C., Nietz, J., Quinn, K.P., Sacchi, K.L., Seubert, P.A., Shopp, G.M., Thorsett, E.D., Tung, J.S., Wu, J., Yang, S., Yin, C.T., Schenk, D.B., May, P.C., Altstiel, L.D., Bender, M.H., Boggs, L.N., Britton, T.C., Clemens, J.C., Czilli, D.L., Dieckman-McGinty, D.K., Droste, J.J., Fuson, K.S., Gitter, B.D., Hyslop, P.A., Johnstone, E.M., Li, W.Y., Little, S.P., Mabry, T.E., Miller, F.D., and Audia, J.E. (2001). Functional gamma-secretase inhibitors reduce beta-amyloid peptide levels in brain. J. Neurochem. *76*, 173-181.

Dower, W.J., Miller, J.F., and Ragsdale, C.W. (1988). High efficiency transformation of E. coli by high voltage electroporation. Nucleic acids Res. *16*, 6127-6145.

Duchen, M.R. (1999). Contributions of mitochondria to animal physiology: from homeostatic sensor to calcium signalling and cell death. J. Physiol. *516 (Pt 1)*, 1-17.

Eckert, G.P., Cairns, N.J., Maras, A., Gattaz, W.F., and Muller, W.E. (2000). Cholesterol modulates the membrane-disordering effects of beta-amyloid peptides in the hippocampus: specific changes in Alzheimer's disease. Dement. Geriatr. Cogn. Disord. *11*, 181-186.

Edbauer, D., Willem, M., Lammich, S., Steiner, H., and Haass, C. (2002a). Insulin-degrading enzyme rapidly removes the beta-amyloid precursor protein intracellular domain (AICD). J. Biol. Chem. *277*, 13389-13393.

Edbauer, D., Winkler, E., Haass, C., and Steiner, H. (2002b). Presenilin and nicastrin regulate each other and determine amyloid beta-peptide production via complex formation. Proc. Natl. Acad. Sci. U. S. A *99*, 8666-8671.

Edbauer, D., Winkler, E., Regula, J.T., Pesold, B., Steiner, H., and Haass, C. (2003). Reconstitution of gamma-secretase activity. Nat. Cell Biol. *5*, 486-488.

Ermekova, K.S., Zambrano, N., Linn, H., Minopoli, G., Gertler, F., Russo, T., and Sudol, M. (1997). The WW domain of neural protein FE65 interacts with proline-rich motifs in Mena, the mammalian homolog of Drosophila enabled. J. Biol. Chem. *272*, 32869-32877.

Ertekin-Taner, N., Graff-Radford, N., Younkin, L.H., Eckman, C., Adamson, J., Schaid, D.J., Blangero, J., Hutton, M., and Younkin, S.G. (2001). Heritability of plasma amyloid beta in typical late-onset Alzheimer's disease pedigrees. Genet. Epidemiol. *21*, 19-30.

Esch, F.S., Keim, P.S., Beattie, E.C., Blacher, R.W., Culwell, A.R., Oltersdorf, T., McClure, D., and Ward, P.J. (1990). Cleavage of amyloid beta peptide during constitutive processing of its precursor. Science *248*, 1122-1124.

Esler, W.P. and Wolfe, M.S. (2001). A portrait of Alzheimer secretases--new features and familiar faces. Science *293*, 1449-1454.

Etcheberrigaray, R., Hirashima, N., Nee, L., Prince, J., Govoni, S., Racchi, M., Tanzi, R.E., and Alkon, D.L. (1998). Calcium responses in fibroblasts from asymptomatic members of Alzheimer's disease families. Neurobiol. Dis. *5*, 37-45.

Evans, D.A., Funkenstein, H.H., Albert, M.S., Scherr, P.A., Cook, N.R., Chown, M.J., Hebert, L.E., Hennekens, C.H., and Taylor, J.O. (1989). Prevalence of Alzheimer's disease in a community population of older persons. Higher than previously reported. J. Am. Med. Assoc. *262*, 2551-2556.

Fiore, F., Zambrano, N., Minopoli, G., Donini, V., Duilio, A., and Russo, T. (1995). The regions of the Fe65 protein homologous to the phosphotyrosine interaction/phosphotyrosine binding domain of Shc bind the intracellular domain of the Alzheimer's amyloid precursor protein. J. Biol. Chem. *270*, 30853-30856.

Fisher, S., Gearhart, J.D., and Oster-Granite, M.L. (1991). Expression of the amyloid precursor protein gene in mouse oocytes and embryos. Proc. Natl. Acad. Sci. U. S. A *88*, 1779-1782.

Forloni, G., Demicheli, F., Giorgi, S., Bendotti, C., and Angeretti, N. (1992). Expression of amyloid precursor protein mRNAs in endothelial, neuronal and glial cells: modulation by interleukin-1. Brain Res. Mol. Brain Res. *16*, 128-134.

Frame, S. and Cohen, P. (2001). GSK3 takes centre stage more than 20 years after its discovery. Biochem. J. *359*, 1-16.

Francis, R., McGrath, G., Zhang, J., Ruddy, D.A., Sym, M., Apfeld, J., Nicoll, M., Maxwell, M., Hai, B., Ellis, M.C., Parks, A.L., Xu, W., Li, J., Gurney, M., Myers, R.L.,

Franzini-Armstrong, C. and Protasi, F. (1997). Ryanodine receptors of striated muscles: a complex channel capable of multiple interactions. Physiol. Rev. *77*, 699-729.

Gao, Y. and Pimplikar, S.W. (2001). The gamma -secretase-cleaved C-terminal fragment of amyloid precursor protein mediates signaling to the nucleus. Proc. Natl. Acad. Sci. U. S. A *98*, 14979-14984.

Gertler, F.B., Niebuhr, K., Reinhard, M., Wehland, J., and Soriano, P. (1996). Mena, a relative of VASP and Drosophila Enabled, is implicated in the control of microfilament dynamics. Cell *87*, 227-239.

Gibson, G.E., Zhang, H., Toral-Barza, L., Szolosi, S., and Tofel-Grehl, B. (1996). Calcium stores in cultured fibroblasts and their changes with Alzheimer's disease. Biochim. Biophys. Acta *1316*, 71-77.

Gibson, G.E., Vestling, M., Zhang, H., Szolosi, S., Alkon, D., Lannfelt, L., Gandy, S., and Cowburn, R.F. (1997). Abnormalities in Alzheimer's disease fibroblasts bearing the APP670/671 mutation. Neurobiol. Aging *18*, 573-580.

Glenner, G.G., and Wong, C.W. (1984). Alzheimer's disease: initial report of the purification and characterization of a novel cerebrovascular amyloid protein. Biochem.Biophys.Res.Commun. *120*, 885-890.

Golde, T.E., Estus, S., Younkin, L.H., Selkoe, D.J., and Younkin, S.G. (1992). Processing of the amyloid protein precursor to potentially amyloidogenic derivatives. Science *255*, 728-730.

Goldgaber, D., Lerman, M.I., McBride, O.W., Saffiotti, U., and Gajdusek, D.C. (1987). Characterization and chromosomal localization of a cDNA encoding brain amyloid of Alzheimer's disease. Science *235*, 877-880.

Goodman, Y. and Mattson, M.P. (1994). Secreted forms of beta-amyloid precursor protein protect hippocampal neurons against amyloid beta-peptide-induced oxidative injury. Exp. Neurol. *128*, 1-12.

Gossen, M. and Bujard, H. (1992). Tight control of gene expression in mammalian cells by tetracycline-responsive promoters. Proc. Natl. Acad. Sci. U. S. A *89*, 5547-5551.

Gouras, G.K., Xu, H., Jovanovic, J.N., Buxbaum, J.D., Wang, R., Greengard, P., Relkin, N.R., and Gandy, S. (1998). Generation and regulation of beta-amyloid peptide variants by neurons. J. Neurochem. *71*, 1920-1925.

Goutte, C., Tsunozaki, M., Hale, V.A., and Priess, J.R. (2002). APH-1 is a multipass membrane protein essential for the Notch signaling pathway in Caenorhabditis elegans embryos. Proc. Natl. Acad. Sci. U. S. A *99*, 775-779.

Graef, I.A., Mermelstein, P.G., Stankunas, K., Neilson, J.R., Deisseroth, K., Tsien, R.W., and Crabtree, G.R. (1999). L-type calcium channels and GSK-3 regulate the activity of NF-ATc4 in hippocampal neurons. Nature *401*, 703-708.

Grundke-Iqbal, I., Iqbal, K., Quinlan, M., Tung, Y.C., Zaidi, M.S., and Wisniewski, H.M. (1986a). Microtubule-associated protein tau. A component of Alzheimer paired helical filaments. J. Biol. Chem. *261*, 6084-6089.

Grundke-Iqbal, I., Iqbal, K., Tung, Y.C., Quinlan, M., Wisniewski, H.M., and Binder, L.I. (1986b). Abnormal phosphorylation of the microtubule-associated protein tau (tau) in Alzheimer cytoskeletal pathology. Proc. Natl. Acad. Sci. U. S. A *83*, 4913-4917.

Grynkiewicz, G., Poenie, M., and Tsien, R.Y. (1985). A new generation of Ca2+ indicators with greatly improved fluorescence properties. J. Biol. Chem. *260*, 3440-3450.

Gunter, K.K. and Gunter, T.E. (1994). Transport of calcium by mitochondria. J. Bioenerg. Biomembr. *26*, 471-485.

Gunter, T.E., Gunter, K.K., Sheu, S.S., and Gavin, C.E. (1994). Mitochondrial calcium transport: physiological and pathological relevance. Am. J. Physiol. *267*, C313-C339.

Guo, Q., Furukawa, K., Sopher, B.L., Pham, D.G., Xie, J., Robinson, N., Martin, G.M., and Mattson, M.P. (1996). Alzheimer's PS-1 mutation perturbs calcium homeostasis and sensitizes PC12 cells to death induced by amyloid beta-peptide. Neuroreport *8*, 379-383.

Guo, Q., Sopher, B.L., Furukawa, K., Pham, D.G., Robinson, N., Martin, G.M., and Mattson, M.P. (1997). Alzheimer's presenilin mutation sensitizes neural cells to apoptosis induced by trophic factor withdrawal and amyloid beta-peptide: involvement of calcium and oxyradicals. J. Neurosci. *17*, 4212-4222.

Guo, Q., Christakos, S., Robinson, N., and Mattson, M.P. (1998a). Calbindin D28k blocks the proapoptotic actions of mutant presenilin 1: reduced oxidative stress and preserved mitochondrial function. Proc. Natl. Acad. Sci. U. S. A *95*, 3227-3232.

Guo, Q., Robinson, N., and Mattson, M.P. (1998b). Secreted beta-amyloid precursor protein counteracts the proapoptotic action of mutant presenilin-1 by activation of NF-kappaB and stabilization of calcium homeostasis. J. Biol. Chem. *273*, 12341-12351.

Guo, Q., Fu, W., Holtsberg, F.W., Steiner, S.M., and Mattson, M.P. (1999a). Superoxide mediates the cell-death-enhancing action of presenilin-1 mutations. J. Neurosci. Res. *56*, 457-470.

Guo, Q., Sebastian, L., Sopher, B.L., Miller, M.W., Ware, C.B., Martin, G.M., and Mattson, M.P. (1999b). Increased vulnerability of hippocampal neurons from presenilin-1 mutant knock-in mice to amyloid beta-peptide toxicity: central roles of superoxide production and caspase activation. J. Neurochem. *72*, 1019-1029.

Haass, C., Koo, E.H., Mellon, A., Hung, A.Y., and Selkoe, D.J. (1992a). Targeting of cell-surface beta-amyloid precursor protein to lysosomes: alternative processing into amyloid-bearing fragments. Nature *357*, 500-503.

Haass, C., Schlossmacher, M.G., Hung, A.Y., Vigo-Pelfrey, C., Mellon, A., Ostaszewski, B.L., Lieberburg, I., Koo, E.H., Schenk, D., Teplow, D.B., and . (1992b). Amyloid beta-peptide is produced by cultured cells during normal metabolism. Nature *359*, 322-325.

Haass, C., Hung, A.Y., Schlossmacher, M.G., Teplow, D.B., and Selkoe, D.J. (1993). beta-Amyloid peptide and a 3-kDa fragment are derived by distinct cellular mechanisms. J. Biol. Chem. *268*, 3021-3024.

Haass, C. and Selkoe, D.J. (1993). Cellular processing of beta-amyloid precursor protein and the genesis of amyloid beta-peptide. Cell *75*, 1039-1042.

Haass, C., Capell, A., Citron, M., Teplow, D.B., and Selkoe, D.J. (1995a). The vacuolar H(+)-ATPase inhibitor bafilomycin A1 differentially affects proteolytic processing of mutant and wild-type beta-amyloid precursor protein. J. Biol. Chem. *270*, 6186-6192.

Haass, C., Lemere, C.A., Capell, A., Citron, M., Seubert, P., Schenk, D., Lannfelt, L., and Selkoe, D.J. (1995b). The Swedish mutation causes early-onset Alzheimer's disease by beta-secretase cleavage within the secretory pathway. Nat. Med. *1*, 1291-1296.

Hanahan, D. (1983). Studies on transformation of Escherichia coli with plasmids. J. Mol. Biol. *166*, 557-580.

Hansson, C.A., Frykman, S., Farmery, M.R., Tjernberg, L.O., Nilsberth, C., Pursglove, S.E., Ito, A., Winblad, B., Cowburn, R.F., Thyberg, J., and Ankarcrona, M. (2004). Nicastrin, presenilin, APH-1, and PEN-2 form active gamma-secretase complexes in mitochondria. J. Biol. Chem. *279*, 51654-51660.

Hardy, J. (1997). Amyloid, the presenilins and Alzheimer's disease. Trends Neurosci. *20*, 154-159.

Hardy, J.A. and Higgins, G.A. (1992). Alzheimer's disease: the amyloid cascade hypothesis. Science *256*, 184-185.

Harkany, T., Abraham, I., Konya, C., Nyakas, C., Zarandi, M., Penke, B., and Luiten, P.G. (2000). Mechanisms of beta-amyloid neurotoxicity: perspectives of pharmacotherapy. Rev. Neurosci. *11*, 329-382.

Hartmann, T., Bieger, S.C., Bruhl, B., Tienari, P.J., Ida, N., Allsop, D., Roberts, G.W., Masters, C.L., Dotti, C.G., Unsicker, K., and Beyreuther, K. (1997). Distinct sites of intracellular production for Alzheimer's disease A beta40/42 amyloid peptides. Nat. Med. *3*, 1016-1020.

Heber, S., Herms, J., Gajic, V., Hainfellner, J., Aguzzi, A., Rulicke, T., von Kretzschmar, H., Von Koch, C., Sisodia, S., Tremml, P., Lipp, H.P., Wolfer, D.P., and Muller, U. (2000). Mice with combined gene knock-outs reveal essential and partially redundant functions of amyloid precursor protein family members. J. Neurosci. *20*, 7951-7963.

Herms, J., Schneider, I., Dewachter, I., Caluwaerts, N., Kretzschmar, H., and Van Leuven, F. (2003). Capacitive calcium entry is directly attenuated by mutant presenilin-1, independent of the expression of the amyloid precursor protein. J. Biol. Chem. *278*, 2484-2489.

Herms, J., Anliker, B., Heber, S., Ring, S., Fuhrmann, M., Kretzschmar, H., Sisodia, S., and Muller, U. (2004). Cortical dysplasia resembling human type 2 lissencephaly in mice lacking all three APP family members. EMBO J. *23*, 4106-4115.

Himes, C.S., Hiebsch, R., Ruble, C., Nye, J.S., and Curtis, D. (2002). aph-1 and pen-2 are required for Notch pathway signaling, gamma-secretase cleavage of betaAPP, and presenilin protein accumulation. Dev. Cell *3*, 85-97.

Hirashima, N., Etcheberrigaray, R., Bergamaschi, S., Racchi, M., Battaini, F., Binetti, G., Govoni, S., and Alkon, D.L. (1996). Calcium responses in human fibroblasts: a diagnostic molecular profile for Alzheimer's disease. Neurobiol. Aging *17*, 549-555.

Holsinger, R.M., McLean, C.A., Beyreuther, K., Masters, C.L., and Evin, G. (2002). Increased expression of the amyloid precursor beta-secretase in Alzheimer's disease. Ann. Neurol. *51*, 783-786.

Homayouni, R., Rice, D.S., Sheldon, M., and Curran, T. (1999). Disabled-1 binds to the cytoplasmic domain of amyloid precursor-like protein 1. J. Neurosci. *19*, 7507-7515.

Hoshi, M., Takashima, A., Noguchi, K., Murayama, M., Sato, M., Kondo, S., Saitoh, Y., Ishiguro, K., Hoshino, T., and Imahori, K. (1996). Regulation of mitochondrial pyruvate dehydrogenase activity by tau protein kinase I/glycogen synthase kinase 3beta in brain. Proc. Natl. Acad. Sci. U. S. A *93*, 2719-2723.

Hoyer, S., Nitsch, R., and Oesterreich, K. (1990). Ammonia is endogenously generated in the brain in the presence of presumed and verified dementia of Alzheimer type. Neurosci. Lett. *117*, 358-362.

Hoyer, S. (1992). Oxidative energy metabolism in Alzheimer brain. Studies in early-onset and late-onset cases. Mol. Chem. Neuropathol. *16*, 207-224.

Hughes, K., Nikolakaki, E., Plyte, S.E., Totty, N.F., and Woodgett, J.R. (1993). Modulation of the glycogen synthase kinase-3 family by tyrosine phosphorylation. EMBO J. *12*, 803-808.

Hussain, I., Powell, D., Howlett, D.R., Tew, D.G., Meek, T.D., Chapman, C., Gloger, I.S., Murphy, K.E., Southan, C.D., Ryan, D.M., Smith, T.S., Simmons, D.L., Walsh, F.S., Dingwall, C., and Christie, G. (1999). Identification of a novel aspartic protease (Asp 2) as beta-secretase. Mol. Cell. Neurosci. *14*, 419-427.

Hutton, M. and Hardy, J. (1997). The presenilins and Alzheimer's disease. Hum. Mol. Genet. *6*, 1639-1646.

Ito, E., Oka, K., Etcheberrigaray, R., Nelson, T.J., McPhie, D.L., Tofel-Grehl, B., Gibson, G.E., and Alkon, D.L. (1994). Internal Ca2+ mobilization is altered in fibroblasts from patients with Alzheimer disease. Proc. Natl. Acad. Sci. U. S. A *91*, 534-538.

Iwatsubo, T. (2004). The gamma-secretase complex: machinery for intramembrane proteolysis. Curr. Opin. Neurobiol. *14*, 379-383

Kang, J., Lemaire, H.G., Unterbeck, A., Salbaum, J.M., Masters, C.L., Grzeschik, K.H., Multhaup, G., Beyreuther, K., and Muller-Hill, B. (1987). The precursor of Alzheimer's disease amyloid A4 protein resembles a cell-surface receptor. Nature *325*, 733-736.

Kaufman, R.J. (1999). Stress signaling from the lumen of the endoplasmic reticulum: coordination of gene transcriptional and translational controls. Genes Dev. *13*, 1211-1233.

Keller, J.N., Guo, Q., Holtsberg, F.W., Bruce-Keller, A.J., and Mattson, M.P. (1998). Increased sensitivity to mitochondrial toxin-induced apoptosis in neural cells expressing mutant presenilin-1 is linked to perturbed calcium homeostasis and enhanced oxyradical production. J. Neurosci. *18*, 4439-4450.

Khachaturian, Z.S. (1989). Calcium, membranes, aging, and Alzheimer's disease. Introduction and overview. Ann. N. Y. Acad. Sci. *568*, 1-4.

Kim, H.S., Lee, J.H., Lee, J.P., Kim, E.M., Chang, K.A., Park, C.H., Jeong, S.J., Wittendorp, M.C., Seo, J.H., Choi, S.H., and Suh, Y.H. (2002). Amyloid beta peptide induces cytochrome C release from isolated mitochondria. Neuroreport *13*, 1989-1993.

Kim, H.S., Kim, E.M., Lee, J.P., Park, C.H., Kim, S., Seo, J.H., Chang, K.A., Yu, E., Jeong, S.J., Chong, Y.H., and Suh, Y.H. (2003). C-terminal fragments of amyloid precursor protein exert neurotoxicity by inducing glycogen synthase kinase-3beta expression. FASEB J. *17*, 1951-1953.

Kim, S.H., Yin, Y.I., Li, Y.M., and Sisodia, S.S. (2004). Evidence that assembly of an active gamma-secretase complex occurs in the early compartments of the secretory pathway. J. Biol. Chem. *279*, 48615-48619.

Kimberly, W.T., Xia, W., Rahmati, T., Wolfe, M.S., and Selkoe, D.J. (2000). The transmembrane aspartates in presenilin 1 and 2 are obligatory for gamma-secretase activity and amyloid beta-protein generation. J. Biol. Chem. *275*, 3173-3178.

Kimberly, W.T., Zheng, J.B., Guenette, S.Y., and Selkoe, D.J. (2001). The intracellular domain of the beta-amyloid precursor protein is stabilized by Fe65 and translocates to the nucleus in a notch-like manner. J. Biol. Chem. *276*, 40288-40292.

Kimberly, W.T., LaVoie, M.J., Ostaszewski, B.L., Ye, W., Wolfe, M.S., and Selkoe, D.J. (2003). Gamma-secretase is a membrane protein complex comprised of presenilin, nicastrin, Aph-1, and Pen-2. Proc. Natl. Acad. Sci. U. S. A *100*, 6382-6387.

Kirischuk, S. and Verkhratsky, A. (1996). Calcium homeostasis in aged neurones. Life Sci. *59*, 451-459.

Klein, P.S. and Melton, D.A. (1996). A molecular mechanism for the effect of lithium on development. Proc. Natl. Acad. Sci. U. S. A *93*, 8455-8459.

Knops, J., Suomensaari, S., Lee, M., McConlogue, L., Seubert, P., and Sinha, S. (1995). Cell-type and amyloid precursor protein-type specific inhibition of A beta release by bafilomycin A1, a selective inhibitor of vacuolar ATPases. J. Biol. Chem. *270*, 2419-2422.

Koizumi, S., Ishiguro, M., Ohsawa, I., Morimoto, T., Takamura, C., Inoue, K., and Kohsaka, S. (1998). The effect of a secreted form of beta-amyloid-precursor protein on intracellular Ca2+ increase in rat cultured hippocampal neurones. Br. J. Pharmacol. *123*, 1483-1489.

Koo, E.H. and Squazzo, S.L. (1994). Evidence that production and release of amyloid beta-protein involves the endocytic pathway. J. Biol. Chem. *269*, 17386-17389.

Kopan, R. and Goate, A. (2000). A common enzyme connects notch signaling and Alzheimer's disease. Genes Dev. *14*, 2799-2806.

Kosik, K.S., Joachim, C.L., and Selkoe, D.J. (1986). Microtubule-associated protein tau (tau) is a major antigenic component of paired helical filaments in Alzheimer disease. Proc. Natl. Acad. Sci. U. S. A *83*, 4044-4048.

Kruman, I., Guo, Q., and Mattson, M.P. (1998). Calcium and reactive oxygen species mediate staurosporine-induced mitochondrial dysfunction and apoptosis in PC12 cells. J. Neurosci. Res. *51*, 293-308.

Kume, H., Maruyama, K., and Kametani, F. (2004). Intracellular domain generation of amyloid precursor protein by epsilon-cleavage depends on C-terminal fragment by alpha-secretase cleavage. Int. J. Mol. Med. *13*, 121-125.

Lai, A., Sisodia, S.S., and Trowbridge, I.S. (1995). Characterization of sorting signals in the beta-amyloid precursor protein cytoplasmic domain. J. Biol. Chem. *270*, 3565-3573.

Lai, J.C. and Cooper, A.J. (1991). Neurotoxicity of ammonia and fatty acids: differential inhibition of mitochondrial dehydrogenases by ammonia and fatty acyl coenzyme A derivatives. Neurochem. Res. *16*, 795-803.

Lammich, S., Kojro, E., Postina, R., Gilbert, S., Pfeiffer, R., Jasionowski, M., Haass, C., and Fahrenholz, F. (1999). Constitutive and regulated alpha-secretase cleavage of Alzheimer's amyloid precursor protein by a disintegrin metalloprotease. Proc. Natl. Acad. Sci. U. S. A *96*, 3922-3927.

Lee, V.M., Balin, B.J., Otvos, L., Jr., and Trojanowski, J.Q. (1991). A68: a major subunit of paired helical filaments and derivatized forms of normal Tau. Science *251*, 675-678.

Leissring, M.A., Parker, I., and LaFerla, F.M. (1999a). Presenilin-2 mutations modulate amplitude and kinetics of inositol 1, 4,5-trisphosphate-mediated calcium signals. J. Biol. Chem. *274*, 32535-32538.

Leissring, M.A., Paul, B.A., Parker, I., Cotman, C.W., and LaFerla, F.M. (1999b). Alzheimer's presenilin-1 mutation potentiates inositol 1,4,5-trisphosphate-mediated calcium signaling in Xenopus oocytes. J. Neurochem. *72*, 1061-1068.

Leissring, M.A., Akbari, Y., Fanger, C.M., Cahalan, M.D., Mattson, M.P., and LaFerla, F.M. (2000). Capacitative calcium entry deficits and elevated luminal calcium content in mutant presenilin-1 knockin mice. J. Cell Biol. *149*, 793-798.

Leissring, M.A., Murphy, M.P., Mead, T.R., Akbari, Y., Sugarman, M.C., Jannatipour, M., Anliker, B., Muller, U., Saftig, P., De Strooper, B., Wolfe, M.S., Golde, T.E., and LaFerla, F.M. (2002). A physiologic signaling role for the gamma -secretase-derived intracellular fragment of APP. Proc. Natl. Acad. Sci. U. S. A *99*, 4697-4702.

Leissring, M.A., Farris, W., Wu, X., Christodoulou, D.C., Haigis, M.C., Guarente, L., and Selkoe, D.J. (2004). Alternative translation initiation generates a novel isoform of insulin-degrading enzyme targeted to mitochondria. Biochem. J. *383*, 439-446.

Lorent, K., Overbergh, L., Moechars, D., De Strooper, B., Van Leuven, F., and Van den, B.H. (1995). Expression in mouse embryos and in adult mouse brain of three members of the amyloid precursor protein family, of the alpha-2-macroglobulin receptor/low density lipoprotein receptor-related protein and of its ligands apolipoprotein E, lipoprotein lipase, alpha-2-macroglobulin and the 40,000 molecular weight receptor-associated protein. Neuroscience *65*, 1009-1025.

Magelhaes, P.J., Andreu, A.L., and Schon, E.A. (1998). Evidence for the presence of 5s rRNA in mammalian mitochondria. Mol. Biol. Cell 9, 2375-2382.

Martlnez, A., Vitorica, J., and Satrustegui, J. (1988). Cytosolic free calcium levels increase with age in rat brain synaptosomes. Neurosci. Lett. *88*, 336-342.

Mason, M.J., Garcia-Rodriguez, C., and Grinstein, S. (1991). Coupling between intracellular Ca2+ stores and the Ca2+ permeability of the plasma membrane. Comparison of the effects of thapsigargin, 2,5-di-(tert-butyl)-1,4-hydroquinone, and cyclopiazonic acid in rat thymic lymphocytes. J. Biol. Chem. *266*, 20856-20862.

Mastrogiacomo, F., Bergeron, C., and Kish, S.J. (1993). Brain alpha-ketoglutarate dehydrogenase complex activity in Alzheimer's disease. J. Neurochem. *61*, 2007-2014.

Matsuda, S., Yasukawa, T., Homma, Y., Ito, Y., Niikura, T., Hiraki, T., Hirai, S., Ohno, S., Kita, Y., Kawasumi, M., Kouyama, K., Yamamoto, T., Kyriakis, J.M., and Nishimoto, I. (2001). c-Jun N-terminal kinase (JNK)-interacting protein-1b/islet-brain-1 scaffolds Alzheimer's amyloid precursor protein with JNK. J. Neurosci. *21*, 6597-6607.

Mattson, M.P., Cheng, B., Davis, D., Bryant, K., Lieberburg, I., and Rydel, R.E. (1992). beta-Amyloid peptides destabilize calcium homeostasis and render human cortical neurons vulnerable to excitotoxicity. J. Neurosci. *12*, 376-389.

Mattson, M.P., Cheng, B., Culwell, A.R., Esch, F.S., Lieberburg, I., and Rydel, R.E. (1993a). Evidence for excitoprotective and intraneuronal calcium-regulating roles for secreted forms of the beta-amyloid precursor protein. Neuron *10*, 243-254.

Mattson, M.P., Tomaselli, K.J., and Rydel, R.E. (1993b). Calcium-destabilizing and neurodegenerative effects of aggregated beta-amyloid peptide are attenuated by basic FGF. Brain Res. *621*, 35-49.

Mattson, M.P. (1994). Secreted forms of beta-amyloid precursor protein modulate dendrite outgrowth and calcium responses to glutamate in cultured embryonic hippocampal neurons. J. Neurobiol. *25*, 439-450.

Mattson, M.P. (1997). Cellular actions of beta-amyloid precursor protein and its soluble and fibrillogenic derivatives. Physiol. Rev. *77*, 1081-1132.

McCormack, J.G., Halestrap, A.P., and Denton, R.M. (1990). Role of calcium ions in regulation of mammalian intramitochondrial metabolism. Physiol. Rev. *70*, 391-425.

Mehta, P.D., Pirttila, T., Patrick, B.A., Barshatzky, M., and Mehta, S.P. (2001). Amyloid beta protein 1-40 and 1-42 levels in matched cerebrospinal fluid and plasma from patients with Alzheimer disease. Neurosci. Lett. *304*, 102-106.

Michikawa, M. and Yanagisawa, K. (1999). Inhibition of cholesterol production but not of nonsterol isoprenoid products induces neuronal cell death. J. Neurochem. *72*, 2278-2285.

Minopoli, G., de Candia, P., Bonetti, A., Faraonio, R., Zambrano, N., and Russo, T. (2001). The beta-amyloid precursor protein functions as a cytosolic anchoring site that prevents Fe65 nuclear translocation. J. Biol. Chem. *276*, 6545-6550.

Mitchell, P. and Moyle, J. (1969). Estimation of membrane potential and pH difference across the cristae membrane of rat liver mitochondria. Eur. J. Biochem. *7*, 471-484.

Mok, S.S., Clippingdale, A.B., Beyreuther, K., Masters, C.L., Barrow, C.J., and Small, D.H. (2000). A beta peptides and calcium influence secretion of the amyloid protein precursor from chick sympathetic neurons in culture. J. Neurosci. Res. *61*, 449-457.

Mulder, M., Ravid, R., Swaab, D.F., de Kloet, E.R., Haasdijk, E.D., Julk, J., van der Boom, J.J., and Havekes, L.M. (1998). Reduced levels of cholesterol, phospholipids, and fatty acids in cerebrospinal fluid of Alzheimer disease patients are not related to apolipoprotein E4. Alzheimer Dis. Assoc. Disord. *12*, 198-203.

Muller, U., Cristina, N., Li, Z.W., Wolfer, D.P., Lipp, H.P., Rulicke, T., Brandner, S., Aguzzi, A., and Weissmann, C. (1994). Behavioral and anatomical deficits in mice homozygous for a modified beta-amyloid precursor protein gene. Cell *79*, 755-765.

Mungarro-Menchaca, X., Ferrera, P., Moran, J., and Arias, C. (2002). beta-Amyloid peptide induces ultrastructural changes in synaptosomes and potentiates mitochondrial dysfunction in the presence of ryanodine. J. Neurosci. Res. *68*, 89-96.

Nicholls, D.G. (1974). The influence of respiration and ATP hydrolysis on the proton-electrochemical gradient across the inner membrane of rat-liver mitochondria as determined by ion distribution. Eur. J. Biochem. *50*, 305-315.

Nicholls, D.G. and Crompton, M. (1980). Mitochondrial calcium transport. FEBS Lett. *111*, 261-268.

Nicholls, D.G. and Budd, S.L. (2000). Mitochondria and neuronal survival. Physiol. Rev. *80*, 315-360.

Nicholls, D.G., Vesce, S., Kirk, L., and Chalmers, S. (2003). Interactions between mitochondrial bioenergetics and cytoplasmic calcium in cultured cerebellar granule cells. Cell Calcium *34*, 407-424.

Nukina, N. and Ihara, Y. (1986). One of the antigenic determinants of paired helical filaments is related to tau protein. J. Biochem. (Tokyo) *99*, 1541-1544.

Octave, J.N. (1995). The amyloid peptide and its precursor in Alzheimer's disease. Rev. Neurosci. *6*, 287-316.

Perez, R.G., Zheng, H., Van der Ploeg, L.H., and Koo, E.H. (1997). The beta-amyloid precursor protein of Alzheimer's disease enhances neuron viability and modulates neuronal polarity. J. Neurosci. *17*, 9407-9414.

Perez, R.G., Soriano, S., Hayes, J.D., Ostaszewski, B., Xia, W., Selkoe, D.J., Chen, X., Stokin, G.B., and Koo, E.H. (1999). Mutagenesis identifies new signals for beta-amyloid precursor protein endocytosis, turnover, and the generation of secreted fragments, including Abeta42. J. Biol. Chem. *274*, 18851-18856.

Perry, E.K., Perry, R.H., Tomlinson, B.E., Blessed, G., and Gibson, P.H. (1980). Coenzyme A-acetylating enzymes in Alzheimer's disease: possible cholinergic 'compartment' of pyruvate dehydrogenase. Neurosci. Lett. *18*, 105-110.

Peterson, C. and Goldman, J.E. (1986). Alterations in calcium content and biochemical processes in cultured skin fibroblasts from aged and Alzheimer donors. Proc. Natl. Acad. Sci. U. S. A *83*, 2758-2762.

Pike, C.J., Walencewicz, A.J., Glabe, C.G., and Cotman, C.W. (1991). In vitro aging of beta-amyloid protein causes peptide aggregation and neurotoxicity. Brain Res. *563*, 311-314.

Plyte, S.E., Hughes, K., Nikolakaki, E., Pulverer, B.J., and Woodgett, J.R. (1992). Glycogen synthase kinase-3: functions in oncogenesis and development. Biochim. Biophys. Acta *1114*, 147-162.

Pozzan, T., Rizzuto, R., Volpe, P., and Meldolesi, J. (1994). Molecular and cellular physiology of intracellular calcium stores. Physiol. Rev. *74*, 595-636.

Putney, J.W., Jr. (1986). A model for receptor-regulated calcium entry. Cell Calcium *7*, 1-12.

Robakis, N.K., Ramakrishna, N., Wolfe, G., and Wisniewski, H.M. (1987). Molecular cloning and characterization of a cDNA encoding the cerebrovascular and the neuritic plaque amyloid peptides. Proc. Natl. Acad. Sci. U. S. A *84*, 4190-4194.

Rogaev, E.I., Sherrington, R., Wu, C., Levesque, G., Liang, Y., Rogaeva, E.A., Ikeda, M., Holman, K., Lin, C., Lukiw, W.J., de Jong, P.J., Fraser, P.E., Rommens, J.M., and George-Hyslop, P. (1997). Analysis of the 5' sequence, genomic structure, and alternative splicing of the presenilin-1 gene (PSEN1) associated with early onset Alzheimer disease. Genomics *40*, 415-424.

Rosen, D.R., Martin-Morris, L., Luo, L.Q., and White, K. (1989). A Drosophila gene encoding a protein resembling the human beta-amyloid protein precursor. Proc. Natl. Acad. Sci. U. S. A *86*, 2478-2482.

Ryves, W.J. and Harwood, A.J. (2001). Lithium inhibits glycogen synthase kinase-3 by competition for magnesium. Biochem. Biophys. Res. Commun. *280*, 720-725.

Schaefer, A., Magocsi, M., Stocker, U., Kosa, F., Marquardt, H. (1994). Early transient suppression of c-myb mRNA levels and induction of differentiation in Friend erythroleukemia cells by the [Ca2+]i-increasing agents cyclopiazonic acid and thapsigargin. J. Biol. Chem. *269*, 8786-8791.

Scheinfeld, M.H., Ghersi, E., Laky, K., Fowlkes, B.J., and D'Adamio, L. (2002). Processing of beta-amyloid precursor-like protein-1 and -2 by gamma-secretase regulates transcription. J. Biol. Chem. *277*, 44195-44201.

Scheinfeld, M.H., Matsuda, S., and D'Adamio, L. (2003). JNK-interacting protein-1 promotes transcription of A beta protein precursor but not A beta precursor-like proteins, mechanistically different than Fe65. Proc. Natl. Acad. Sci. U. S. A *100*, 1729-1734.

Schneider, W.C. (1948). Intracellular distribution of enzymes III. The oxidation of octanoic acid by rat liver fractions. J. Biol. Chem. *176*, 259-267.

Schubert, D., Jin, L.W., Saitoh, T., and Cole, G. (1989). The regulation of amyloid beta protein precursor secretion and its modulatory role in cell adhesion. Neuron *3*, 689-694.

Selkoe, D.J. (1994). Cell biology of the amyloid beta-protein precursor and the mechanism of Alzheimer's disease. Annu. Rev. Cell Biol. *10*, 373-403.

Selkoe, D.J. (1998). The cell biology of beta-amyloid precursor protein and presenilin in Alzheimer's disease. Trends Cell Biol. *8*, 447-453.

Seubert, P., Vigo-Pelfrey, C., Esch, F., Lee, M., Dovey, H., Davis, D., Sinha, S., Schlossmacher, M., Whaley, J., and Swindlehurst, C. (1992). Isolation and quantification of soluble Alzheimer's beta-peptide from biological fluids. Nature *359*, 325-327.

Seubert, P., Oltersdorf, T., Lee, M.G., Barbour, R., Blomquist, C., Davis, D.L., Bryant, K., Fritz, L.C., Galasko, D., and Thal, L.J. (1993). Secretion of beta-amyloid precursor protein cleaved at the amino terminus of the beta-amyloid peptide. Nature *361*, 260-263.

Shoji, M., Golde, T.E., Ghiso, J., Cheung, T.T., Estus, S., Shaffer, L.M., Cai, X.D., McKay, D.M., Tintner, R., Frangione, B., and . (1992). Production of the Alzheimer amyloid beta protein by normal proteolytic processing. Science *258*, 126-129.

Sims, N.R., Bowen, D.M., Allen, S.J., Smith, C.C., Neary, D., Thomas, D.J., and Davison, A.N. (1983a). Presynaptic cholinergic dysfunction in patients with dementia. J. Neurochem. *40*, 503-509.

Sims, N.R., Bowen, D.M., Neary, D., and Davison, A.N. (1983b). Metabolic processes in Alzheimer's disease: adenine nucleotide content and production of 14CO2 from [U-14C] glucose in vitro in human neocortex. J. Neurochem. *41*, 1329-1334.

Sinha, S., Anderson, J.P., Barbour, R., Basi, G.S., Caccavello, R., Davis, D., Doan, M., Dovey, H.F., Frigon, N., Hong, J., Jacobson-Croak, K., Jewett, N., Keim, P., Knops, J., Lieberburg, I., Power, M., Tan, H., Tatsuno, G., Tung, J., Schenk, D., Seubert, P., Suomensaari, S.M., Wang, S., Walker, D., John, V., and . (1999). Purification and cloning of amyloid precursor protein beta-secretase from human brain. Nature *402*, 537-540.

Sinha, S. and Lieberburg, I. (1999). Cellular mechanisms of beta-amyloid production and secretion. Proc. Natl. Acad. Sci. U. S. A *96*, 11049-11053.

Sisodia, S.S., Koo, E.H., Beyreuther, K., Unterbeck, A., and Price, D.L. (1990). Evidence that beta-amyloid protein in Alzheimer's disease is not derived by normal processing. Science *248*, 492-495.

Slunt, H.H., Thinakaran, G., Von Koch, C., Lo, A.C., Tanzi, R.E., and Sisodia, S.S. (1994). Expression of a ubiquitous, cross-reactive homologue of the mouse beta-amyloid precursor protein (APP). J. Biol. Chem. *269*, 2637-2644.

Small, D.H. (1998). The role of the amyloid protein precursor (APP) in Alzheimer's disease: does the normal function of APP explain the topography of neurodegeneration? Neurochem. Res. *23*, 795-806.

Smith, I.F., Boyle, J.P., Vaughan, P.F., Pearson, H.A., Cowburn, R.F., and Peers, C.S. (2002). Ca(2+) stores and capacitative Ca(2+) entry in human neuroblastoma (SH-SY5Y) cells expressing a familial Alzheimer's disease presenilin-1 mutation. Brain Res. *949*, 105-111.

Somlyo, A.P., Somlyo, A.V., and Shuman, H. (1979). Electron probe analysis of vascular smooth muscle. Composition of mitochondria, nuclei, and cytoplasm. J. Cell Biol. *81*, 316-335.

Sorbi, S., Bird, E.D., and Blass, J.P. (1983). Decreased pyruvate dehydrogenase complex activity in Huntington and Alzheimer brain. Ann. Neurol. *13*, 72-78.

Spillantini, M.G. and Goedert, M. (1998). Tau protein pathology in neurodegenerative diseases. Trends Neurosci. *21*, 428-433.

Steiner, H., Duff, K., Capell, A., Romig, H., Grim, M.G., Lincoln, S., Hardy, J., Yu, X., Picciano, M., Fechteler, K., Citron, M., Kopan, R., Pesold, B., Keck, S., Baader, M., Tomita, T., Iwatsubo, T., Baumeister, R., and Haass, C. (1999a). A loss of function mutation of presenilin-2 interferes with amyloid beta-peptide production and notch signaling. J. Biol. Chem. *274*, 28669-28673.

Steiner, H., Romig, H., Pesold, B., Philipp, U., Baader, M., Citron, M., Loetscher, H., Jacobsen, H., and Haass, C. (1999b). Amyloidogenic function of the Alzheimer's disease-associated presenilin 1 in the absence of endoproteolysis. Biochemistry *38*, 14600-14605.

Steiner, H. and Haass, C. (2000). Intramembrane proteolysis by presenilins. Nat. Rev. Mol. Cell Biol. *1*, 217-224.

Steiner, H., Winkler, E., Edbauer, D., Prokop, S., Basset, G., Yamasaki, A., Kostka, M., and Haass, C. (2002). PEN-2 is an integral component of the gamma-secretase complex required for coordinated expression of presenilin and nicastrin. J. Biol. Chem. *277*, 39062-39065.

Strittmatter, W.J. and Roses, A.D. (1995). Apolipoprotein E and Alzheimer disease. Proc. Natl. Acad. Sci. U. S. A *92*, 4725-4727.

Sullivan, P.G. and Brown, M.R. (2005). Mitochondrial aging and dysfunction in Alzheimer's disease. Prog. Neuropsychopharmacol. Biol. Psychiatry *29*, 407-410.

Svennerholm, L. and Gottfries, C.G. (1994). Membrane lipids, selectively diminished in Alzheimer brains, suggest synapse loss as a primary event in early-onset form (type I) and demyelination in late-onset form (type II). J. Neurochem. *62*, 1039-1047.

Tanahashi, H. and Tabira, T. (1999). X11L2, a new member of the X11 protein family, interacts with Alzheimer's beta-amyloid precursor protein. Biochem. Biophys. Res. Commun. *255*, 663-667.

Tandon, A., Rogaeva, E., Mullan, M., and George-Hyslop, P.H. (2000). Molecular genetics of Alzheimer's disease: the role of beta-amyloid and the presenilins. Curr. Opin. Neurol. *13*, 377-384.

Tandon, A. and Fraser, P. (2002). The presenilins. Genome Biol. *3*,3014.1-3014.9

Tanzi, R.E., Gusella, J.F., Watkins, P.C., Bruns, G.A., George-Hyslop, P., Van Keuren, M.L., Patterson, D., Pagan, S., Kurnit, D.M., and Neve, R.L. (1987). Amyloid beta protein gene: cDNA, mRNA distribution, and genetic linkage near the Alzheimer locus. Science *235*, 880-884.

Taylor, C.W. and Laude, A.J. (2002). IP3 receptors and their regulation by calmodulin and cytosolic Ca2+. Cell Calcium *32*, 321-334.

Toescu, E.C. and Verkhratsky, A. (2000). Assessment of mitochondrial polarization status in living cells based on analysis of the spatial heterogeneity of rhodamine 123 fluorescence staining. Pflugers Arch. *440*, 941-947.

Van Gassen, G. and Van Broeckhoven, C. (2000). Molecular genetics of Alzheimer's disease: what have we learned? Acta Neurol. Belg. *100*, 65-76.

Van Uden, E., Kang, D.E., Koo, E.H., and Masliah, E. (2000). LDL receptor-related protein (LRP) in Alzheimer's disease: towards a unified theory of pathogenesis. Microsc. Res. Tech. *50*, 268-272.

Vassar, R., Bennett, B.D., Babu-Khan, S., Kahn, S., Mendiaz, E.A., Denis, P., Teplow, D.B., Ross, S., Amarante, P., Loeloff, R., Luo, Y., Fisher, S., Fuller, J., Edenson, S., Lile, J., Jarosinski, M.A., Biere, A.L., Curran, E., Burgess, T., Louis, J.C., Collins, F., Treanor, J., Rogers, G., and Citron, M. (1999). Beta-secretase cleavage of Alzheimer's amyloid precursor protein by the transmembrane aspartic protease BACE. Science *286*, 735-741.

Villalba, M., Pereira, R., Martinez-Serrano, A., and Satrustegui, J. (1995). Altered cell calcium regulation in synaptosomes and brain cells of the 30-month-old rat: prominent effects in hippocampus. Neurobiol. Aging *16*, 809-816.

von Rotz, R.C., Kohli, B.M., Bosset, J., Meier, M., Suzuki, T., Nitsch, R.M., and Konietzko, U. (2004). The APP intracellular domain forms nuclear multiprotein complexes and regulates the transcription of its own precursor. J. Cell Sci. *117*, 4435-4448.

Walsh, D.M., Fadeeva, J.V., LaVoie, M.J., Paliga, K., Eggert, S., Kimberly, W.T., Wasco, W., and Selkoe, D.J. (2003). gamma-Secretase cleavage and binding to FE65 regulate the nuclear translocation of the intracellular C-terminal domain (ICD) of the APP family of proteins. Biochemistry *42*, 6664-6673.

Wang, R., Meschia, J.F., Cotter, R.J., and Sisodia, S.S. (1991). Secretion of the beta/A4 amyloid precursor protein. Identification of a cleavage site in cultured mammalian cells. J. Biol. Chem. *266*, 16960-16964.

Wasco, W., Bupp, K., Magendantz, M., Gusella, J.F., Tanzi, R.E., and Solomon, F. (1992). Identification of a mouse brain cDNA that encodes a protein related to the Alzheimer disease-associated amyloid beta protein precursor. Proc. Natl. Acad. Sci. U. S. A *89*, 10758-10762.

Wasco, W., Gurubhagavatula, S., Paradis, M.D., Romano, D.M., Sisodia, S.S., Hyman, B.T., Neve, R.L., and Tanzi, R.E. (1993). Isolation and characterization of APLP2 encoding a homologue of the Alzheimer's associated amyloid beta protein precursor. Nat. Genet. *5*, 95-100.

Weidemann, A., Konig, G., Bunke, D., Fischer, P., Salbaum, J.M., Masters, C.L., and Beyreuther, K. (1989). Identification, biogenesis, and localization of precursors of Alzheimer's disease A4 amyloid protein. Cell *57*, 115-126.

Weidemann, A., Eggert, S., Reinhard, F.B., Vogel, M., Paliga, K., Baier, G., Masters, C.L., Beyreuther, K., Evin, G. (2002). A novel epsilon-cleavage within the transmembrane domain of the Alzheimer amyloid precursor protein demonstrates homology with Notch processing. Biochemistry *41*, 2825-2835.

Wischik, C.M., Novak, M., Edwards, P.C., Klug, A., Tichelaar, W., and Crowther, R.A. (1988). Structural characterization of the core of the paired helical filament of Alzheimer disease. Proc. Natl. Acad. Sci. U. S. A *85*, 4884-4888.

Wolfe, M.S., Xia, W., Ostaszewski, B.L., Diehl, T.S., Kimberly, W.T., and Selkoe, D.J. (1999). Two transmembrane aspartates in presenilin-1 required for presenilin endoproteolysis and gamma-secretase activity. Nature *398*, 513-517.

Wood, J.G., Mirra, S.S., Pollock, N.J., and Binder, L.I. (1986). Neurofibrillary tangles of Alzheimer disease share antigenic determinants with the axonal microtubule-associated protein tau (tau). Proc. Natl. Acad. Sci. U. S. A *83*, 4040-4043.

Xiong, J., Verkhratsky, A., and Toescu, E.C. (2002). Changes in mitochondrial status associated with altered Ca2+ homeostasis in aged cerebellar granule neurons in brain slices. J. Neurosci. *22*, 10761-10771.

Yan, R., Bienkowski, M.J., Shuck, M.E., Miao, H., Tory, M.C., Pauley, A.M., Brashier, J.R., Stratman, N.C., Mathews, W.R., Buhl, A.E., Carter, D.B., Tomasselli, A.G., Parodi, L.A., Heinrikson, R.L., and Gurney, M.E. (1999). Membrane-anchored aspartyl protease with Alzheimer's disease beta-secretase activity. Nature *402*, 533-537.

Yang, L.B., Lindholm, K., Yan, R., Citron, M., Xia, W., Yang, X.L., Beach, T., Sue, L., Wong, P., Price, D., Li, R., and Shen, Y. (2003). Elevated beta-secretase expression and enzymatic activity detected in sporadic Alzheimer disease. Nat. Med. *9*, 3-4.

Yoo, A.S., Cheng, I., Chung, S., Grenfell, T.Z., Lee, H., Pack-Chung, E., Handler, M., Shen, J., Xia, W., Tesco, G., Saunders, A.J., Ding, K., Frosch, M.P., Tanzi, R.E., and Kim, T.W. (2000). Presenilin-mediated modulation of capacitative calcium entry. Neuron *27*, 561-572.

Yu, G., Chen, F., Nishimura, M., Steiner, H., Tandon, A., Kawarai, T., Arawaka, S., Supala, A., Song, Y.Q., Rogaeva, E., Holmes, E., Zhang, D.M., Milman, P., Fraser, P.E., Haass, C., and George-Hyslop, P.S. (2000a). Mutation of conserved aspartates affects maturation of both aspartate mutant and endogenous presenilin 1 and presenilin 2 complexes. J. Biol. Chem. *275*, 27348-27353.

Yu, G., Nishimura, M., Arawaka, S., Levitan, D., Zhang, L., Tandon, A., Song, Y.Q., Rogaeva, E., Chen, F., Kawarai, T., Supala, A., Levesque, L., Yu, H., Yang, D.S., Holmes, E., Milman, P., Liang, Y., Zhang, D.M., Xu, D.H., Sato, C., Rogaev, E., Smith, M., Janus, C., Zhang, Y., Aebersold, R., Farrer, L.S., Sorbi, S., Bruni, A., Fraser, P., and George-Hyslop, P. (2000b). Nicastrin modulates presenilin-mediated notch/glp-1 signal transduction and betaAPP processing. Nature *407*, 48-54.

Zhang, H., Komano, H., Fuller, R.S., Gandy, S.E., and Frail, D.E. (1994). Proteolytic processing and secretion of human beta-amyloid precursor protein in yeast. Evidence for a yeast secretase activity. J. Biol. Chem. *269*, 27799-27802.

Zheng, H., Jiang, M., Trumbauer, M.E., Hopkins, R., Sirinathsinghji, D.J., Stevens, K.A., Conner, M.W., Slunt, H.H., Sisodia, S.S., Chen, H.Y., and Van der Ploeg, L.H. (1996). Mice deficient for the amyloid precursor protein gene. Ann. N. Y. Acad. Sci. *777*, 421-426.

Zhong, S., Wu, K., Black, I.B., and Schaar, D.G. (1996). Characterization of the genomic structure of the mouse APLP1 gene. Genomics *32*, 159-162.

Zhong, Z., Higaki, J., Murakami, K., Wang, Y., Catalano, R., Quon, D., and Cordell, B. (1994). Secretion of beta-amyloid precursor protein involves multiple cleavage sites. J. Biol. Chem. *269*, 627-632.

Acknowledgements

*I take the opportunity to acknowledge the debt I owe to **Prof. Dr. Jochen Herms** for his supervision and mentorship that has contributed significantly to my understanding of the subject. His remarkable enthusiasm and constant encouragement assisted a lot to accomplish this work.*

*I am grateful to **Prof.Dr.Hans Kretzschmar**, Director, Centre of Neuropathology und Prion Research for accepting me to pursue my doctoral study in this institute.*

*I am thankful to **Prof.Dr.Christian Haass**, **Dr.Ellen Kilger** and **Dr.Andreas Reichert** for their collaboration and the interest shown in this project.*

*I would like to express my deepest indebtness to my coulleagues **Antje Strack**, **Christina Burkhardt** and **Martin Fuhrmann** for always maintaining a wonderful friendly environment to work in and who have always assisted in one way or the other during the whole tenure of this work. I thank them for their selfless support, suggestions and timeless discussions.*

*I am thankful to **Gerda Mitteregger** for her perfect management to provide enough supply of experimental mice.*

*I am thankful to **Dr.Joachim Ubl**,* Olympus Biosystems GmbH *for giving me basics of Calcium imaging.*

*I would like to express my special thanks to **Krebs Bjarne**, **Rüdiger Schmalzbauer, Uwe Bertsch** and **Kathrin Barnewitz** for their scientific discussions and suggestions.*

*I would like to thank **Dorothee Rieger**, **Antje Strack, Martin Fuhrmann and Marko Maringer** for their insightful critique on draft of this thesis that has been immensely useful in helping me clearly communicate my sometimes inchoate thoughts.*

*I acknowledge and greatly appreciate **Doris Schechinger** for her excellent technical assistance.*

*My special thanks to **Ben Vanmassenhove** for his cheery help and always being a translator for me whenever I was stucked up communicating with my house master in German.*

To all the staff of Centre of Neuropathology and Prion Research whose name I am unable to acknowledge due to space constraints, I feel greatly indebted.

I am grateful to my friends ***Ritu Rawat****,* ***Farid Ahmed****,* ***Aniruddha Deshpande****,* ***Irfan Tamboli*** *and* ***Poorvi Kakariya****. Their friendship and support have made my stay worth in Munich.*

I have had a great fortune to be with the family of ***Vijay Rawat****, his wife* ***Ritu*** *and being a "bua" of their two loving sons* ***Shivam*** *and* ***Aditya****. I thank them for giving me uncountable number of cherishable moments I spent with them.*

*I greatly acknowledge the love and support of my husband "****Arif****". His constant support, encouragement and faith have played a key role in accomplishing this work successfully.*

Last but not least, I acknowledge, treasure the blessings and return the love of my whole "Khan ***family****" without whom "I would be lost".* ***My parents*** *and my sisters* ***Samina*** *and* ***Hiba,*** *are the wonderful gift I am blessed with. Their love, inspiration and trust have given me courage of spending a long time thousands of miles away from them.*

Runa Hamid

Curriculum Vitae

Personal Data

Name: Runa Hamid

Date of Birth: 26th August, 1978

Place of Birth: Barreilly, India

Nationality: Indian

Academic Qualification

2002 – 2006	PhD student at Center of Neuropathology and Prion research, LMU, Munich, Germany.
1999 – 2001	MSc., Biotechnology, University of Pune, Pune, India.
1995 – 1999	BSc., Zoology, Botany and Chemistry B.R.A. University, Agra, India.

Achievements

Qualified “**General Aptitude Test for Engineers**” in 2001 with 90 percentile score.

Qualified “**CSIR-UGC NET examination** “ in 2000 and awarded **Lectureship** by UGC.

Awarded scholarship for two years by DBT, Government of India for pursuing MSc. in Biotechnology.

Publications and Presentation

Hamid, R., Kilger, E., Willem, M., Kostka, M., Bornhoevd C., Kretzschmar, H.A., Haass, C., and Herms, J. (2006). APP intracellular domain modulates cellular calcium homeostasis and cellular ATP content. *Submitted to J. Neuroscience.*

Hamid, R., Willem, M., Edbauer, D., Steiner, H., Müller, U., Wünsch, G., Kretzschmar, H.A., Haass, C., and Herms, J. β–amyloid precursor protein intracellular domain (AICD) strongly enhances resting free cytosolic calcium levels. Presented at *9th International Conference on Alzheimer's Disease and Related Disorders, Philadelphia, Pennsylvania, USA, July, 17-22, 2004.*

(Runa Hamid)